Defining a Role for DPP4 In Inflammation and Atherosclerosis

Andrew Clément

This thesis is submitted to the University of Ottawa in partial fulfillment of the requirements for the degree of Master of Science in Biochemistry

Department of Biochemistry, Microbiology, and Immunology

Faculty of Medicine

University of Ottawa

Abstract

Atherosclerosis is an accumulation of lipid-rich plaques within arteries and a leading cause of death worldwide. Chronic low-grade inflammation is characteristic of atherosclerosis, where monocytes and macrophages play a critical role in the progression or regression of plaque. Dipeptidyl peptidase 4 (DPP4) is increased in conditions of metabolic dysfunction, and there is a strong association between monocyte DPP4 and the development of atherosclerosis. However, a causal mechanism linking increased monocyte DPP4 activity and atherogenesis remains to be revealed. We hypothesize that DPP4 regulates proteins in circulation and in macrophages to drive inflammation and atherosclerosis progression. Using *in vivo* and *in vitro* inflammatory models, we identified that DPP4 activity is increased during inflammation, and *Dpp4* mRNA is upregulated in pro-inflammatory polarized macrophages. We also found that mononuclear phagocyte DPP4 may have a role in regulating circulating immune cell populations. Ependymin-related 1 (EPDR1) was identified as a DPP4 substrate via N-terminal enrichment mass spectrometry, where transcript expression was decreased in pro-inflammatory and anti-inflammatory polarized BMDMs from males. Additionally, we found correlations between circulating DPP4 protein and Hba1c and LDLc, while both DPP4 activity and protein correlated with HDLc in patients. EPDR1 increased with age and correlated with LDLc and plasma triglycerides in *apoe*$^{-/-}$ mice, while EPDR1 decreased with age in patients. These data suggest a role of DPP4 and EPDR1 in inflammation, macrophage phenotype, and metabolic dysfunction.

Co-Authorship Statement

Andrew Clément did experiments, analysis, data presentation and thesis preparation with the exception of:

Dr. Erin E. Mulvihill provided intellectual input and scientific expertise with experimental designs, project scope and hypothesis.

The University of Ottawa Animal Care Veterinary Services (ACVS) provided care for all animals used for experiments.

Natasha Trzaskalski aided in technical expertise, HYTANE, metabolic tests, animal sacrifices, tissue processing, and LPS injections.

Dr. My-Anh Nguyen aided in technical expertise, experiments, animal sacrifices, tissue processing, and the development of histological slides.

Nadya Morrow aided in metabolic tests, animal sacrifices, tissue processing, and processing and analyzing circulating blood components.

Dr. Ilka Lorenzen-Schmidt aided in the management of the mouse colonies and genotyping.

Dr. Majid Nikpay aided in the statistical analyses of patient samples.

We want to thank the University of Ottawa Heart Institute Biobank and donors.

Acknowledgments

First and foremost, I would like to thank my graduate supervisor, Dr. Erin E. Mulvihill, for allowing me to pursue this degree in her laboratory. I sincerely appreciate all of her support, patience, guidance, and ability to push me out of my comfort zone and develop throughout my time in her laboratory. I am fortunate to have been under her tutelage for the past few years and am grateful to start my career in her laboratory.

I would also like to acknowledge and thank my thesis advisory committee, Dr. Katey Rayner, and Dr. Morgan Fullerton, for their guidance and support throughout my studies. Their direction and encouragement have been imperative for shaping this project and thesis.

I express the deepest gratitude to my present and former lab members – Natasha Trzaskalski, Nadya Morrow, Serena Pulente, Cassie Locatelli, Antonio Hanson, Dr. My-Anh Nguyen, Dr. Ilka Lorenzen-Schmidt – for providing an enriching environment that encourages professional and personal growth. I am grateful to be a part of such a good environment that drove me to pursue this research.

Finally, I would like to thank my family, girlfriend, and friends for their patience, unconditional support, and care through the ebbs and flows of my master's degree.

Table of Contents

List of Figures

List of Tables

List of Abbreviations

AAV	Adeno-Associated Virus
DAPI	4′,6-diamidino-2-phenylindole
ACEi	ACE Inhibitor
acLDL	Acetylated Low-Density Lipoprotein
ADA	Adenine Deaminase
ADP	Adenine Diphosphate
ATP	Adenine Triphosphate
aggLDL	Aggregated Low-Density Lipoprotein
ARB	Angiotensin Receptor Blockers
ANOVA	Analysis of Variance
apoe	Apolipoprotein E
ARG-1	Arginase-1
Abca1	ATP Binding Cassette Subfamily A Member 1
Actβ	Beta-Actin
BMDM	Bone Marrow-Derived Macrophages
BSA	Bovine Serum Albumin
CVA	Cerebral Vascular Accident
CHF	Chronic Heart Failure
CD4	Cluster of Differentiation 4
CD45	Cluster of Differentiation 45
CABG	Coronary Artery Bypass Surgery
CAD	Coronary Artery Disease

Cx3cr1	CX3C motif chemokine receptor 1
DPP4i	Dipeptidyl Peptidase-4 Inhibitor
DPP4	Dipeptidyl-Peptidase 4
DPP8	Dipeptidyl-Peptidase 8
DPP9	Dipeptidyl-Peptidase 9
DMEM	Dulbecco's Modified Eagle Medium
ELISA	Enzyme-Linked Immunosorbent Assay
EPDR1	Ependymin-Related 1
ER	Estrogen Receptor
FBS	Fetal Bovine Serum
GLP-1R	Glucagon-Like Peptide-1 Receptor
GLP-1RA	Glucagon-Like Peptide-1 Receptor Agonist
GLP-1	Glucagon-Like-Peptide 1
GLUT	Glucose Transporter
GIP	Glucose-Dependent Insulinotropic Polypeptide
HBSS	Hanks' Balanced Salt Solution
Hba1c	Hemoglobin A1C
HDLc	High-Density Lipoprotein Cholesterol
HYTANE	Hydrophobic Tagging-Assisted N-Termini Enrichment
Hmbs	Hydroxymethylbilane Synthase
Hprt	Hypoxanthine-Guanine Phosphoribosyltransferase
IFNγ	Interferon gamma
IL4	Interleukin 4

Il1β	Interleukin-1 beta
iBAT	Interscapular Brown Adipose Tissue
LPS	Lipopolysaccharide
Lxrα	Liver X receptor alpha
Ldlr	Low Density Lipoprotein Receptor
LDLc	Low-Density Lipoprotein Cholesterol
mRNA	Messenger RNA
Nox1	NADPH oxidase 1
NADPH	Nicotinamide Adenine Dinucleotides Phosphate
iNOS	Nitric Oxide Synthase
oGTT	Oral Glucose Tolerance Test
oLTT	Oral Lipid Tolerance Test
oxLDL	Oxidized Low-Density Lipoprotein
PFA	Paraformaldehyde
PCI	Percutaneous Coronary Intervention
pWAT	Perigonadal White Adipose Tissue
PAD	Peripheral Artery Disease
PPARγ	Peroxisome Proliferator-Activated Receptor Gamma
PBS	Phosphate Buffer Saline
PCSK9	Proprotein Convertase Subtilisin/Kexin Type 9
ROS	Reactive Oxygen Species
RT-qPCR	Real-Time Quantitative Polymerase Chain Reaction
Retnla	Resistin Like Alpha

RNA	Ribonucleic Acid
Scarb1	Scavenger Receptor Class B Type 1
SEM	Standard Error of the Mean
sWAT	Subcutaneous White Adipose Tissue
Stx5a	Syntaxin 5A
TBG	Thyroxine-Binding Globulin
TRIF	TIR-Domain-Containing Adapter-Inducing Interferon-β
TIR	Toll/interleukin-1 receptor
TLR4	Toll-Like Receptor 4
TIA	Transient Ischaemic Attack
TG	Triglycerides
Tnf	Tumor Necrosis Factor
T1DM	Type 1 Diabetes Mellitus
T2DM	Type 2 Diabetes Mellitus
T2D	Type-2 Diabetes
Mφ	Unpolarized BMDM

1. Introduction

1.1 The Cardiovascular System and Cardiovascular Disease

Cardiovascular disease (CVD) remains the leading cause of death worldwide, accounting for almost 20 million deaths in 2021, where coronary artery disease (CAD), strokes and other arterial diseases account for over 60% of CVD-related deaths in the United States. CVD cost on the healthcare system has a profound economic impact on healthcare and society, the total cost of CVD in the United States alone totaled $422.3 billion between 2019 and 2020(1), and are predicted to increase to $1.2 trillion by 2035(2). Identifying the importance of shifting care from late-stage intervention to less resource-dependent pharmacological options.

The cardiovascular system consists of blood vessels (veins, capillaries, arterioles, and arteries) and the heart. Its function is to circulate blood to body tissues and remove waste products(3). Cardiovascular disease is a term used to describe a multitude of non-communicable diseases affecting the cardiovascular system(4), typically leading to the dysfunctional circulation of blood(5).

1.1.1 Atherosclerosis

Atherosclerosis is a subset of arteriosclerosis, which translates to “artery” and “hardening,” a defining characteristic of both is arterial wall thickening and the narrowing of the lumen, with a decreased ability to dilate(6–8). It is a maladaptive, chronic immunometabolic disease that develops over decades(9–11).

1.1.1.1 Atherosclerosis Development

The tunica intima is an essential part of the artery, it comprises endothelial cells connected by extracellular matrix components, elastin, and smooth muscle cells. It

separates the lumen from the tunica media and is important in maintaining hemodynamic homeostasis by secreting anti-clotting agents and vasodilators like nitric oxide (NO)(12, 13). Hemodynamic changes can cause dysregulation of endothelial cells, and endothelial mechanoreceptors stimulate downstream signals to alter the landscape of the endothelium. These changes include a thickening of the tunica intima, an increased expression of adhesion molecules on the endothelial lining, and increased cell proliferation. Atherosclerotic plaques typically develop in areas of high disturbed flow and low or oscillatory shear stress, such as in arterial bifurcations and curvatures in the blood vessels. A common site with atheroma is the interior curvature between the ascending and descending aorta. This curvature causes a gradient change in hemodynamic properties, where there is high-velocity laminar blood flow in the outer curvature but disturbed turbulent blood flow in the inner curvature(13–15). The turbulent blood influences shear stress and causes endothelial phenotypic changes, leading to decreased arterial integrity, increasing permeability, cell turnover, adhesiveness, and increased intimal thickening(14, 16). Traditionally, these changes are described as the initial injury(17). On the other hand, homeostasis is maintained on the outer curvature of the artery, with maintained laminar blood flow, dilatory NO production, and expressions of genes involved in cell-cycle arrest(13, 15).

Immune cells like monocytes migrate to the developing lesion and there is retention of low-density lipoproteins (LDL) between the tunica intima and tunica media(15, 18–20). This increased retention of LDL through transcytosis (21–24) causes further endothelial disturbance, including decreasing NO production(25). The lipid accumulation can be visualized and is known as the “fatty streak”(17, 26).

Simultaneously, as the lesion develops, macrophage infiltration increases(27, 28). These macrophages come from monocyte migration and tissue-resident niches, and can increase inflammation within the developing lesion, increasing inflammatory cytokine and chemokine secretion (TNF-alpha, IL-6, IL-1(9, 29), MCP1(30), CCL2(31), and CCL5(32)). This increases the expression of endothelial selectins and immune cell integrins increasing the migration of circulating immune cells(33) and forming the intermediate lesion.

The process of immune cell migration is like that of a regular non-sterile immune response. Leukocytes, like monocytes, undergo extravasation when they encounter endothelial cell selectins like E- and P-selectins. These bind transiently, causing the rolling of the cells (margination)(34–36). Activated monocyte integrins ligands for VCAM-1, ICAM-1, and PECAM-1 increase adherence of cells(37) to begin the diapedesis process into the developing lesion(34–37). Immune cells enter the lesion to stimulate phenotypical changes in cells in the lesion(27, 38–41). Some of these phenotypic changes include the migration of vascular smooth muscle cells (VSMC) into the plaque, forming a layer of VSMCs underneath the endothelial lining and beginning to form a fibrous cap(42). Due to these environmental signals, VSMC can also increase their propensity to become pro-atherogenic foam cells(42, 43).

Both immune cells and VSMC contribute to the development of a necrotic core(17, 26, 44). In homeostatic conditions, cells undergo regulated cell death like apoptosis and surrounding macrophages undergo efferocytosis to remove apoptotic remnants. However, in the plaque milieu, the microenvironment is very complex, there are inflammatory cytokines, cholesterol crystals, and oxidized LDL (oxLDL) which can

influence induction of regulated and unregulated cell death including apoptosis, necroptosis, pyroptosis, ferroptosis, and necrosis, leading to release of damage-associated molecular patterns (DAMPs) and more inflammation(27, 39, 44–47). Additionally, there is the dysregulation of efferocytosis due to oxidized phospholipids (oxPL), inhibiting the recognition of debris by macrophages, paired with macrophage dysfunction, leading to decreased clearance of dead cell remnants(44, 46). In necrotic cores, homeostatic mechanisms are dysregulated, leading to a positive feedback loop of inflammation and cell death, and macrophages cannot handle this accumulation of DAMPs, oxLDL, oxPL, cholesterol crystals, and more. These can be characterized as vulnerable plaques, capable of forming a thrombus, and occluding the artery, as seen in myocardial infarcts and strokes(26, 40, 47).

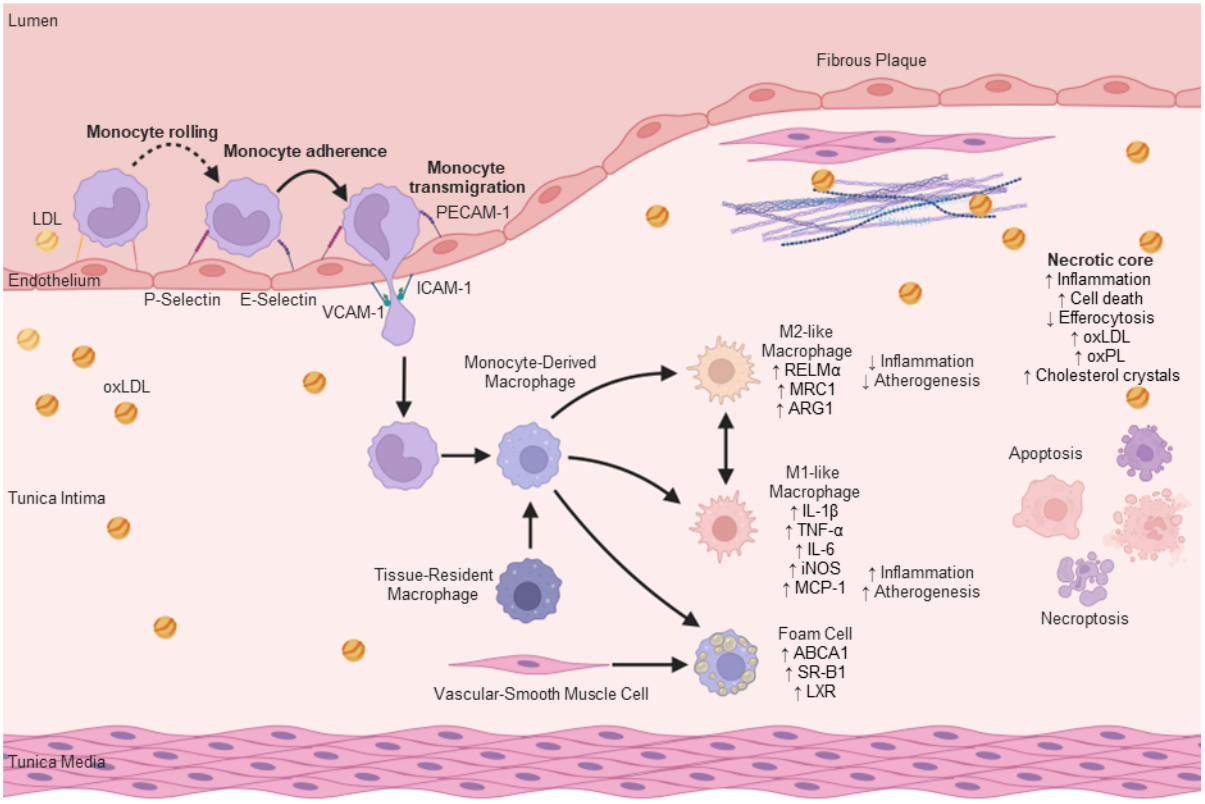

Figure 1. Macrophage polarization in atherosclerosis.

High turbulent blood flow causes hemodynamic changes and dysregulation in endothelial cells, leading to the thickening, retention of LDL, and development of a fatty streak and immune cell migration. Phenotypic changes in the developing lesions can lead to plaque rupture, typically seen in vulnerable plaque, or plaque erosion, commonly seen in more stable plaques. Either mechanism can lead to acute coronary occlusion, leading to partial or full occlusion of the artery.

1.1.1.2 Plaque Architecture

Atherosclerotic plaque begins between the tunica intima and tunica media. More advanced plaques are made up of a fibrous cap containing endothelial cells, ECM proteins, collagen, elastin and VSMC that migrated from the tunica media(26). This fibrous cap localizes and encapsulates the lesion(42). It provides structural support and elasticity and separates the developing atheroma from blood components(14, 15, 26). This defence mechanism is a response to cytokines like platelet-derived growth factor (PDGF), transforming growth factor-beta (TGF beta), and vascular endothelial growth factor (VEGF) from foam cells and endothelial cells that stimulate ECM component secretion, collagen production, and VSMC migration and proliferation(26, 42, 48). There is a balance between growth and deterioration of the fibrous cap, in more vulnerable plaques, there is increased inflammation and inflammatory M1-like macrophages, which increase matrix metalloproteases (MMP), like MMP9 that breakdown the ECM and collagen. On the other hand, in more stable plaques, pro-resolving, anti-inflammatory M2-like macrophages secrete fibrous cap growth factors(27, 28, 41, 47). Atheroma's have complex microenvironments made up of various immune cells like T-cells, neutrophils, macrophages(9, 33, 49), modified lipids like cholesterol crystals and oxLDL, macrophage and VSMC-derived foam cells, VSMCs, cell death remnants, and more, followed by the tunica media and adventitia(12).

1.1.1.3 Changes in the microenvironment

As previously mentioned, plaques evolve and progress, and depending on the microenvironment, there can be different plaque phenotypes. Stable plaques are

favourable and have thick fibrous caps, greater than 65 μm in coronary arteries and greater than 165 μm in carotid arteries in humans(50, 51), their microenvironment is composed of a greater proportion of anti-atherosclerotic cells, like M2-like macrophages(27, 28, 41, 47). In humans, there can also be vulnerable plaque with thinner fibrous caps and a greater proportion of pro-atherosclerotic cells in the atheroma milieu, like M1-like macrophages, foam cells, etc.(27, 28, 41, 47). Morphological changes of plaque are dependent on microenvironment signalling, and are capable of shifting phenotypes.

1.1.1.4 Mechanisms of Acute Arterial Occlusion

Acute arterial occlusion occurs due to the formation of a thrombus that partially or completely occludes an artery, leading to decreased or no blood flow to the tissue downstream. This occurs due to plaque ruptures or plaque erosion, leading to the formation of a thrombus, however, these tend to arise in different plaque phenotypes. Acute arterial occlusions occur in acute coronary syndrome (myocardial infarcts, unstable angina), stroke, and acute limb ischemia(50, 52–55).

1.1.1.4.1 Plaque Rupture

Over 60% of acute coronary syndromes are caused by plaque rupture. This presentation of acute arterial occlusion is seen in vulnerable and unstable atherosclerotic plaques(50, 52–55). These plaques have thin fibrous caps and typically a discontinuous intimal layer, leading to a weakness within a certain area of the fibrous cap. Over time, the fibrous cap can get degraded by MMPs, along with a large necrotic core and high levels of inflammation(14, 26). This microenvironment is ideal for the dysregulation of the endothelium that can eventually lead to rupture of

the atheroma, spilling pro-thrombotic elements, exposing ECM components and collagen to circulating blood and activating circulating platelets, causing the formation of a thrombus and quick occlusion of the artery(52–55). This leads to the fast onset of acute symptoms seen in myocardial infarction and strokes.

1.1.1.4.2 Plaque Erosion

Plaque erosion arises less frequently than plaque rupture, occurring in around 40% of patients presenting with a myocardial infarct(50). The etiology of this acute arterial occlusion is endothelial cell sloughing from the fibrous cap, exposing ECM components and collagen, activating circulating platelets and forming a thrombus, occluding the artery. For this reason, this form of arterial occlusion can present in both unstable and stable atherosclerotic lesions; however, is more frequent in larger stable plaques, as vulnerable lesions rupture before eroding. It is thought that changes in shear stress caused by turbulent blood flow for an extended period are the cause of endothelial sloughing(52–55).

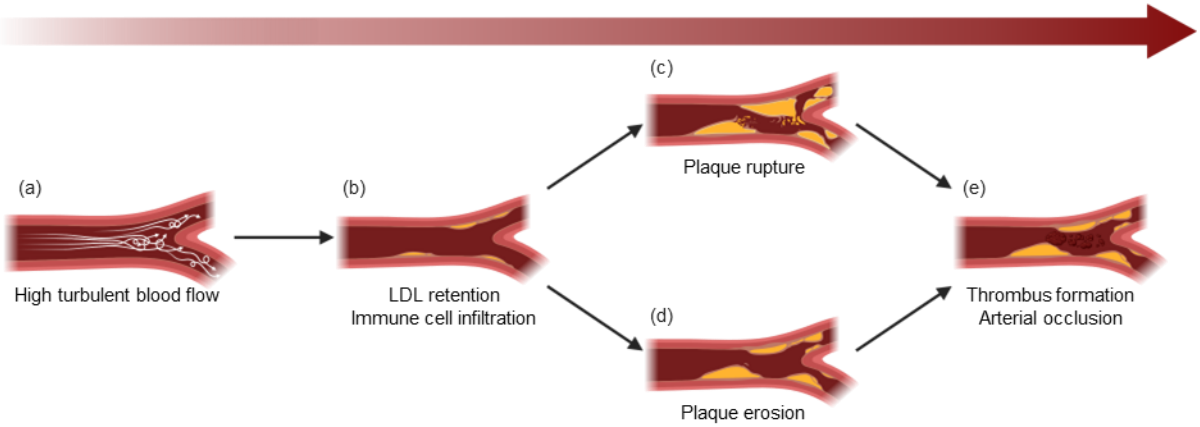

Figure 2. Mechanisms of acute arterial occlusion.

High turbulent blood flow causes hemodynamic changes dysregulation in endothelial cells (a), leading to the thickening, retention of LDL, and development of a fatty streak and immune cell migration (b). Phenotypic changes in the developing lesions can lead to plaque rupture (c), typically seen in vulnerable plaque, or plaque erosion (d), commonly seen in more stable plaques. Either mechanism can lead to acute coronary occlusion, leading to partial or full occlusion of the artery (e).

1.2.1 Metabolic Dysfunction in Cardiovascular Disease

1.2.1.1 Glucose Metabolism in Cardiovascular Disease

In healthy individuals, glucose metabolism is maintained in a narrow range with the use of two main glucoregulatory hormones: insulin and glucagon(56, 57). These proteins regulate glucose transport proteins on tissues, its absorption, glycogen anabolism and catabolism, and gluconeogenesis, ultimately keeping glucose in homeostasis(58). However, dysregulation within this system is a strong risk factor for cardiovascular disease, as seen in individuals with diabetes(59, 60). Increased blood glucose levels caused by defects in insulin secretion, action, or both can lead to endothelial dysfunction and chronic inflammation in circulation. Hyperglycemia can result in increased oxidative stress(6, 61), advanced glycation end products(62–64), reduced nitric oxide production(65), and activation of inflammatory pathways like nuclear factor κB (NFκB) in endothelial cells(66). This leads to dysfunction and increased rigidity of arteries(61, 67) and permeability of the endothelial layer(7), which disrupts blood flow and increases the risk for atherosclerosis and other cardiovascular diseases.

1.2.1.2 Lipid Metabolism in Cardiovascular Disease

Triglycerides, phospholipids, and sterols are hydrolyzed by lipases beginning in the oral cavity into the small intestine enterocytes, into free fatty acids, monoacylglycerols, lysophospholipids, and cholesterol, and absorbed by enterocytes and repackaged into triglycerides in the cells. Following resynthesis, it is packaged as chylomicrons, a triglyceride-rich lipoprotein and secreted into circulation, where it can interact with lipoprotein lipase to release free fatty acids for tissue energy production (68, 69). Endogenous lipoproteins are synthesized in the liver, first as triglyceride-rich,

very low-density lipoproteins (VLDL). Where metabolized, VLDL turns into cholesterol and triglyceride-rich intermediate density lipoproteins (IDL) and then cholesterol-rich low-density lipoproteins (LDL), which can deliver cholesterol to many tissues and can be taken up by different tissues, mainly the liver(70, 71). LDL cholesterol has been identified as a causal factor for the development of atherosclerosis(72, 73) through the retention and deposition of particles into the arterial wall and the development of plaque, as described previously.

High-density lipoprotein (HDL) is synthesized in the liver and the intestine(68, 74, 75), where its role is to transport phospholipids and cholesterol that have been effluxed out of cells through the actions of two ATP-binding cassette transporters (ABC): ABCA1 and ABCG1(74, 76). Additionally, it can receive phospholipids and cholesterol from VLDL and chylomicrons during LPL-mediated lipolysis(70). Cells accumulate cholesterol mainly through deposition by circulating lipoproteins and *de novo* cholesterol synthesis(70, 77). Most cells do not have mechanisms for the catabolism of excess cholesterol, but some cell types can convert cholesterol into steroid hormones, and some cell types on epithelial tissues can secrete cholesterol. However, most cells cannot decrease their cholesterol transport intrinsically and need a different mechanism(70, 78, 79). HDL-mediated reverse cholesterol transport is essential in removing excess cholesterol from cells. As noted, ABCA1 and ABCG1 are important in cholesterol efflux to HDL. As intracellular cholesterol increases, so does the formation of oxysterols, activating the transcription factor liver X receptor (LXR)(76). This results in increased ABCA1 and ABCG1 and enhanced cholesterol efflux from the cell. After cholesterol efflux onto HDL, it can travel to the liver and interact with hepatic scavenger receptor class B type 1 (SR-B1), resulting in the

selective uptake of cholesterol from HDL and conversion and secretion of cholesterol into bile acids(68, 70).

Dysregulation of circulating blood lipoproteins, as seen in dyslipidemia, is a strong risk factor for cardiovascular disease(80, 81). This imbalance in blood lipids can be a result of poor diet, physical inactivity, obesity, and the use of tobacco and is estimated to affect more than half the global population(29, 82). LDL cholesterol has been proposed as a stimulator of inflammation through a macrophage CD36-TLR4-TLR6 pathways activating the NLRP3 inflammasome and the NFκB pathways(29, 83).

1.3 The Immune System

The immune system is a collection of tissues, cells, and chemicals that protect the body from “foreign” pathogens(84, 85). There are structural barriers like epithelial barriers like the skin or the lining of our respiratory tract and digestive tract, or endothelial barriers like endothelial cells in the vasculature(86). Immune system defences are tailored towards specific functions and include the innate immune system, which acts quickly and is the first line of defence against “foreign” pathogens, and the adaptive immune system, tailored towards immunological memory, mounting more sophisticated, specific responses toward previously exposed pathogens, which takes longer to mount an attack. These systems are interconnected in their abilities to fight pathogens through indirect cytokine signaling and direct cell-cell communication(87).

1.3.1 The Innate Immune System

The innate immune system is responsible for early defences from perceived pathogens and response to injury. It uses mechanical or physical (epithelial and

mucosal membranes, mucus, etc.), chemical (microbicidal peptides, defensins, enzymes, pH regulation, etc.) barriers, as well as cell-mediated innate defences when those fail. These innate cell-mediated defenses include tissue-resident cells and incoming recruited cells(86, 88, 89). However, in many cases, soluble mediators like pro-inflammatory cytokines and chemokines, secreted by immune cells, discussed later, can stimulate increased myelopoiesis and travelling of these newly acquired cells to the site of injury(90, 91).

1.3.1.1 Organs in the Innate Immune System

Multiple tissues are involved in the development, differentiation, and detection of pathogens in the immune system. Primary lymphoid organs like the bone marrow and the thymus are responsible for the production of the cells(87) or further differentiation(92, 93); where the hematopoiesis occurs in the bone marrow, giving rise to myeloid cells and naive lymphoid cells(87, 88, 94, 95), and the thymus trains and further differentiate naive T-cells into effector cells(92, 93). There are also secondary lymphoid organs, which are important in recognizing pathogens and stimulating the immune response. These tissues include the spleen, lymph nodes, and mucosal-associated lymphoid tissues (MALT)(96). The spleen is the first line of defense against blood-borne pathogens. The spleen can be broken down into red and white pulp and contain passing red blood cells and immune cells like macrophages, dendritic cells (DC), and B- and T-cells, respectively(97, 98). Upon discovering blood-born pathogens, antigen-presenting cells (APCs) like macrophages and DCs phagocytose the pathogen and present it to lymphoid cells. Lymph capillaries are an important entrance of APCs to the lymph nodes, where lymphoid cells can be

activated and matured to stimulate the immune system(96, 99, 100). MALT can be found near epithelial layers and give rise to tissue-resident immune cells to protect from oncoming pathogens and stimulate the immune system if necessary(96).

1.3.1.2 Hematopoiesis

The cellular components of blood are made in the red bone marrow found in the long bones of the body, starting with niches of self-renewing, pluripotent hematopoietic stem cells (HPCs) that can differentiate into many different cell types(87). Cell fate determination of HPCs is dependent on microenvironmental cues where cytokines, growth factors, and cell-cell communication between HPCs and stromal cells determine whether lymphopoiesis or myelopoiesis take precedence and what specific cell types(87, 94, 95). There are two lineages: lymphoid and myeloid. The lymphoid lineage gives rise to natural killer cells, T-cells, and B-cells, with the possibility of long-term immunological memory as a characteristic of T- and B-cells(87, 94). The myeloid lineage gives rise to all other cellular components, from cells of the innate immune system to erythrocytes and megakaryocytes to produce platelets(88, 95). In short, myelopoiesis occurs when HPCs differentiate into common myeloid progenitors, then to granulocyte/macrophage (GM) progenitors or megakaryocyte/erythrocyte progenitors. GM progenitor cells can differentiate into most cells of the innate immune system, dependent on microenvironmental signalling(87, 94, 95). This can be used *ex vivo* to stimulate the differentiation of cells to specific cell types. For example, to get bone-marrow-derived macrophages, you can use GM-CSF (colony-stimulating factor) and M-CSF (macrophage-colony

stimulating factor) to generate bone-marrow-derived monocytes and macrophages(101, 102).

1.3.1.3 Cells of the Innate Immune System

Each cell in the immune system has a specific role, sometimes overlapping, but all can work together to overcome pathogens, and sometimes molecules stimulate sterile inflammation when there is an immune system activation without the presence of an exogenous pathogen or in response to injury, as described earlier with the example of increased accumulation of LDL particles. Some cells of the innate immune system can be categorized based on appearance and functions, such as, phagocytes, APCs, and other cells of the immune system(86, 88, 90, 91). The phagocytes encompass neutrophils, dendritic cells, monocytes, and macrophages, as they can use phagocytosis to kill microbes(103, 104). These can be subcategorized based on histological and morphological properties of their nucleus, where neutrophils are polymorphonuclear phagocytes(49, 90, 105), and dendritic cells, monocytes and macrophages are mononuclear phagocytes(103, 106–108). APCs are important in ingesting microbes and pathogens and identifying antigens to lymphocytes to stimulate the adaptive immune systems and immunological memory. These cells include dendritic cells, macrophages, and lymphocytic B-cells(109–112). Furthermore, other cells of the innate immune system include mast cells, basophils, and eosinophils, important in allergic reactions, inflammation, and anti-parasitic activity(86, 88), respectively.

1.3.1.4 The Innate Immune Response

Upon initiation of the innate immune system due to the presence of DAMPs or pathogen-associated molecular patterns (PAMPs)(86, 91), tissue-resident macrophages or neutrophils are typically the first to respond within seconds to minutes(38, 45, 49, 90, 105, 113), followed by monocytes entering the tissue or lesions and differentiating into macrophages(39, 45, 108). Together, they mount an attack, releasing reactive oxygen species (ROS) and ingesting pathogens and cellular debris(90, 104, 107, 108). Additionally, support is called upon via secretion of nitric oxide, chemokines, and other cytokines like histamines and bradykinin sensitizing the area, causing vasodilation to increase blood flow and recruitment to the tissue, contraction of endothelial cells to increase leakiness of the vessels, and expression of selectins and other adhesion molecules to increase margination and extravasation of immune cells into the tissue(9, 84–86, 114).

An important feature of the innate immune system is the lack of receptor specificity. For example, monocytes use pattern recognition receptors (PRRs) that recognize common molecular features and structures on PAMPs or DAMPs. This non-specificity allows for quick recognition of PAMPs and DAMPs in a diverse landscape of molecular patterns(86, 88, 91). Many PRRs recognize many different molecules. A well-characterized PRR is toll-like receptor 4 (TLR4), which classically recognizes the lipid A portion of lipopolysaccharide (LPS) on the membrane of gram-negative bacteria(115).

1.3.2 Macrophages in Atherosclerosis

Macrophages are part of the mononuclear phagocyte family, meaning that they can utilize PRRs to recognize a diverse range of molecular patterns(38, 39, 108). In the developing lesion, macrophages come from differentiated monocytes from circulation or proliferating tissue-resident macrophages, typically located in the intima and the adventitia of arteries. They are important in removing DAMPs and PAMPs from the lesion, utilizing mainly three different mechanisms, depending on the recognized molecule: phagocytosis through scavenger receptors like CD36 and SR-B1, micropinocytosis, and efferocytosis. However, utilization of these mechanisms is very dependent on the polarization spectrum of the macrophages, as microenvironmental signals alter macrophage phenotype, mechanisms of ingestions will either be up- or downregulated(27, 28, 38, 39, 41, 47).

Once macrophages are in the lesion, they begin ingesting pathogenic material like oxLDL and dead tissue. This is done by the recognition of PAMP or DAMP by subcategories of PRR like scavenger receptors, mediating non-opsonic uptake of pathogens(116–118). After phagocytosis, macrophages can secrete cytokines to stimulate a variety of functions like pro-inflammatory cytokines to increase the inflammatory response or pro-resolving cytokines to initiate tissue repair(119–121). These macrophages can also break down these pathogens and present them via MHC class I and II markers to lymphocytes to potentiate the adaptive immune response(91, 112).

Macrophage phenotypes have a unique plasticity that gives them the power to regulate their microenvironment(27, 28, 38, 39, 41, 47). However, there is a reciprocal

mechanism where cues in their environment can regulate their phenotype, for example, the necrotic core is filled with oxLDL, cholesterol crystals, and cell debris dsDNA, which can activate downstream pro-inflammatory pathways, in addition to being an oxygen-poor environment. This environment can regulate cellular metabolism, like increasing glycolysis, while decreasing oxidative phosphorylation, leading to a more pro-inflammatory macrophage phenotype(29, 40, 47, 83, 122).

Macrophage phenotype can heavily influence lesion stability, and there are multiple identified phenotypes, although it is more of a spectrum and macrophages can alternate, or display components of multiple phenotypes depending on microenvironmental signalling (27, 28, 38, 39, 41, 47). Classically activated M1-like macrophages are the main driver of inflammation within the plaque and are pro-atherogenic(123). They express high levels of pro-inflammatory molecules like IL-1β, TNF-α, IL-6, iNOS, and MCP-1. These cells have an increased rate of glycolysis, upregulated GLUT1 and hexokinase protein expression, and increased ROS generation. Important in generating this phenotype *in vivo* is stimulation by pro-inflammatory factors like IFNγ, TNF-α, and the hypoxic microenvironment, leading to upregulation of HIF1-α, increasing glycolytic genes to mitigate this imbalance in oxygen supply and demand, and increase pro-inflammatory gene expression, and NLRP3 activity(27, 28, 38, 39, 41, 47, 124). This phenotype can be stimulated *in vitro* with LPS and IFNγ(101, 102).

On the other side of the spectrum are alternatively activated M2-like anti-inflammatory and atheroprotective macrophages. They produce high levels of pro-resolving genes like TGF-β, RELMα, MRC1, and ARG1 and promote wound healing

by stimulating ECM remodelling, collagen production, and removal of cell debris via efferocytosis(28, 28, 41, 125). Important to note is that there are subtypes to this phenotype, from M2a to M2d, to suit their environment best. M2a macrophages are induced by IL-4 and IL-13 and are characterized by their increased phagocytic capabilities and expression of pro-resolving genes. This phenotype can be stimulated *in vitro* with IL-4 and or IL-13. M2b are induced by immune complexes, TLR signalling, and pro-inflammatory cytokine IL-1β. They secrete both pro- and anti-inflammatory proteins to modulate their environment based on what is needed(126). M2c is characterized as important in mediating the clearance of DAMPs via efferocytosis and is stimulated by TGF-β, and IL-10 within the plaque(126, 127). M2d macrophages secrete high levels of VEGF to induce VSMC migration after TLR activation and adenosine A_{2A} receptor activation(128, 129).

Foam cells are very pro-atherogenic and can be derived from macrophages or VSMC due to unregulated oxLDL ingestion(17, 41, 42, 47). VSMC can undergo a phenotypic switch to a macrophage-like foam cell phenotype. Surprisingly, these cells, although pro-atherogenic, are not the main source of inflammation within the plaque(123); they upregulate genes involved in reverse cholesterol transport like ABCA1, ABCG1 SR-B1, and LXR, as well as processes involved in fatty acid transport, oxidative phosphorylation, fibrous cap degeneration, and lysosomal activity(17, 41, 123, 130). Additionally, due to the increased intracellular cholesterol, metabolic flux shifts towards glycolysis, rather than oxidative phosphorylation and fatty acid oxidation. This intracellular pool of free cholesterol and free fatty acids is generated through ingestion of oxLDL and digestion in the lysosome, however, this

accumulation of free cholesterol is cytotoxic and causes endoplasmic reticulum stress, stimulating the unfolded protein response and cell death. In homeostatic conditions, it stimulates apoptosis, however, in cases of acute, large increases of cytotoxic free cholesterol can result in necroptosis and necrosis(122, 131, 132). Further dysregulation of foam cells mediated by free cholesterol, is the formation of cholesterol crystals, increasing NFκB pathways, NLRP3 activation, and inflammatory signalling(47, 83).

Other macrophage phenotypes lie more in the spectrum of the aforementioned phenotypes. M4, Mox, M(Hb), and Mhem are all stimulated by different signals(27, 28, 38, 39, 41, 47, 124). Of these, M4 and Mox macrophages are pro-inflammatory, proatherogenic phenotypes. M4 macrophages are activated by pro-inflammatory chemokine, CXCL4, and have decreased phagocytic capabilities, and increased matrix metalloprotease expression. These cells are more prevalent in vulnerable plaque(133). In comparison, Mox responds to oxPL and has increased glycolytic capabilities and oxidative phosphorylation to promote high levels of inflammation(134). On the other hand, M(Hb) and Mhem macrophages are anti-inflammatory and atheroprotective. M(Hb) are activated by hemoglobin and haptoglobin, whereas Mhem phenotypes are stimulated by haem, as the name suggests, these are typically seen in lesions that have ruptured, where macrophages ingest red blood cells. There is an increase in genes involved in reverse cholesterol transport like LXRa and ABCA1 that prevent foam cell formation, promote angiogenesis and vascular permeability(135–138).

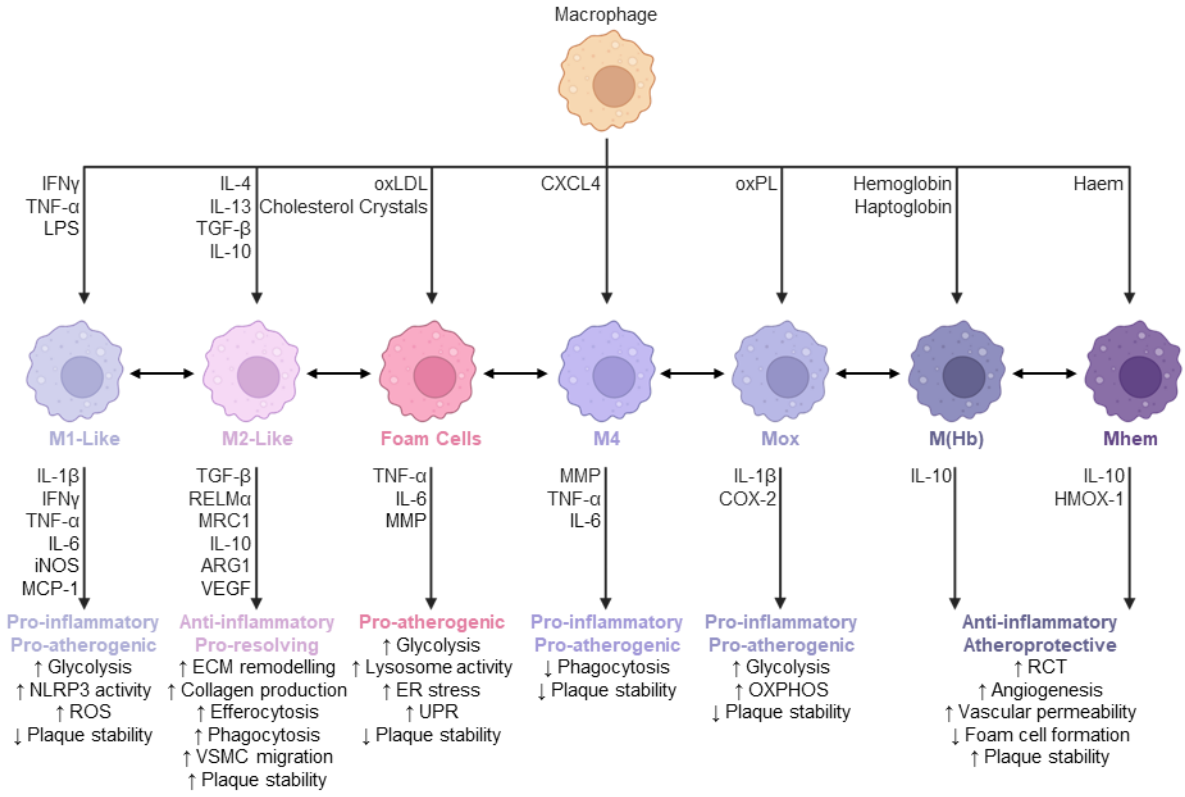

Figure 3. Macrophage phenotypes in atherosclerosis.

Macrophage plasticity during atherosclerosis depends on microenvironmental signalling and can lead to various atherosclerotic plaque phenotypes, such as increased or decreased plaque stability.

1.4 DPP4

Dipeptidyl peptidase 4 (DPP4), also known as cluster of differentiation 26 (CD26), is a type II transmembrane serine protease that can be membrane-bound or cleaved to release a soluble form(139). Circulating DPP4 protein and activity levels are upregulated in metabolic disease, including obesity and atherosclerosis (140, 141). Additionally, LPS activity through TLR4 signalling in monocytes can increase membrane expression(142).

1.4.1 Enzymatic Activity of DPP4

DPP4 cleaves a dipeptide from the N-terminal of proteins that display an alanine, serine, or proline at the penultimate position. It has been characterized as an important regulator of several bioactive peptides(139).

1.4.2 DPP4 In the Incretin Effect

The bioactivity of glucagon-like peptide 1 (GLP1) and glucose-dependent insulinotropic polypeptide (GIP) are regulated by DPP4 cleavage(141, 143). GLP1 and GIP are secreted by L-(144) and K(145) cells in the duodenum in response to nutrients entering the small intestine(144, 146–148). They are secreted into circulation, acting quickly on their respective receptors on pancreatic beta cells, stimulating glucose-dependent insulin secretion to regulate blood glucose levels. The incretins have a short half-life due to DPP4 cleavage, which prevents receptor activation and potentiation of glucose stimulated insulin release (141). DPP4i are widely used in treating diabetes for their ability to increase endogenous intact GLP1 and GIP levels(139, 149–151). Additionally, mice lacking DPP4 are resistant to the

development of obesity and hyperinsulinemia, as seen in early-stage diabetes, and they have improved post-prandial glucose response(152, 153).

1.4.3 DPP4 in Cardiovascular Disease

DPP4 is upregulated in metabolic disease, as seen in obesity, diabetes, and cardiovascular disease(140, 141) and has been proposed to contribute to atherogenesis by reducing incretin signaling(143), and increasing atherogenic monocyte and macrophage phenotypes(154–156). Importantly, DPP4 may have a role in the development of metabolic syndrome and is correlated with an increased BMI(157). This multifaceted metabolic dysregulation can lead to the development of diabetes and cardiovascular disease(158). The inflammatory toll/interleukin-1 receptor domain-containing adaptor protein inducing interferon beta (TRIF)-TLR4 pathway can stimulate membrane DPP4 expression(142), and DPP4 inhibition has been shown to decrease foam formation in a human macrophage cell model(155, 156).

1.4.3.1 DPP4 Inhibitors

DPP4i is a common treatment used in diabetes to help regulate blood glucose(139, 149–151). Interestingly, DPP4i in preclinical models has shown cardiovascular benefit(159), with decreased atherosclerosis development by reducing migration of macrophages into the developing atheroma, and decreased pro-inflammatory cytokines within the plaque(159, 160), and has also been shown to decrease macrophage foam cell formation(156, 159, 160). Additionally, DPP4i can regulate macrophage phenotypes by inducing a phenotypic switch of M1-like macrophages to M2-like macrophages *in vitro*(160). Further preclinical studies have identified decreased inflammation in circulation(155).

Despite the positive outcomes of DPP4i use in preclinical models, multiple cardiovascular safety trials have shown no cardiovascular benefit in patients(161–167).

1.4.4 DPP4 in the Immune System

Although ubiquitously expressed, in the immune system, DPP4 is predominantly expressed in lymphocytes like T cells, B cells, natural killer cells, and myeloid cells like monocytes, macrophages, and neutrophils. Interestingly, DPP4 in the bone marrow is important in the regulation of hematopoiesis as it can regulate multiple colony-stimulating factors, where DPP4i's have been shown to increase the action of GM-CSF, G-CSF, and erythropoietin(168, 169). Illustrating a role of DPP4 in HPSCs in myeloid cell differentiation.

1.4.4.1 DPP4 in Monocytes and Macrophages

An emerging role of DPP4 in monocytes and macrophages suggests that it may be implicated with cellular and physiological phenotypes(142, 154–156, 161, 168, 170, 171). Circulating monocytes expressing DPP4 are elevated in patients living with obesity and patients with atherosclerosis, along with its membrane expression. DPP4 expression in these cells is correlated with atherosclerotic burden, non-HDL cholesterol, and plasma triglycerides (170). There are also additional roles to monocyte and macrophage phenotypes, where oxLDL and LPS upregulated surface DPP4 expression on human-derived monocytes through a CD36/TLR4/TRIF dependent mechanism(142). Additionally, DPP4 is implicated with macrophage mobility, where DPP4 inhibition via DPP4i decreases migration into atheroma's(159), and small interfering RNA (siRNA)-mediated downregulation of DPP4 also blocks glucocorticoid-induced migration(172).

1.5 EPDR1

Ependymin-related 1 (EPDR1) was first described as a mammalian homolog of ependymin, termed mammalian-related proteins(173). First identified as a glycoprotein secreted into the cerebrospinal fluid of teleost fish by fibroblasts, it is characterized to increase in many different diseases like cancers(174–177), osteoporosis(178), Dupuytren's disease(179), and glaucoma(180). Like DPP4, it is a type II transmembrane protein, however, unlike DPP4, it has homology to cell adhesion molecules like cadherins and ependymin and is thought to localize to the be lysosome(173, 181). Its crystal structure provides insight into potential actions, as it shares homology with bacterial lipoprotein transporter LolA, highlighting a possible role in lipid metabolism(173).

1.5.2 EPDR1 in Obesity, Diabetes, and Coronary Artery Disease

EPDR1 was recently identified as a batokine, a cytokine highly expressed by brown adipose tissue (BAT) in humans. It was further found to have a role in adipose tissue browning and cellular metabolism. siRNA knockdown decreases oxygen consumption rate in isolated human BAT, BAT activation increases transcript expression, and decreases expression of thermogenic genes like *Dio2,* and *Ucp1*, as well as the glucose transporter *Glut4*(182). EPDR1 was identified as an endocrine factor part of an inter-organ adipose tissue-liver cross-tissue gene regulatory network associated with the clinical severity of CAD; where *Epdr1* transcript expression in both visceral and subcutaneous adipose tissue correlated with BMI, fasting plasma triglycerides, and Hba1c. Additionally, injection of recombinant EPDR1 for three days at 1μg/g in wild-type mice decreased plasma total cholesterol, with no effect on HDLc, suggesting a decrease in non-HDL cholesterol, reduced plasma glucose, but

increased plasma triglycerides(183). Transcript expression is also upregulated in pancreatic islets of people diagnosed with type 2 diabetes mellitus and is correlated with the BMI of patients with and without diabetes, Hba1c, and glucose-stimulated insulin secretion (GSIS) in islets of non-diabetic donors. On the other hand, *Epdr1* expression in islets from diabetic donors negatively correlated with Hba1c and increased as GSIS increased. They identified that EPDR1 has a role in regulating TCA cycle intermediates, where siRNA knockdown increased lactate production, and decreased pyruvate production and induction into the TCA cycle, in addition to reduced citrate, succinate, alpha-ketoglutarate and malate. This change in glycolysis and the TCA cycle led to decreased insulin secretion, as there was an imbalance in ADP: ATP ratios(184). These data identify an underlying mechanism of EPDR1 in regulating lipid and glucose metabolism through modulation of cellular metabolism, which identified it as a possible target for CAD and modulation of inflammation through immunometabolism.

1.6 Rationale, Hypothesis, and Objectives

There is evidence that DPP4 is regulated by inflammation(140, 142, 170), and it may have a role in inflammatory signaling(156, 168, 171, 185). It has been identified that membrane-bound DPP4 is upregulated after LPS treatment in human-derived monocytes through a TLR4-dependent mechanism(142). Additionally, treatment of macrophages with DPP4i can increase polarization towards an anti-inflammatory M2-like phenotype(171), illustrating a potential relationship between DPP4 and inflammation. In patients with atherosclerosis, a chronic inflammatory disease, monocyte DPP4 expression is increased and is associated with atherosclerotic burden and risk factors for atherosclerosis(170). In preclinical models, DPP4 may

have a larger role in monocyte motility and migration to developing lesions, and the regulation of inflammation within the plaque(155, 159, 172).

Interestingly, DPP4i has not shown cardiovascular benefits in humans(161, 162, 164–167), but its therapies based on its substrate, GLP1 receptor agonists have shown strong cardiovascular benefits (186, 187). However, there is a lack of sensitivity in assays to detect cleaved proteins and identify novel substrates. Using HYTANE, we identified EPDR1 as a novel target of DPP4(188). EPDR1 has been shown to regulate risk factors for atherosclerosis, like lipid and glucose metabolism(182–184), as well as cellular metabolism(182, 184), modulating cellular energy levels within beta cells and regulating insulin secretion(184).

The thesis will address the following hypothesis: Macrophage DPP4 is required for the response to inflammation, and the DPP4 substrate EPDR1 regulates body composition, and lipid and glucose metabolism.

Objective 1: Determine if DPP4 responds to LPS *in vivo* and in cultured macrophages.

Objective 2: Identify EPDR1 as a novel DPP4 substrate and determine its role in lipid and glucose metabolism.

Objective 3: Detect associations between circulating DPP4 and EPDR1 with risk factors for atherosclerosis.

2. Methods

2.1 Animals, Diets, Housing

Mouse experiments were performed adhering to the approved protocols of the University of Ottawa Animal Care Committee and the Canadian Council on Animal Care (Protocol #HI-2920). Male and female mice were housed under a 12-hour light/dark cycle at the University of Ottawa Heart Institute and had free access to water and a standard lab diet (Harlan Teklad) unless otherwise noted.

2.2 *Dpp4*$^{-/-}$, *Epdr1*$^{-/-}$, *Dpp4*$^{Cx3cr1-/-}$, *apoe*$^{-/-}$ mice.

Whole-body *Dpp4* deletions were re-derived from a mouse colony that has been described previously in C57BL/6 mice(153)

To generate germline full-body deletion of *Epdr1, Epdr1*$^{fl/fl}$ mice from the Toronto Centre for Phenogenomics (C57BL/6N-Epdr1<tm1a(NCOM)Mfgc>/Tcp, the Canadian Mouse Mutant repository) were crossed with Ella-Cre expressing mice(189) (B6.FVB-Tg(EIIa-cre)C5379Lmgd/J, obtained from The Jackson Laboratory, 003724), generating *Epdr1*$^{fl/+}$ expressing one copy of Ella-Cre. These mice were crossed to generate *Epdr1*$^{-/-}$ with the deletion in exon 2 of the *Epdr1* gene.

Dpp4$^{fl/fl}$ (Merck Research Laboratories) were crossed with Cx3cr1 Cre-ER expressing mice(190) (B6.129P2(C)-Cx3cr1tm2.1(cre/ERT2)Jung/J, The Jackson Laboratory, 020940), generating *Dpp4*$^{+/fl}$, expressing *Cx3cr1* Cre-ER. These mice were crossed to generate *Dpp4*$^{fl/fl}$, expressing *Cx3cr1* Cre-ER. Cx3cr1 Cre-ER activation is induced by administering 5mg to males and 2.5mg to females of tamoxifen in corn oil via gavage three times in week 1, followed by a 1-week break, and three more tamoxifen administrations in week 3. This induces exon 22 excision

from the *Dpp4* gene, where the catalytic serine active site is located; the following week, the mice are used for experiments.

Table 1. Primers for genotyping *Dpp4*$^{Cx3cr1-/-}$.

	Forward	**Reverse**
Dpp4$^{fl/fl}$	GAA TAT GAT CCT TGT CAG AGC AGC C	CTG CAC TCA GAA GTC TCA CTG
Cre	ATC CGA AAA GAA AAC GTT GA	ATC CAG GTT ACG GAT ATA GT

2.3 Blood and Tissue Collection and Preservation

Blood samples were collected from cardiac puncture with an EDTA-coated syringe, or via the tail vein in EDTA-coated blood-collection microvette tubes (Sarstedt, 16.444.100), and plasma was isolated via centrifugation at 13523xg for 10 minutes at 4°C. For EPDR1 analysis, blood was mixed with 10% TED (5,000 KIU/mL Trasylol, 1.2 mg/mL EDTA, and 0.1 nmol/L Diprotin A) (vol/vol) prior to centrifugation. All plasma was stored at -80°C for further analysis. Mice were euthanized by CO_2 inhalation and cervical dislocation, was used as a secondary method of euthanasia. Tissues were isolated and snap-frozen in liquid nitrogen and stored at -80°C for further analysis. Analysis for plasma triglycerides, total cholesterol, LDLc, HDLc, and glucose was performed by The Centre for Phenogenomics (Toronto, Ontario).

2.4 LPS injections

To determine *in vivo* if LPS increases circulating DPP4 through macrophage-targeted signalling. Wild-type mice underwent intraperitoneal injection with saline or 0.3mg/kg of body weight of LPS (Sigma-Aldrich, L2880). Additionally, control or *Dpp4*$^{Cx3cr1-/-}$ were injected with 0.3mg/kg of body weight of LPS in sterile saline, tail snip blood was taken before and 24-hours post-injection for DPP4 protein and activity analysis and circulating blood components (red blood cells, platelets, white blood cells, neutrophils, monocytes, basophils, eosinophils, and lymphocytes) via Element HT5.

2.5 Bone Marrow-Derived Macrophage Cell Culture

To better understand the role of *Dpp4* in macrophage phenotypes, male and female wild-type and *Dpp4*$^{-/-}$ mice between the ages of 8-12 weeks were sacrificed, and bone marrow (BM) was isolated from the femurs and tibias of both hind legs. The

cells were allowed to grow and differentiate into bone marrow-derived macrophages (BMDM) in BMDM Media (DMEM High Glucose media (Gibco, 11965092) supplemented with 20% L929 conditioned media (gift from Dr. Katey Rayner) to differentiate the BM into BMDMs, 10% heat-inactivated FBS (Gibco, 12483020) to provide growth factors and nutrients, 1:100 penicillin/streptomycin (Gibco, 15140122)) to prevent bacterial contamination for six days at 37°C, 5% CO_2. The BMDMs were then washed with filter-sterilized 1X PBS, incubated with 1X HBSS (Gibco, 14185052) with 50mM EDTA (1.8% w/v NaOH (Fisher, S318-1), pH 8, 18.7% w/v $Na_2{\cdot}EDTA{\cdot}2H_2O$ (Fisher, BP120-500) in double distilled H_2O) for 10 minutes at 4°C, lifted and transferred at $1.7x10^5$ cells/cm^2 in cell culture treated plates at 37°C, 5% CO_2 for 24 hours. BMDMs were treated in duplicates with only treatment media (DMEM High Glucose media supplemented with 5% L929 conditioned media, 2% heat-inactivated FBS, 1:100 penicillin/streptomycin) LPS (Sigma, L4391) and IFNγ (Sigma-Aldrich, I4777) to induce a pro-inflammatory phenotype, IL4 (R&D Systems, 404-ML) to induce a anti-inflammatory phenotype, oxLDL, acLDL, aggLDL (gift from Dr. Katey Rayner) to induce foam cell formation for either 24, 48, or 72 hours at 37°C, 5% CO_2.

2.6 Protein Isolation

To isolate protein from 100-150mg of whole tissues, they were homogenized with RIPA buffer supplemented with Halt™ Protease Inhibitor Cocktail for or homogenization buffer for DPP4 analysis in microcentrifuge tubes with 2.0mm zirconium oxide beads (FroggaBio, ZROB20) and homogenized at 30hz for 10 minutes at 4°C for physical lysis. To isolate protein from frozen bone marrow, it was

centrifuged at 1300xg for 5 minutes, and the pellet was used as described without zirconium oxide beads. The resulting solution was incubated at 4°C for 30 minutes.

2.7 Total Protein Analysis

Following the manufacturer's instructions, the total protein in BMDM and whole tissue extracts was measured using the colorimetric Pierce Rapid Gold BCA Protein Assay Kit (Thermo Scientific, A53226).

2.8 DPP4 Activity Assay

DPP4 activity was measured in isolated protein from cell or tissue samples, or plasma samples using a fluorometric assay. Samples were diluted in 80mM $MgCl_2$ and incubated with 50µL of AMC substrate (10 mM H-Gly-Pro-AMC HBr, Bachem, I-1225), for a final volume of 100µL in a black 96-well plate for 20 minutes. Fluorescence was read at 450nm, and DPP4 activity was calculated in µM/min/mL from a standard curve based on bank-corrected standards (AMC, Bachem, Q-1025). Tissue DPP4 activity was normalized to the total protein concentration in the sample.

2.9 Mouse DPP4 ELISA

DPP4 protein was measured using a colorimetric sandwich DPPIV/CD26 Duoset ELISA kit (R&D Systems, AF954) following manufacturer instructions. Plasma samples were diluted 1/100, BMDM samples were diluted 1/10, and whole tissue lysate was diluted from 1/10-1/100.

2.10 BMDM Protein Isolation

To isolate protein from BMDMs, the cells were washed with filter-sterilized 1X PBS and treated with RIPA buffer (20mM Tris-HCl pH 8.0 (60.57g Tris-HCl (Fisher, BP120-500, 150mM NaCl, 0.1% SDS, 1% deoxycholic acid, 1% triton X-100, in double-distilled H_2O) supplemented with Halt™ Protease Inhibitor Cocktail

(ThermoScientific, 78430) for DPP4 substrate analysis, or homogenization buffer (50mM Tris-HCl, pH 8, 1mM EDTA, 1% glycerol (Sigma, G5516-100ML), 0.0067% Brij-35 (Fisher, BP345-500)) for DPP4 analysis and were incubated at 4°C for 30 minutes to induce chemical lysis. Cells underwent physical lysis using a syringe plunger, and the protein lysate was collected and centrifuged at 21130xg for 20 minutes. The supernatant was collected and stored at -80°C if not used immediately.

2.11 BMDM RNA Isolation, Reverse Transcription and Transcript expression

To isolate RNA from BMDMs, the cells were washed with filter-sterilized 1X PBS, treated with 1mL TriZol reagent (Invitrogen, 15596026) per well, and mixed by pipetting. The solution was transferred and incubated for 5 minutes at room temperature to lyse the cells, 200µL/1mL of TriZol of chloroform (Fisher Scientific, C298-4) was added to each sample and mixed vigorously for 15 seconds and incubated at room temperature for 10 minutes. Samples were then centrifuged at 12000xg for 15 minutes at 4°C, the aqueous phase was aliquoted into a clean tube, 500µL/1mL of TriZol of cold isopropanol (Fisher bioreagents, CAS 67-63-0) was added with 1µL of glycogen (Roche, 10901393001), and incubated at -80°C overnight. The next day, samples were thawed and centrifuged at 12000xg for 10 minutes at 4°C, the supernatant was discarded, and 1mL of 75% ethanol (Comercial Alcohols, P006EAAN) was added, centrifuged at 7500xg for 5 minutes, the supernatant was removed, and repeated once more. Then, the pellet was dried and resuspended in RNase-free water (Thermo Scientific, 10977015) and stored at -80°C. The RNA was thawed and reverse transcribed using a High-Capacity cDNA Reverse Transcription Kit (Fisher Scientific, 43-688-14). cDNA was quantified via RT-qPCR using the ΔΔCt method using Applied Biosystems TaqMan Gene Expression Master Mix (4369016).

BMDM expression was normalized to the geometric mean of *Actb*, *Hprt*, *Stx5a*, and *Hmbs,* in order to minimize the variability of results caused by housekeeping transcript expression.

2.12 Blood Cell Analysis

Circulating blood cell components in samples collected from cardiac puncture or the tail vein (15-20μL) were analyzed using the Element HT5. The number and percent of red blood cells, platelets, lymphocytes, monocytes, neutrophils, eosinophils, and basophils were determined.

2.13 Identification of EPDR1 as a novel DPP4 substrate

The identification of DPP4 substrates has been hindered due to the lack of sensitivity of assays to detect cleavage of a dipeptide from the N-termini of proteins. In collaboration with Dr. Shen Zhang, our lab has identified novel *in vivo* substrates via proteomics screening analysis: hydrophobic tagging-assisted N-terminal enrichment (HYTANE)(188). Wild-type mice were treated with 90mg/kg of streptozotocin (STZ) to induce diabetes, fed a high-fat diet, then mice were randomized into saline-injected mice, or mice treated with 18mg/kg DPP4 inhibitor (DPP4i) MK-0626 ((2S,3S)-1-(3,3-difluropyrrolidin-1-yl)-4-(dimethylamino)-1,4-dioxo-3-(4-[1,2,4]triazolo[1,5-A]pyridin-6-ylphenyl)butan-2-aminium chloride) mixed in their diet, and finally the mice underwent transverse aortic arch banding to induce pressure-overload heart failure, as described previously(191). The plasma of these mice was isolated, DPP4 substrates were isolated via HYTANE, and cleavage was identified via liquid chromatography with tandem mass spectrometry (Figure 5). Following the identification of peptides, validation of DPP4 cleaves was performed via incubation of

the peptide with or without DPP4, followed by ultra-performance liquid chromatography-mass spectrometry.

2.14 Cold Exposure

To further characterize if EPDR1 is regulated by DPP4, Wild-type and *Dpp4*$^{-/-}$, were acclimatized to new cages at room temperature in the cold temperature chamber overnight, followed by 16°C for at least 24 hours, followed by 6°C for 14 weeks. Interscapular brown adipose tissue (iBAT), subcutaneous white adipose tissue (sWAT), perigonadal white adipose tissue (pWAT), liver, and bone marrow were isolated for transcript expression and plasma was isolated for EPDR1 protein, DPP4 protein and activity. At the 2-week timepoint, wild-type and *Dpp4*$^{-/-}$ mice underwent an oral glucose tolerance test. At the 6-week time point, an oil gavage lipid tolerance test was performed, and body composition was quantified using echo MRI.

2.15 Tissue RNA Isolation

To isolate RNA from tissues, they were treated with 1mL TriZol reagent (Invitrogen, 15596026) in microcentrifuge tubes with 2.0mm zirconium oxide beads (FroggaBio, ZROB20) and homogenized at 30hz for 10 minutes at 4°C for tissue homogenization. To isolate RNA from preserved bone marrow, it was centrifuged at 1300xg for 5 minutes, and the pellet was used as described without zirconium oxide beads. The solution was incubated for 5 minutes at room temperature to lyse the cells, 200µL/1mL of TriZol of chloroform was added to each sample, mixed vigorously for 15 seconds, and incubated at room temperature for 10 minutes. Samples were then centrifuged at 12000xg for 15 minutes at 4°C, the aqueous phase was aliquoted into a clean tube, 500µL/1mL of TriZol of cold isopropanol was added and incubated at -80°C overnight. The next day, samples were thawed and centrifuged at 12000xg for

10 minutes at 4°C, the supernatant was discarded, and 1mL of 75% ethanol was added, centrifuged at 7500xg for 5 minutes, the supernatant was removed, and repeated once more. Then, the pellet was dried, resuspended in RNase-free water, and stored at -80°C.

2.16 Reverse Transcription and Transcript expression

The RNA was reverse transcribed using a High-Capacity cDNA Reverse Transcription Kit (Fisher Scientific 43-688-14). cDNA was quantified via RT-qPCR (QuantStudio 5) using the ΔΔCt method, or the standard curve method, using Applied Biosystems TaqMan Gene Expression Master Mix (4369016).

2.17 Oral Glucose Tolerance Tests

Male and female Control and *Epdr1*$^{-/-}$ mice were fasted for 5 hours and gavaged with 2g/kg D-Glucose, and tail snip blood was collected at baseline and 15 minutes while glucose was measured using a glucometer (StatStrip Xpress) at baseline, 15, 30, 45, 60, 90, 120 minutes.

2.18 Weight and Body Composition

Fat, lean, and total water mass were determined in awake mice by EchoMRI (EchoMRI-100 machine, Echo Medical Systems, Houston, TX, USA).

2.19 Mouse EPDR1 ELISA

Circulating and tissue EPDR1 was quantified in mice using the Mouse Mammalian ependymin-related protein 1 ELISA kit (Abbexa, abx522131) following manufacturer instructions.

2.20 Aortic Sinus Immunofluorescence Microscopy

Slides of aortic sinuses from *apoe*$^{-/-}$ mice fed a high-fat diet for 26 weeks were fixed with 10% formalin for 10 minutes at room temperature and washed with PBS.

Then, heat-induced epitope retrieval was performed with sodium citrate buffer (10mM, pH 6, with 0.05% Tween-20) for 2 minutes in a microwave, followed by washes with double distilled water and PBS. The slides were permeabilized with 0.2% triton X-100 in PBS, washed with PBS, blocked with 10% donkey serum in sterile PBS and incubated with the primary antibody diluted in 1% donkey serum sterile PBS at 4°C overnight in a low light exposure humidity chamber. The following day, the slides were washed with PBS and incubated with the secondary antibody in 1% donkey serum with sterile PBS for 1 hour at room temperature in a dark humidity chamber, washed with PBS, stained with DAPI (Thermo Fisher Scientific 62248, 1:2,000) at room temperature for 5 minutes, washed with PBS, and mounted with anti-fade mounting medium (Abcam, ab104135). The staining of interest included DPP4, EPDR1, Galectin 3 (MAC2) macrophages, and arginase-1 (ARG-1) for anti-inflammatory macrophages (Table 2). A Zeiss AxioImage Z1 epifluorescence microscopy with the 20X objective was used to image the aortic sinuses and analyzed using the Zeiss Zen Blue software.

Table 2. Primary and secondary antibodies used for atherosclerotic lesion staining of *apoe*$^{-/-}$ mice.

Antibody Target	Vendor	Cat #	Tested Dilution	Source	Excitation	Excitation
Mac2	Cedarlane	CL8942AP	1:500	Monoclonal Rat, clone M3/38 IgG2a		
Arginase-1	Millipore	abS535	1:50	Chicken polyclonal IgY		
DPP4	R&D Systems	AF954	1:50	Polyclonal Goat IgG		
Anti-EPDR1	Abcam	ab197932	1:50	Polyclonal Rabbit IgG		
Donkey anti-Rat IgG (H+L) Highly Cross-Adsorbed Secondary Antibody, Alexa Fluor Plus 647	Thermo Scientific	A48272	1:100		658	675
Goat anti-Chicken IgY (H+L) Cross-Adsorbed Secondary Antibody, Alexa Fluor Plus 488	Thermo Scientific	A32931	1:100		493	518
Donkey anti-Rabbit IgG (H+L) Highly Cross-Adsorbed Secondary Antibody, Alexa Fluor Plus 555	Thermo Scientific	A32794	1:100		558	572
Donkey anti-Goat IgG (H+L) Highly Cross-Adsorbed Secondary Antibody, Alexa Fluor Plus 594	Thermo Scientific	A32758	1:100		590	618

2.21 Patient Sample Protein and Transcript expression Analysis

To evaluate the *in vivo* significance of EPDR1 and DPP4, participants recruited from 2015 to 2022 from the University of Ottawa Heart Institute Biobank Facility (OHSN-REB Protocol #: 20220419-01H, Study Title: Linking of Metabolic and Cardiovascular Disease) were chosen based on patients with high-risk factors for cardiovascular diseases (coronary artery disease (CAD) group) and a control group. The CAD patients were chosen based on the presence of coronary artery disease, myocardial infarction, coronary artery bypass graph, percutaneous coronary intervention, congestive heart failure, cardiac murmur, atrial fibrillation, valvular diseases, aortic diseases, hypertension, dyslipidemia, diabetes mellitus, obstructive sleep apnea, smoking, or drinks per week. DPP4 protein, DPP4 activity, and EPDR1 protein were quantified in patient plasma.

2.22 Human Circulating DPP4

Circulating DPP4 was measured in the plasma of patients (1/4000) with and without CAD using the U-PLEX Human DPPIV Antibody set (Meso Scale Diagnostics, K151D9K) following the U-PLEX Biomarker Group 3 manufacturers instructions.

2.23 Human Circulating EPDR1

Circulating EPDR1 was quantified in the plasma of patients with and without CAD using a Human Mammalian Ependymin Related 1 ELISA kit (, MBS9316185) following manufacturer instructions.

2.24 Statistical Analysis

All data were graphed, and statistical analyses were performed on GraphPad Prism (version 10.2.0). Data are expressed at mean ± SEM. 1-way or 2-way ANOVA evaluated statistical differences between groups with Tukey's multiple comparisons

post-hoc test, and between two groups were measured by a 2-tailed or 1-tailed unpaired t-test with Welch correction. Human data analysis was evaluated using linear regression models with no covariates or adjustment covariates.

3. Results

3.1 Low-dose LPS administration increases circulating DPP4 activity without affecting DPP4 protein.

DPP4 upregulation has been identified in metabolic disease states, and DPP4 activity increases after multiple injections of LPS(192). To test the sensitivity of our model we used saline or low-dose LPS (0.3mg/kg) intraperitoneal injection over 24 hours to stimulate inflammation in the mice, then we measured spleen weight (Figure 4A), plasma DPP4 activity (Figure 4B), and plasma DPP4 protein (Figure 4C). A subsequent increase in spleen weight in LPS-treated mice (Figure 4A) confirmed general inflammation and a 45% increase in DPP4 activity (Figure 4B). Interestingly, there was no change in circulating DPP4 protein (Figure 4C). This suggests a role of inflammation in regulating circulating DPP4 activity.

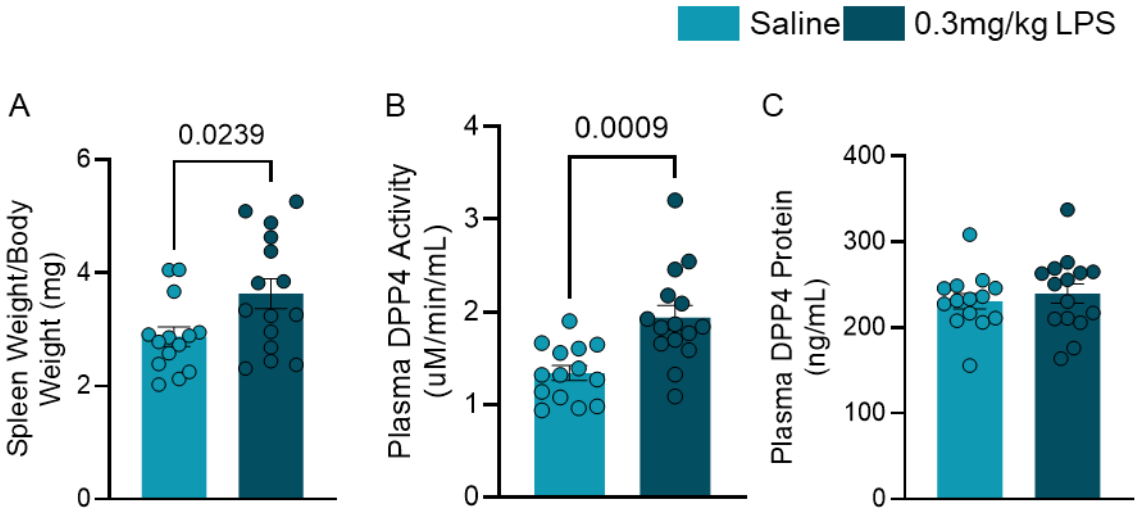

Figure 4. Low-dose LPS injection increases circulating DPP4 activity with no effect on circulating DPP4 protein.

Blood taken via cardiac puncture was taken from wild-type mice, injected intraperitoneally with either saline or 0.3mg/kg LPS. Spleen weight normalized to body weight (A), circulating plasma DPP4 activity (B) and circulating plasma DPP4 protein (D) were measured. Data is shown as mean ± SEM. Significance was determined by an unpaired student t-test with welch correction (A-C). Graphs display males and females, n=14-15.

3.2 *Dpp4* transcript expression increases in pro-inflammatory BMDMs.

To identify the role of *Dpp4* in inflammation in BMDMs, bone marrow was isolated from male and female *Dpp4*$^{+/+}$ and *Dpp4*$^{-/-}$ mice and differentiated into BMDMs. Once differentiated, they were treated with pro-inflammatory cytokine IFNγ and cytotoxin LPS to polarize them to a pro-inflammatory state or anti-inflammatory cytokine IL4 to polarize them into anti-inflammatory BMDMs, then *Dpp4* gene and protein expression were measured. There was a 15.5-fold and 7.5-fold increase in *Dpp4* mRNA expression in pro-inflammatory macrophages in males and females (Figure 5A-B), respectively. However, this did not coincide with DPP4 protein expression (Figure 5C-D). However, DPP4 protein expression is decreased by 40% and 37% in anti-inflammatory BMDMs from males when compared to BMDMs and pro-inflammatory BMDMs, respectively (Figure 5C). While there were no changes in DPP4 protein expression in BMDMs from females (Figure 5D). We identified that *Dpp4* transcript expression is upregulated in pro-inflammatory BMDMs, with a greater fold-increase in BMDMs from males compared to females, and that although this increase in mRNA does not translate to an increase in protein, there is a reduction in DPP4 protein in anti-inflammatory BMDMs from males, identifying sex-specific differences in *ex-vivo* BMDMs.

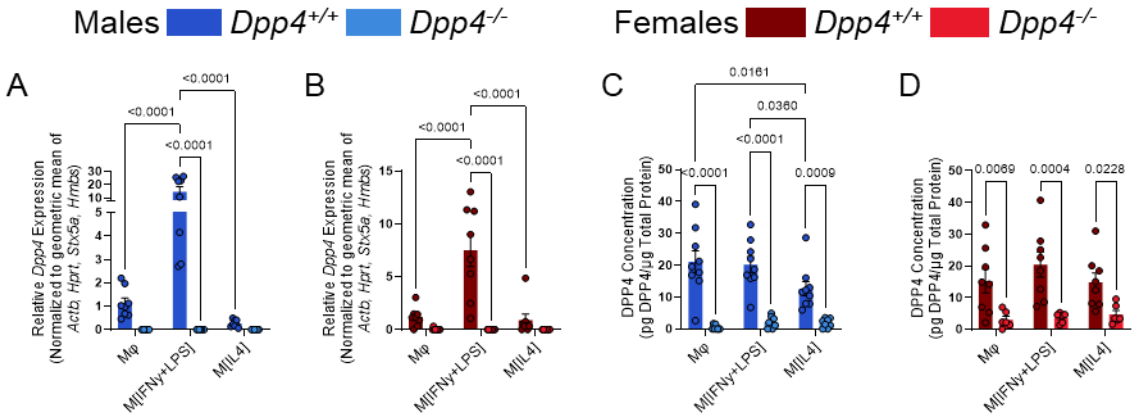

Figure 5. *Dpp4* transcript expression is increased in male and female pro-inflammatory macrophages.

Bone marrow was isolated from male (blue) and female (red) eight- to twelve-week-old *Dpp4*$^{+/+}$ and *Dpp4*$^{-/-}$ mice and differentiated into BMDMs. After 48h of treatment, BMDMs (Mφ), proinflammatory BMDMs (M[IFNγ+LPS]), or anti-inflammatory BMDMs (M[IL4]):

(A, B) *Dpp4* transcript expression was measured using RT-qPCR in male and female BMDMs, n=8-10.

(B) Cellular DPP4 protein was quantified, n=6-10.

Data is shown as mean ± SEM. Significance was determined by an ordinary two-way ANOVA with Tukey's multiple comparisons (A-D).

3.3 Genetic elimination of *Dpp4* does not change pro-inflammatory phenotypes but may increase anti-inflammatory phenotypes in BMDMs.

To further understand the role of *Dpp4* in inflammation in BMDMs, bone marrow from male and female *Dpp4*$^{+/+}$ and *Dpp4*$^{-/-}$ mice were isolated, differentiated into BMDMs, and treated with polarizing signals to induce a pro-inflammatory or anti-inflammatory phenotype as previously stated. We measured transcript expression of pro-inflammatory genes: *Tnf* (Figure 6A-B), *Il1β* (Figure 6C-D), *Il6* (Figure 6E-F), *Mcp1* (Figure 6G-H), and *Nos2* (Figure 6I-J) and anti-inflammatory genes: *Arg1* (Figure 6K-L), *Mrc1* (Figure 6M-N), and *Retnla* (Figure 6O-P). We discovered that *Il6* transcript expression was increased by 55% in *Dpp4*$^{-/-}$ pro-inflammatory BMDMs from males when compared to *Dpp4*$^{+/+}$ pro-inflammatory BMDMs (Figure 6E), but not in BMDMs from females. Additionally, genetic deletion of *Dpp4* did not alter *Tnf, Il1β,* and *Nos2* pro-inflammatory transcript expression in BMDMs from males or females (Figure 6A-D, F-J). Interestingly, genetic deletion of *Dpp4* resulted in the upregulation of *Arg1* and *Mrc1* in BMDMs from both males and females (Figure 6K-N). This increase in anti-inflammatory transcript expression in *Dpp4*$^{-/-}$ BMDMs may suggest that *Dpp4* decreases the polarization of BMDMs to a anti-inflammatory phenotype.

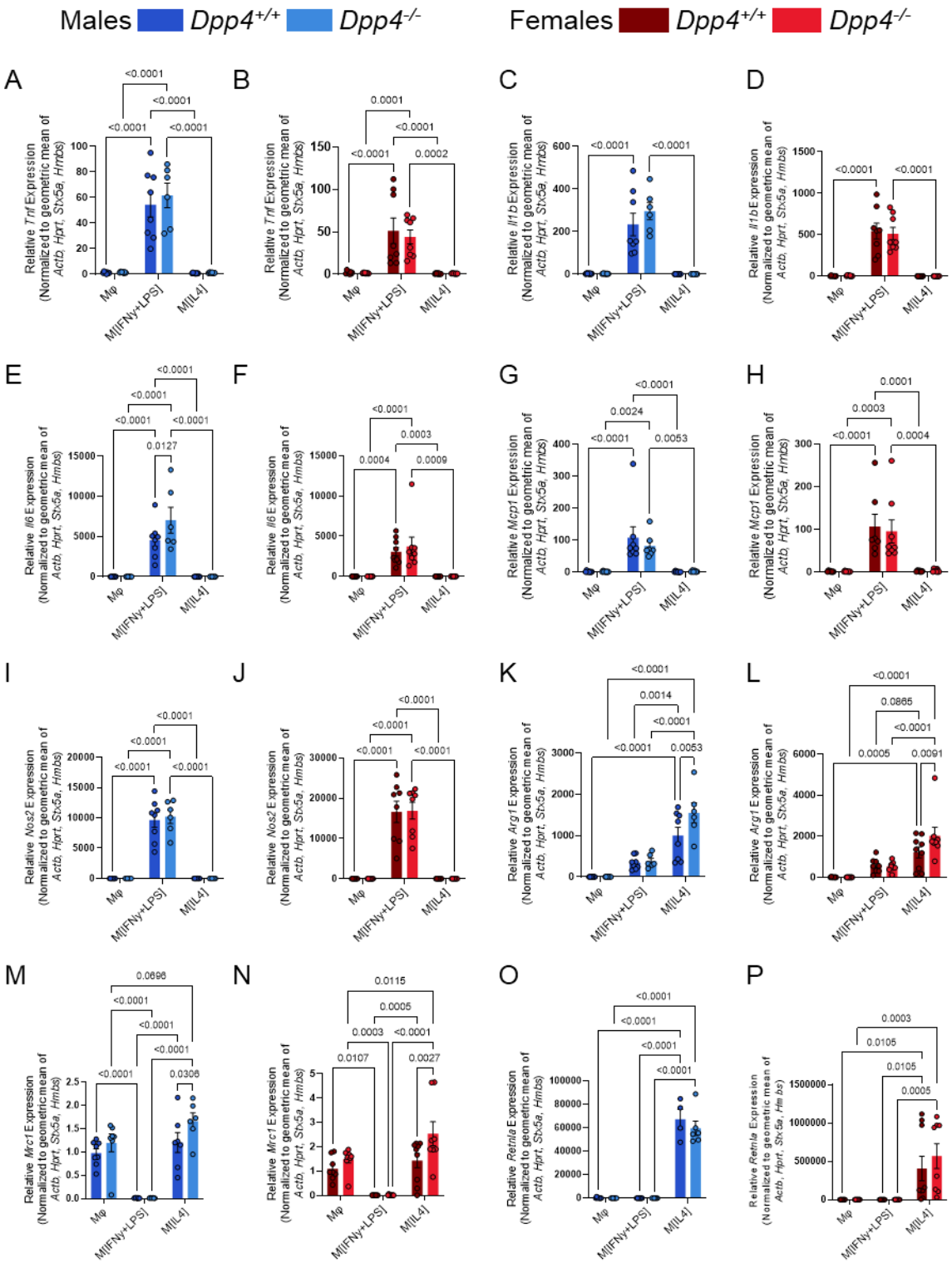
Males Dpp4+/+ Dpp4-/-
Females Dpp4+/+ Dpp4-/-
A
B
C
D
E
F
G
H
I
J
K
L
M
N
O
P
Relative Tnf Expression (Normalized to geometric mean of Actb, Hprt, Stx5a, Hmbs)
Relative Il1b Expression (Normalized to geometric mean of Actb, Hprt, Stx5a, Hmbs)
Relative Il6 Expression (Normalized to geometric mean of Actb, Hprt, Stx5a, Hmbs)
Relative Mcp1 Expression (Normalized to geometric mean of Actb, Hprt, Stx5a, Hmbs)
Relative Nos2 Expression (Normalized to geometric mean of Actb, Hprt, Stx5a, Hmbs)
Relative Arg1 Expression (Normalized to geometric mean of Actb, Hprt, Stx5a, Hmbs)
Relative Mrc1 Expression (Normalized to geometric mean of Actb, Hprt, Stx5a, Hmbs)
Relative Retnla Expression (Normalized to geometric mean of Actb, Hprt, Stx5a, Hmbs)
Mφ
M[IFNγ+LPS]
M[IL4]

Figure 6. Anti-inflammatory *Dpp4*$^{-/-}$ BMDMs have increased *Mrc1* and *Arg1* expression.

Bone marrow was isolated from male (blue) and female (red) eight- to twelve-week-old *Dpp4*$^{+/+}$ and *Dpp4*$^{-/-}$ mice and differentiated into BMDMs. After 48h of treatment with just treatment media (Mφ), proinflammatory BMDMs (M[IFNγ+LPS]), or anti-inflammatory BMDMs (M[IL4]):

(A-H) Transcript expression was measured using RT-qPCR in male (blue) and female (red) BMDMs, n=8-10.

Data is shown as mean ± SEM. Statistical outliers were excluded based off the ROUT method with a false discovery rate of 1%. Significance was determined by an ordinary two-way ANOVA with Tukey's multiple comparisons (A-G).

3.4 *Dpp4* deletion from mononuclear phagocytes does not alter circulating DPP4.

To identify the role of DPP4 in inflammation, we utilized a tamoxifen-inducible model that selectively deletes the *Dpp4* gene in cells expressing *Cx3cr1* (Figure 7A-C). Then we injected a low-dose of LPS in $Dpp4^{+/+}$, $Dpp4^{-/-}$, and $Dpp4^{Cx3cr1-/-}$ mice and measured circulating monocytes (Figure 8B), DPP4 activity (Figure 8C), circulating DPP4 protein (Figure 8D), lymphocytes (Figure 8E), neutrophils (Figure 8F), eosinophils (Figure 8G), red blood cells (Figure 8H), platelets (Figure 8I), before and after injection. We see a reduction in DPP4 protein in the spleen (Figure 7A), and the bone marrow (Figure 7B), as well as partial genetic deletion in the spleen (Figure 7C). There was a reduction in the proportions of circulating monocytes in $Dpp4^{Cx3cr1-/-}$ mice pre-LPS injection, whereas post-LPS injection showed no significant differences in circulating monocytes compared $Dpp4^{+/+}$, $Dpp4^{-/-}$ (Figure 8B). Consistent we our previous observations (Figure 4B-C), we identified that DPP4 activity increases with LPS injection (Figure 8C), but protein does not (Figure 8D). Circulating lymphocyte proportions were increased in $Dpp4^{Cx3cr1-/-}$ mice pre- and post-LPS injection compared to $Dpp4^{+/+}$, $Dpp4^{-/-}$ mice (Figure 8E), with opposite trends in neutrophils (Figure 8F) and eosinophils (Figure 8G), where there is a decrease in circulating proportions. Circulating pools of DPP4 were not affected in $Dpp4^{Cx3cr1-/-}$ mice, identifying that mononuclear phagocytes are not responsible for supplying DPP4 to the circulating pool in response to LPS. However, we identified a possible role of mononuclear phagocyte *Dpp4* in hematopoiesis.

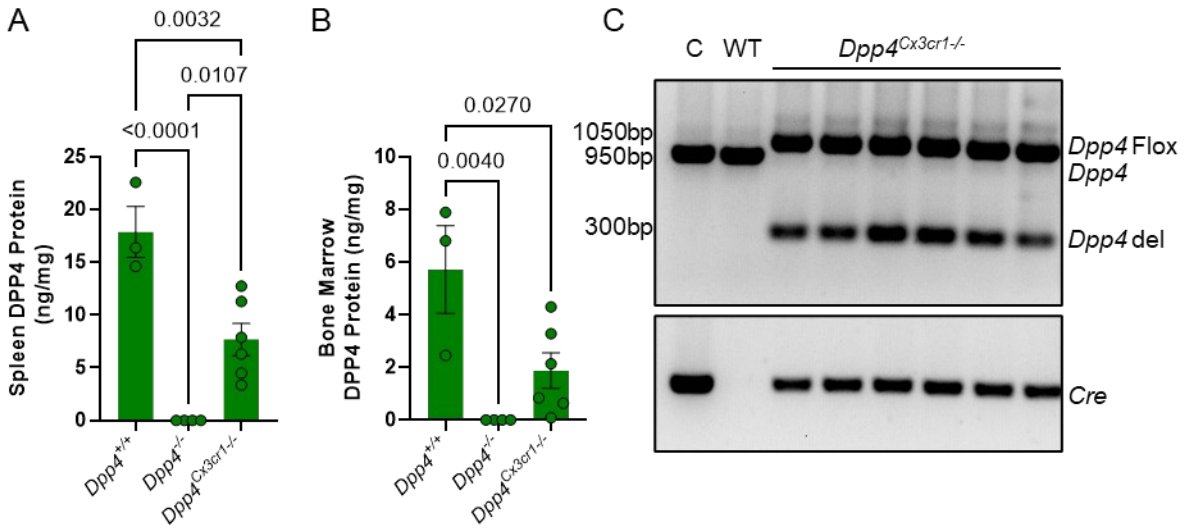

Figure 7. *Dpp4* has been genetically deleted from a subset of cells in *Dpp4*$^{Cx3xr1-/-}$ mice.

DPP4 protein from spleen (A) and bone marrow (B) and spleen PCR amplification of *Dpp4* (C) to validate deletion of *Dpp4*. Data is shown as mean ± SEM. Significance was determined by an ordinary one-way ANOVA with Tukey's multiple comparisons (A-B), n=3-6.

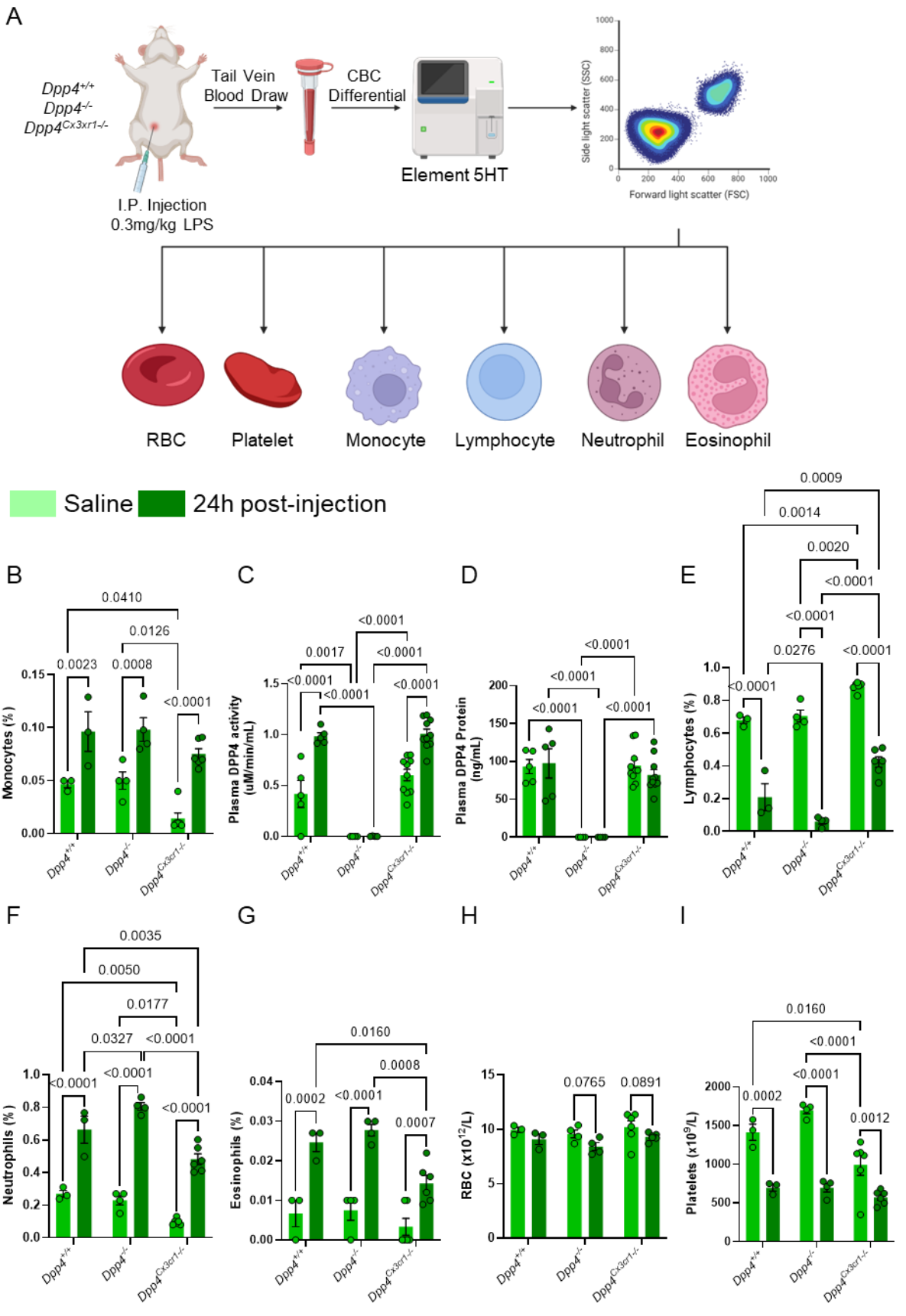
A
Dpp4+/+
Dpp4-/-
Dpp4Cx3xr1-/-
Tail Vein Blood Draw
CBC Differential
Element 5HT
Side light scatter (SSC)
Forward light scatter (FSC)
I.P. Injection 0.3mg/kg LPS
RBC
Platelet
Monocyte
Lymphocyte
Neutrophil
Eosinophil
Saline
24h post-injection
B
Monocytes (%)
C
Plasma DPP4 activity (uM/min/mL)
D
Plasma DPP4 Protein (ng/mL)
E
Lymphocytes (%)
F
Neutrophils (%)
G
Eosinophils (%)
H
RBC (x10^12/L)
I
Platelets (x10^9/L)

Figure 8. *Dpp4*$^{Cx3xr1-/-}$ mice have increased lymphocytes and decreased myeloid populations at baseline and after LPS injection compared to wild-type and *Dpp4*$^{-/-}$ mice.

Tail vein blood was taken from wild-type, *Dpp4*$^{-/-}$, *Dpp4*$^{Cx3xr1-/-}$ mice, before and 24h-post LPS injection (0.3mg/kg). Schematic of complete blood cell differential after LPS injection (A). Tail vein blood was taken from wild-type, *Dpp4*$^{-/-}$, *Dpp4*$^{Cx3xr1-/-}$ mice, before and 24h-post LPS injection. Circulating monocyte (B) DPP4 protein (C), and activity (D) were measured, as well as lymphocytes (E), neutrophils (F), eosinophils (G), red blood cells (RBCs) (H), platelets (I). Data is shown as mean ± SEM. Significance was determined by an ordinary one-way ANOVA with Tukey's multiple comparisons (A-B), or ordinary two-way ANOVA with Tukey's multiple comparisons (D-K), n=3-6.

3.5 DPP4 cleaved sequential dipeptides from EPDR1 in circulation of mice with diabetes and heart failure.

The complexity of DPP4 action is intensified by the vast collection of known substrates, ranging from neuromodulator peptides, chemokines, endocrine hormones, colony-stimulating factors, growth factors, and more. Many DPP4 substrates have been identified *in vitro*, unfortunately, cleavage by DPP4 has not yet been identified as physiologically relevant. Therefore, identifying novel DPP4 substrates is of interest, and identification has been hindered due to the lack of sensitivity of current strategies distinguishing intact and cleaved peptides(139). In collaboration with Dr. Shen Zhang and his laboratory, our lab has identified novel *in vivo* substrates via the proteomics screening analysis HYTANE(188). We identified differentially cleaved peptides in mice with streptozotocin-induced diabetes with transaortic constriction to induce pressure overload heart failure(191). These mice were treated with and without the DPP4i MK-0626, and plasma samples were used for HYTANE (Figure 9A). We identified apolipoprotein C1 (APOC1), growth-hormone binding protein (GHBP), transforming growth factor beta-induced (TGFBI), insulin-like growth factor binding protein 1 (IGFBP1), and namely, EPDR1 (Figure 9B). Interestingly, we found that EPDR1 was cleaved sequentially by DPP4. The identified peptides of interest were validated by incubating samples with and without DPP4 and ultra-performance mass spectrometry (Figure 9C).

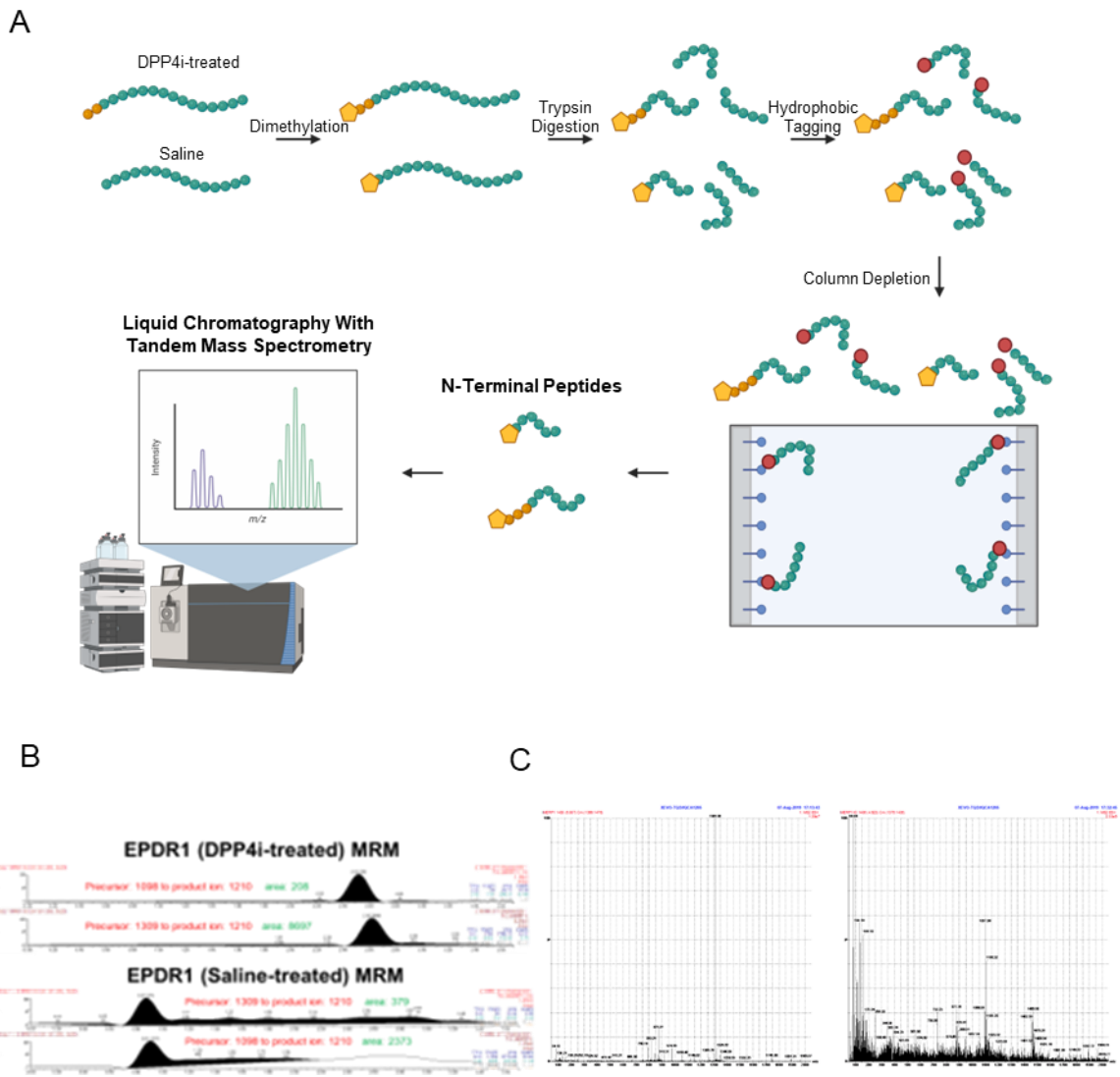

Figure 9. Identification of EPDR1 as a novel DPP4 substrate.

Hydrophobic-tagging assisted N-enrichment (HYTANE) schematic (A) size and abundance of EPDR1 in DPP4 inhibitor (DPP4i) and saline-treated mice (B), EPDR1 substrate validation via incubation of EPDR1 without (left) and with (right) DPP4 protein (C).

3.6 *Epdr1* transcript expression is decreased in anti-inflammatory BMDMs from males.

To understand the role of *Epdr1* in BMDMs, bone marrow was isolated from male and female *Dpp4*$^{+/+}$ and *Dpp4*$^{-/-}$ mice and differentiated into BMDMs. After differentiation, they were treated with pro-inflammatory cytokine IFNγ and cytotoxin LPS to polarize them to a pro-inflammatory phenotype or anti-inflammatory cytokine IL4 to polarize them into anti-inflammatory BMDMs, then *Epdr1* gene and protein expression were measured. Interestingly, *Epdr1* mRNA expression was approximately halved in both pro-inflammatory and anti-inflammatory BMDMs in males, regardless of the presence of *Dpp4* (Figure 10A), while there were no changes in BMDMs from females (Figure 10B). Additionally, this reduction in *Epdr1* transcript expression did not translate to cellular protein reductions (Figure 10C), and interestingly, in male BMDMs, genetic deletion of *Dpp4* increased cellular EPDR1 protein expression by 40%, with no change in polarized BMDMs (Figure 10C). However, there were no changes in protein expression (Figure 10D) in BMDMs from female mice. We found that *Epdr1* transcript expression decreases in polarized BMDMs from males and not females, further suggesting sex-specific phenotypes in the regulation of *Epdr1* in macrophages.

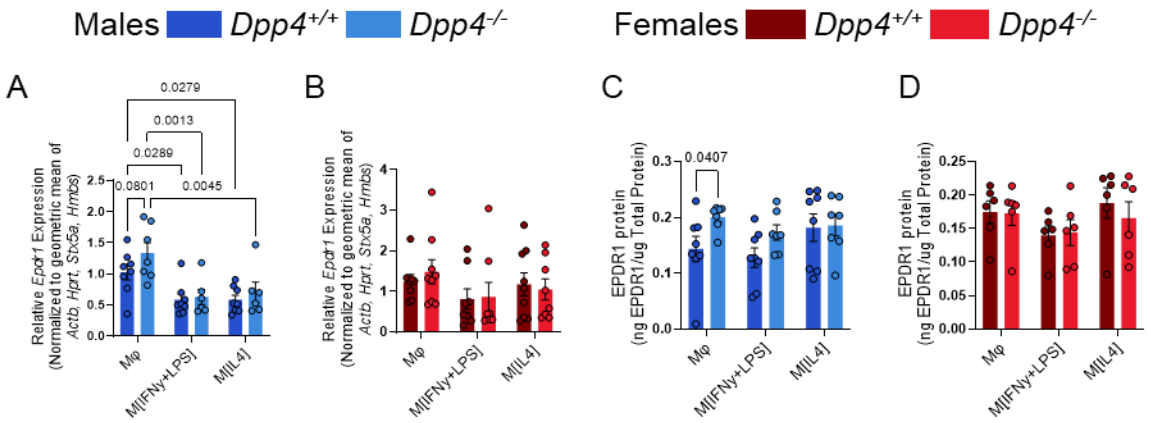

Figure 10. *Epdr1* is downregulated in polarized BMDMs.

Bone marrow was isolated from male (blue) and female (red) eight- to twelve-week-old *Dpp4*$^{+/+}$ and *Dpp4*$^{-/-}$ mice and differentiated into BMDMs. After 48h of treatment, BMDMs (Mφ), proinflammatory BMDMs (M[IFNγ+LPS]), or anti-inflammatory BMDMs (M[IL4]):

(A, B) *Epdr1* transcript expression was measured using RT-qPCR in male and female BMDMs, n=8-10.

(B) Cellular EPDR1 protein was quantified, n=6-10.

Data is shown as mean ± SEM. Significance was determined by an ordinary two-way ANOVA with Tukey's multiple comparisons (A-D).

3.7 Whole-body deletion of *Dpp4* does not affect brown adipose tissue, and glucose metabolism, regardless of cold exposure.

Knowing that EPDR1 is cleaved by DPP4 (Figure 9) and is increased in brown adipose tissue stimulation(182), we wanted to elucidate the role of DPP4 cleavage in EPDR1. We did this by housing *Dpp4*$^{+/+}$ and *Dpp4*$^{-/-}$ mice at either 22°C (warm) or 6°C (cold) for 14 weeks to stimulate the brown adipose tissue. Cold stimulation did not affect interscapular brown adipose tissue (iBAT) mass but did lower subcutaneous and epididymal white adipose tissue mass regardless of genotype (Figure 11A). Additionally, we quantified *Epdr1*, *Ucp1, Pgc1α, and Pparα* transcript expression in iBAT (Figure 11B). Surprisingly, *Epdr1* transcript expression was decreased in both *Dpp4*$^{+/+}$ and *Dpp4*$^{-/-}$ mice cold-housed mice, while *Ucp1* expression was increased. *Pgc1α* expression was increased in cold-housed *Dpp4*$^{-/-}$ mice when compared to warm *Dpp4*$^{-/-}$ mice suggestive of increased BAT activity. *Dpp4*$^{+/+}$, *Dpp4*$^{-/-}$ cold-house mice had a lower baseline fasting plasma triglyceride compared to their warm-housed counterparts (Figure 10D), and *Dpp4*$^{-/-}$ mice housed in the cold have lower total plasma cholesterol compared to both *Dpp4*$^{+/+}$, *Dpp4*$^{-/-}$ warm-housed groups (Figure 10E).

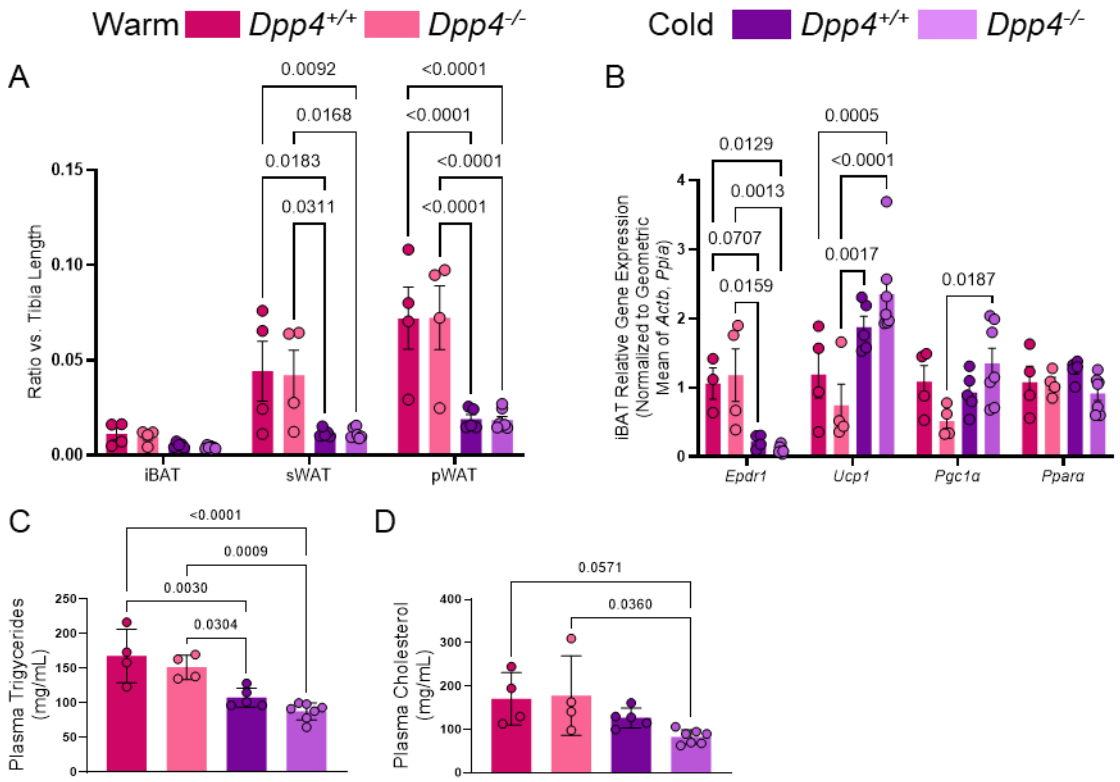

Figure 11. *Epdr1* transcript expression is decreased in cold-housed mice.

Male *Dpp4*$^{+/+}$ and *Dpp4*$^{-/-}$ mice were housed in warm (22°C) and cold (6°C) for 14 weeks. Tissue weight relative to tibia length (A) and transcript expression of *Epdr1* and thermogenic genes were measured in interscapular brown adipose tissue (iBAT), subcutaneous adipose tissue (sWAT), and epididymal adipose tissue (eWAT) (B). Fasting plasma triglycerides (C) and cholesterol (D) were measured. Data is shown as mean ± SEM. Significance was determined by an ordinary two-way (A-B) or one-way (C-F) ANOVA with Tukey's multiple comparisons. * Indicates differences between cold *Dpp4*$^{+/+}$ mice and cold *Dpp4*$^{-/-}$ mice, n=3-7

3.8 DPP4 and EPDR1 are present within atherosclerotic plaque.

To determine if DPP4 and EPDR1 are present within the atherosclerotic plaque, aortic sinuses were serially sectioned from *apoe*$^{-/-}$ mice and stained for macrophages (MAC2), anti-inflammatory macrophages (ARG1), DPP4 and EPDR1 (Figure 12). We identified MAC2 and ARG1 within the lesion, with MAC2 staining surrounding the necrotic core. DPP4 and EPDR1 were also found in the atherosclerotic plaque; however, they surrounded the luminal side of the plaque, likely endothelial cells, or smooth muscle cells (Figure 12). Suggesting that they are present within the plaque microenvironment.

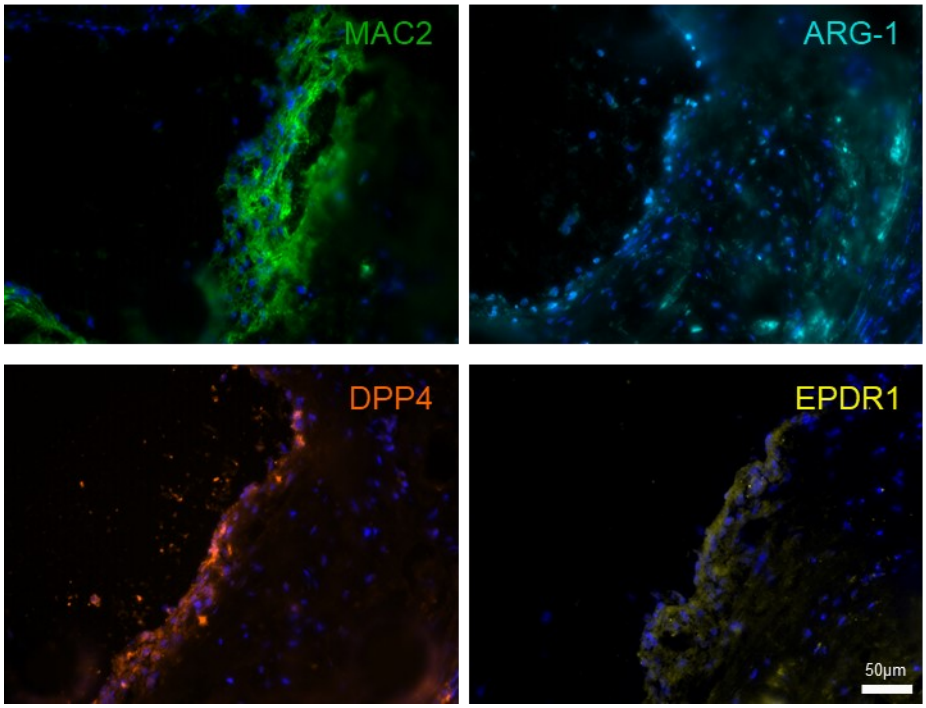

Figure 12. DPP4 and EPDR1 are present within atherosclerotic plaque of *apoe*$^{-/-}$ mice.

Staining of MAC2, ARG1, DPP4, and EPDR1, atherosclerotic lesions of *Apoe*$^{-/-}$ mice aged fed a high-fat diet for 26 weeks by immunohistochemistry. Slides were fixed, permeabilized with Triton X-100, and stained with primary antibodies anti-MAC2 (top left), anti-ARG1 (top right), anti-DPP4 (bottom left), and anti-EPDR1 (bottom right), then treated with a secondary antibody as described under “Methods”.

3.9 Circulating DPP4 is not correlated with lipid or glucose parameters, but circulating EPDR1 protein is correlated with LDLc, and plasma triglycerides in *apoe*$^{-/-}$ mice.

To identify DPP4 as potential molecular markers for dyslipidemia in mice, we measure circulating plasma DPP4 in 16-, 40-, and 79-week-old dyslipidemic *apoe*$^{-/-}$ mice (Table 3). There were no correlations between DPP4 and age (Figure 13A), total cholesterol (Figure 13B), HDL cholesterol (Figure 13C), LDL cholesterol (Figure 13D), plasma triglycerides (Figure 13E) or glucose (Figure 13F). Interestingly, circulating EPDR1 protein increased with age, with a significant increase in the 79-week-old mice (Figure 14A). Additionally, there was a trend between increasing EPDR1 and LDLc (Figure 14D, p=0.0533) and plasma triglycerides (Figure 15E, p=0.0681). These data suggest a developing landscape as the mice age, where EPDR1 may change over time while dyslipidemia progresses.

Table 3. Characteristics of *apoe*$^{-/-}$ mice.

Clinical chemistry of a*poe*$^{-/-}$ mice was measured, total cholesterol, HDL cholesterol, Triglycerides, LDL cholesterol, and plasma glucose were measured in 16-, 40-, and 79-week-old mice.

	Age (Weeks)			
	16	**40**	**79**	**All**
Total Cholesterol (mmol/L)	7.47 ± 0.58	9.97 ± 1.28	7.98 ± 0.97	8.29 ± 0.53
HDLc (mmol/L)	0.55 ± 0.06	0.63 ± 0.06	0.52 ± 0.06	0.57 ± 0.04
Triglycerides (mmol/L)	1.06 ± 0.08	1.26 ± 0.14	1.03 ± 0.12	1.11 ± 0.06
LDLc (mmol/L)	1.02 ± 0.06	1.15 ± 0.10	1.08 ± 0.15	1.07 ± 0.05
Plasma Glucose (mmol/L)	8.88 ± 0.40	9.92 ± 0.30	9.35 ± 0.62	9.28 ± 0.26

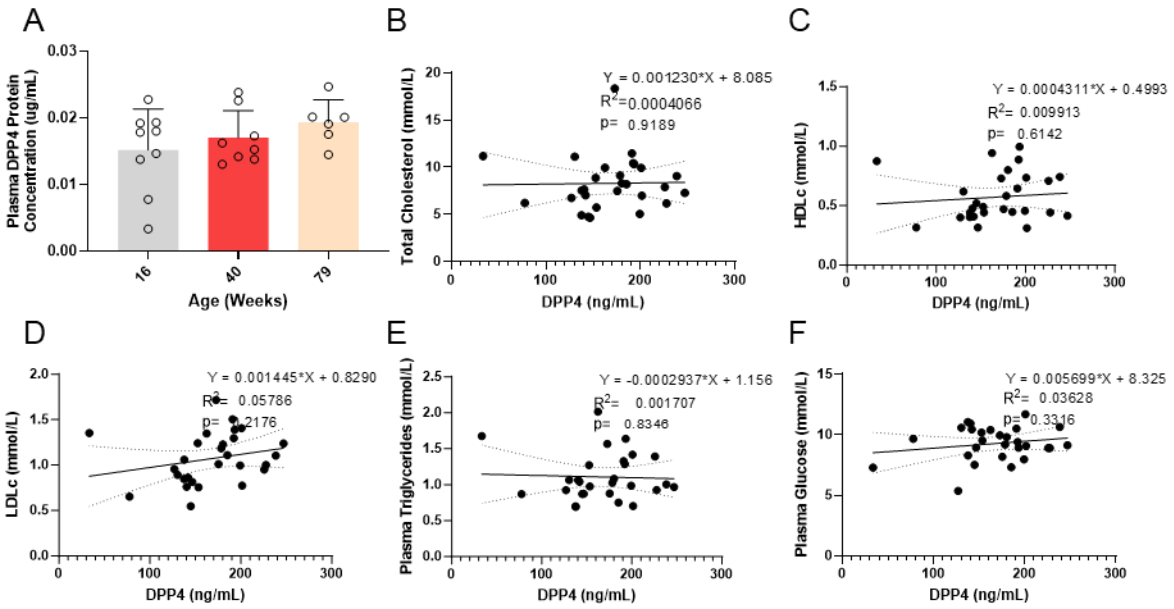

Figure 13. There are no correlations between circulating DPP4 and lipid and glucose parameters in *apoe*$^{-/-}$ mice.

Circulating DPP4, total cholesterol, HDLc, plasma triglycerides, LDLc, and glucose were measured in *apoe*$^{-/-}$ mice aged 16, 40, and 79 weeks old. Statistical analyses performed an ordinary one-way ANOVA with Tukey's Multiple comparisons test (A), or a simple linear regression with the 95% confidence band shown (B-F). Graphs display males and females, n=23.

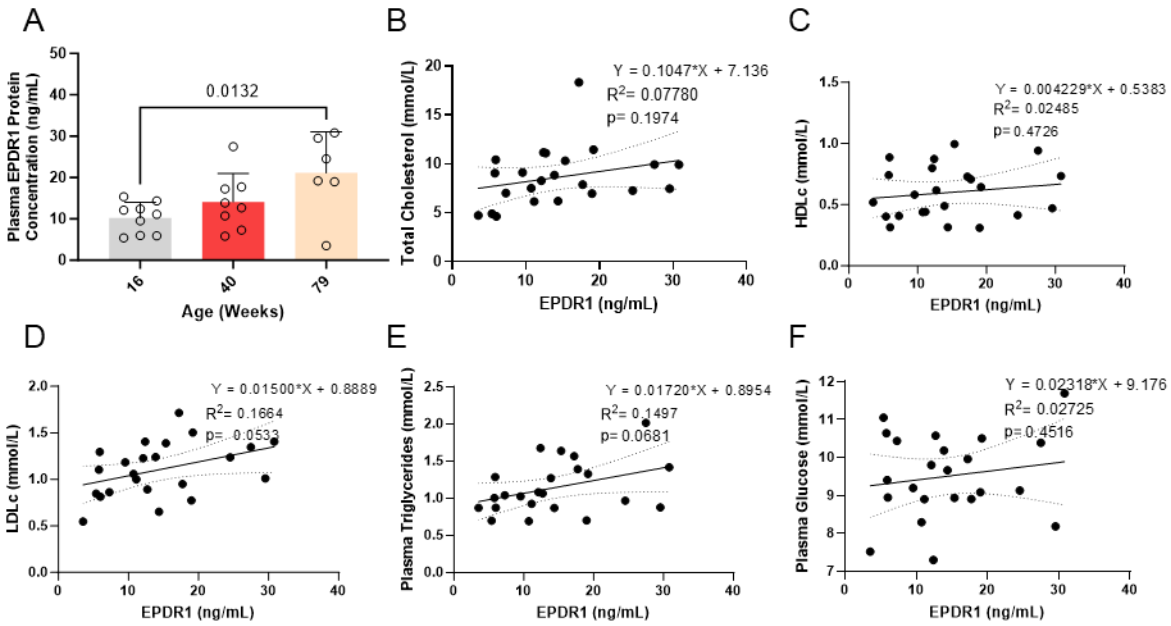

Figure 14. Circulating EPDR1 is increased in 79-week-old mice and trends with LDLc and plasma triglycerides.

Circulating EPDR1, total cholesterol, HDLc, plasma triglycerides, LDLc, and glucose were measured in *apoe*$^{-/-}$ mice aged 16, 40, and 79 weeks old. Statistical analyses performed an ordinary one-way ANOVA with Tukey's Multiple comparisons test (A), or a simple linear regression with the 95% confidence band shown (B-F). Graphs display males and females, n=23.

3.10 Circulating DPP4 protein correlates with total cholesterol, LDLc, and HDLc in patients, while activity only correlates with HDLc, and EPDR1 decreases with age.

DPP4 and EPDR1 have both shown to regulate glucose and lipid metabolism, therefore, we wanted to understand if they increased with different metabolic markers in humans. To do this, male and female plasma samples were isolated from patients who are low risk for cardiovascular disease or patients with confirmed CAD and maintained in the UOHI BioBank (Table 4). We analyzed plasma DPP4 protein, plasma DPP4 activity, and plasma EPDR1 protein and performed linear regressions with BMI, age, Hba1c, plasma triglycerides, total cholesterol, LDL cholesterol, and HDL cholesterol. We found that DPP4 protein was not correlated with BMI (Figure 15A), age (Figure 15B), Hba1c (Figure 15D) or plasma triglycerides (Figure 15E) but was correlated with DPP4 activity (Figure 15C), total cholesterol (Figure 15F). LDLc (Figure 15G), and HDLc (Figure 15H). Similarly, DPP4 activity was correlated with HDLc (Figure 16G) but nothing else (Figure 16A-F). Surprisingly, circulating EPDR1 decreased with age (Figure 17B) but did not correlate with BMI (Figure 17A), DPP4 protein (Figure 17C), DPP4 activity (Figure 17D), Hba1c (Figure 17E), plasma triglycerides (Figure 17F), total cholesterol (Figure 17G), LDLc (Figure 17H), and HDLc (Figure 17I). Contrary to what we saw in the mice, the correlations between circulating DPP4 and lipid parameters suggest it may be a molecular marker in dyslipidemic patients, while EPDR1 is not. However, more work is needed to identify them as biomarkers for metabolic dysregulation in humans.

Table 4. Clinical characteristics of plasma donors used for correlation analysis.

Plasma isolated from male and female patients that are low risk for cardiovascular disease, or patients with confirmed CAD maintained in the UOHI BioBank were used for DPP4 protein, activity and EPDR1 protein analysis. Shown are the clinical characteristics of the patients. Bold numbers in the P-value column indicate statistical significance.

P-values* obtained using unpaired student t-test with welch correction.

		Control Patients (95)		CAD Patients (99)		
		Number ± SEM	%	Number ± SEM	%	P-value*
Male		40	45.45%	76	76.77%	
Female		50	50.51%	23	23.23%	
Age		53.38 ± 1.96		67.05 ± 1.02		1.35E-07
BMI		26.90 ± 0.64		30.85 ± 0.59		1.73E-05
Systolic Blood Pressure (mmHg)		115.16 ± 1.55		124.48 ± 1.56		8.71E-05
Diastolic Blood Pressure (mmHg)		70.10 ± 1.29		73.36 ± 1.06		0.07
Hemoglobin A1C (%)		5.59 ± 0.71		6.56 ± 0.16		5.64E-06
Total Cholesterol (mmol/L)		5.21 ± 0.20		3.76 ± 0.13		6.98E-08
LDLc (mmol/L)		3.06 ± 0.17		1.78 ± 0.12		2.74E-08
HDLc (mmol/L)		1.40 ± 0.08		1.24 ± 0.11		0.25
Triglycerides (mmol/L)		1.73 ± 0.17		2.13 ± 0.21		0.15
DPP4 Protein		584.82 ± 17.40		533.91 ± 19.71		0.05
DPP4 Activity		3.30 ± 0.08		3.01 ± 0.12		0.05
EPDR1 Protein		98.69 ± 12.07		84.97 ± 5.29		0.28
Myocardial Infarct (yes/no)		0	0.0%	55	55.6%	
CABG (yes/no)		0	0.0%	31	31.3%	
PCI (yes/no)		0	0.0%	60	60.6%	
CHF (yes/no)		0	0.0%	11	11.1%	
Cardiomyopathy (yes/no)	**Hypertrophic**	0	0.0%	14	14.1%	
	Dilated	0	0.0%	5	5.1%	
Valvular Disease (yes/no)		0	0.0%	13	13.1%	
Aortic Disease (yes/no)		0	0.0%	6	6.1%	
Hypertension (yes/no)		0	0.0%	94	94.9%	
Dyslipidemia (yes/no)		0	0.0%	98	99.0%	
CVA (yes/no)		1	1.1%	6	6.1%	
TIA (yes/no)		1	1.1%	12	12.1%	
Carotid Artery Disease (yes/no)		0	0.0%	5	5.1%	
PAD (yes/no)		0	0.0%	4	4.0%	
T1DM (yes/no)		0	0.0%	1	1.0%	
T2DM (yes/no)		0	0.0%	35	35.4%	
ACEi (yes/no)		0	0.0%	47	47.5%	
ARB (yes/no)		0	0.0%	23	23.2%	
Beta Blockers (yes/no)		1	1.1%	69	69.7%	
Calcium Channel Blockers (yes/no)		0	0.0%	25	25.3%	
Statins (yes/no)		1	1.1%	92	92.9%	
	Metformin	0	0.0%	28	28.3%	
Hypoglycemic agent (yes/no)	**DPP4i**	0	0.0%	6	6.1%	
	GLP1ra	0	0.0%	2	2.0%	
	Current	87	91.6%	49	49.5%	
Smoking (yes/no)	**Ex-Smoker**	1	1.1%	32	32.3%	
	Never	5	5.3%	17	17.2%	
	Mother	18	18.9%	29	29.3%	
Family History of CAD (yes/no)	**Father**	32	33.7%	49	49.5%	
	Sibling	11	11.6%	31	31.3%	

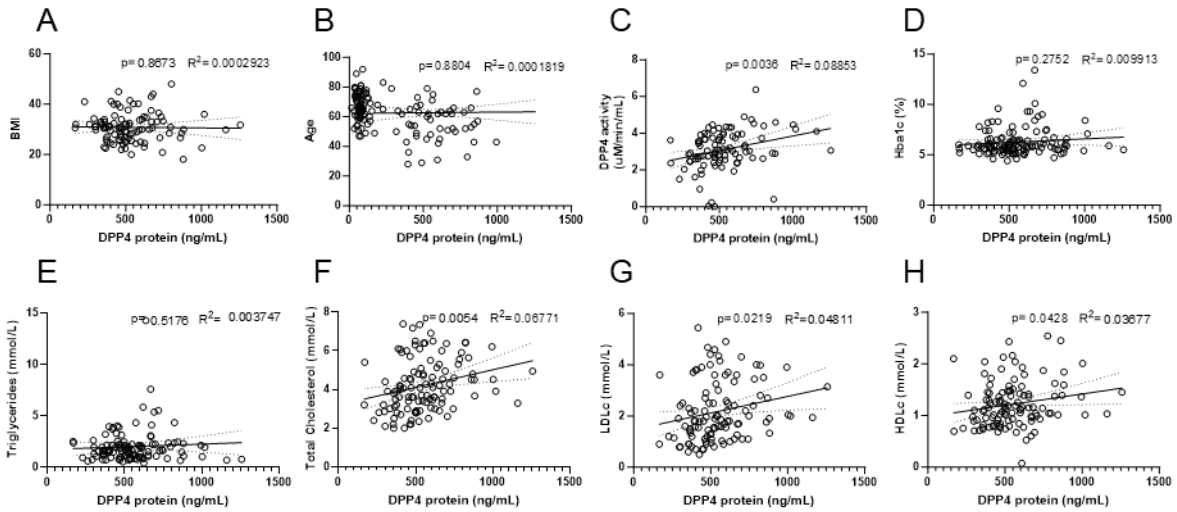

Figure 15. Circulating DPP4 correlates with Hba1c, total cholesterol, LDLc and HDLc.

Plasma DPP4 in patients at low risk for CAD patients with CAD. Circulating DPP4 versus BMI (A) age (B), DPP4 activity (C), Hba1c (D), plasma triglycerides (E), total cholesterol (F), LDL cholesterol (G), HDL cholesterol (H) Statistical analyses performed a simple linear regression with the 95% confidence band shown. Graphs display males and females, N=114-194.

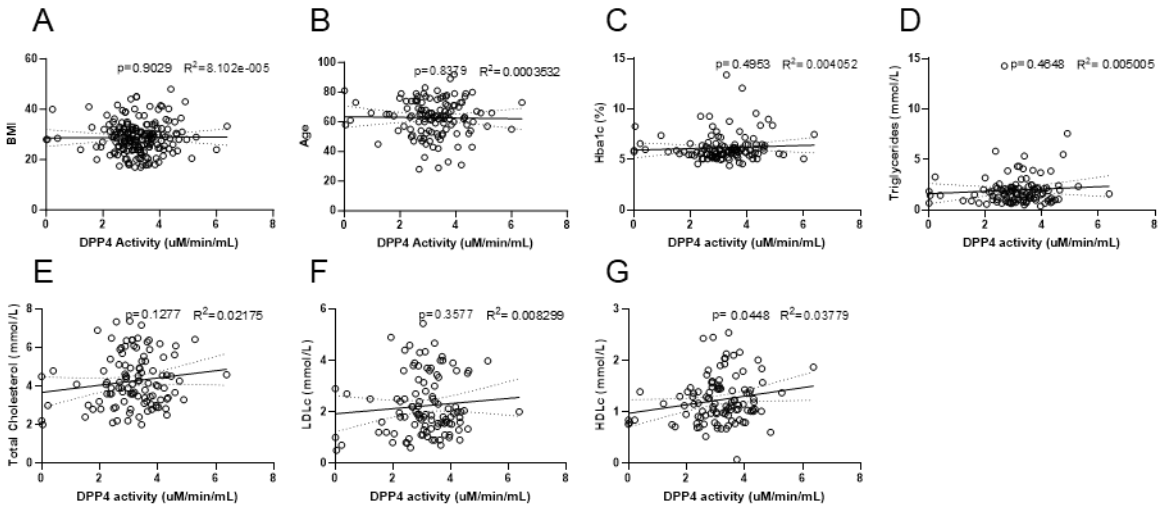

Figure 16. Circulating DPP4 activity increases with HDL.

Plasma DPP4 activity in patients at low risk for CAD patients with CAD. Circulating DPP4 activity versus BMI (A) age (B), Hba1c (C), plasma triglycerides (D), total cholesterol (E), LDL cholesterol (F), HDL cholesterol (G) Statistical analyses performed a simple linear regression with the 95% confidence band shown. Graphs display males and females, N=114-194.

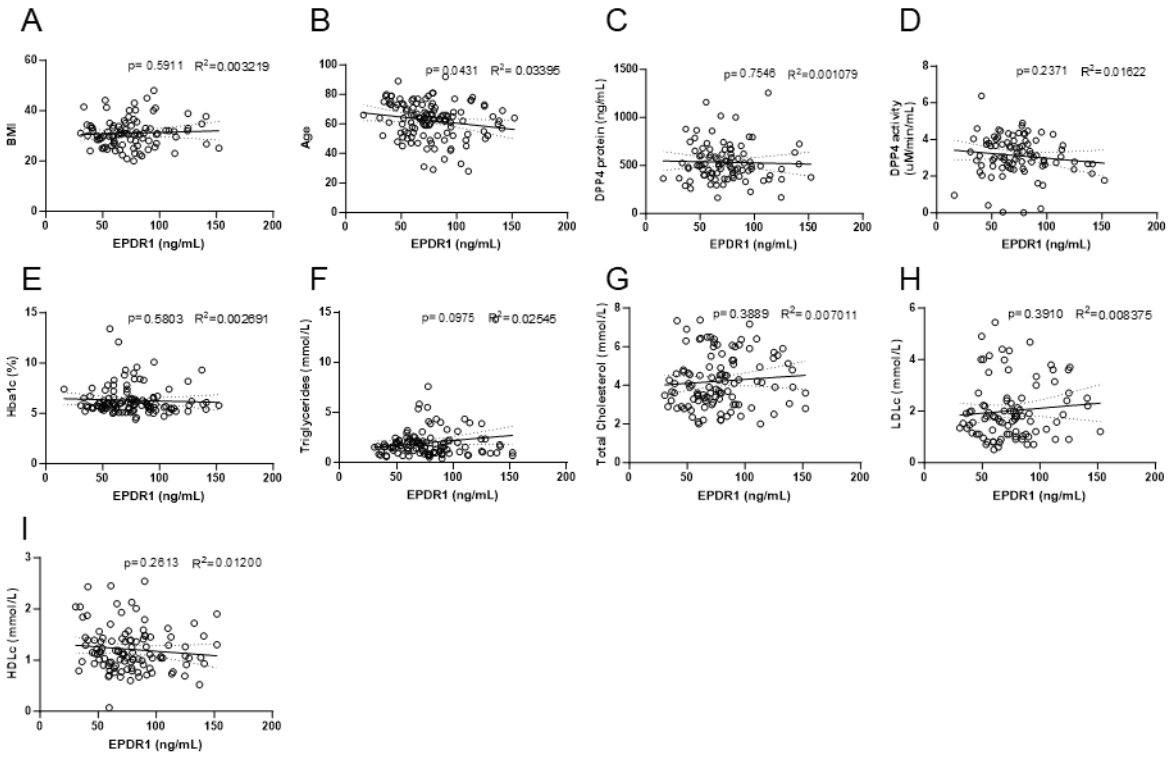

Figure 17. Circulating EPDR1 in decreased in CAD patients and decreases with age.

Plasma EPDR1 in patients at low risk for CAD patients with CAD. Circulating EPDR1 versus BMI (A) age (B), DPP4 Protein (C), DPP4 activity (D), Hba1c (E), plasma triglycerides (F), total cholesterol (G), LDL cholesterol (H), HDL cholesterol (I) Statistical analyses performed a simple linear regression with the 95% confidence band shown. Graphs display males and females, N=114-194.

4. Discussion and Future Directions

4.1 Discussion

4.1.1 DPP4 is regulated by inflammation in circulation in mice and in macrophages.

DPP4 is a serine protease that cleaves dipeptides from the N-terminal of proteins, it is ubiquitously expressed and is shed in circulation(193, 194). Its best-characterized role is the cleavage and regulation of incretin activity, where it inactivates these peptides to decrease insulin secretion, modulating glucose metabolism. It has been shown that the principal site of action of DPP4 inhibitors are vascular endothelial cells, suggesting a significant role of endothelial membrane-bound DPP4 in the regulation of the incretin response(141, 195). However, DPP4 activity seems to be regulated by the tissue that it is shed from, for example, circulating, shed DPP4 that come from hepatocytes and adipose tissue may not regulate the incretin hormones but can contribute to liver and adipose tissue inflammation, hepatocyte-derived DPP4 may be important in regulating inflammation in adipose tissue, identifying a tissue-tissue connection(196). Interestingly, it also seems that there is a responsive regulation of DPP4 protein and its activity in circulation, where the use of DPP4 inhibitors decreases DPP4 enzymatic activity but increases circulating DPP4 protein in mice(140, 196). We show that the rise in DPP4 activity after LPS injection (Figure 4B) does not result in a change in DPP4 protein in circulation (Figure 4C). Previous studies have identified that post-translational modifications can regulate DPP4 activity(197–199). Additionally, LPS-induced inflammation has been shown to cause post-translational modifications in many proteins involved in inflammation(200, 201). Therefore, we hypothesize that either

direct post-translational modifications of DPP4 may regulate its activity because of LPS-induced inflammation or an increase in active shed DPP4 after TLR4-mediated upregulation of membrane-bound DPP4(142) via LPS injection.

Similarly, we observed upregulation of *Dpp4* mRNA expression in both male and female BMDMs stimulated with LPS and IFNγ (Figure 5A-B), with a greater magnitude in BMDMs from males. However, this is not seen at the total cellular protein level, (Figure 5C). This was surprising because it has been shown previously that LPS stimulation increases membrane-bound DPP4 in monocytes, activated macrophages(142) and PBMCs(202). It has been shown that there is constitutive membrane expression of type-II proteins like the transmembrane TNF-α protein(203, 204) upon LPS stimulation, which may mean increased trafficking of DPP4 to the membrane.. After seeing that inflammation can regulate *Dpp4* mRNA in BMDMs, we looked at pro-inflammatory transcript expression, namely *Tnf*, *Il1β*, *Il6*, *Mcp1*, *Nos2* (Figure 6A-J), and saw that it did not change between $Dpp4^{+/+}$ and $Dpp4^{-/-}$ BMDMs; except for *Il6* transcript expression was increased in pro-inflammatory $Dpp4^{-/-}$ compared to $Dpp4^{+/+}$ from male BMDMs. Additionally, we quantified anti-inflammatory transcript expression, such as *Retnla*, *Mrc1*, and *Arg1* (Figure 6K-P). Interestingly, $Dpp4^{-/-}$ BMDMs treated with IL4 from males and females all had increased anti-inflammatory *Arg1*, and *Mrc1* transcript expression (Figure 6J, N), this increase in anti-inflammatory phenotype has been shown in linagliptin-treated and siRNA-mediated knockdown of BMDMs(205). These sex differences could be attributed to a sex-chromosome effect(206) and/or epigenetic differences(207), leading to a changed phenotype, as there is no hormonal input *in vitro*.

Additionally, macrophages from female mice have a greater propensity to favour anti-inflammatory phenotypes in multiple diseased contexts. For example, female mice with bacterial pneumonia have a lower ratio of pro-inflammatory to anti-inflammatory lung macrophages due to an X-linked microRNA, affecting macrophage polarization(208). PBMC-derived M2-like macrophages from women have higher IL4-induced transcript expression signatures(209). Finally, a study looking at macrophages from female mice found enhanced transcriptionally active histone modifications at pro-resolving gene promoters when compared to male mice, and that estrogen supplementation ovariectomized female mice enhanced anti-inflammatory polarization, and the BMDMs from these mice had enhanced IL4-induced pro-resolving transcript expression(210). However, a more in-depth analysis of these sex-specific differences with LPS stimulation is needed.

Seeing the effects of LPS-induced inflammation on DPP4 in circulation and in macrophages, we think that monocyte and macrophage-derived DPP4 is important in the development of inflammation, as DPP4 inhibition has been shown to decrease circulating and hepatic inflammation in LPS-injected mice via the suppression of NFκB(171). So, we generated a tamoxifen-inducible conditional model that deletes the 22nd exon of *Dpp4* in cells expressing transcripts from the *Cx3cr1* promoter, including mononuclear phagocytes, like monocytes, macrophages, and dendritic cells(190). Then we injected *Dpp4*$^{+/+}$, *Dpp4*$^{-/-}$, and *Dpp4*$^{Cx3cr1-/-}$ mice with the same dose of LPS and via tail vein bleed, we measured circulating DPP4 activity (Figure 8C) and protein (Figure 8D), as well as monocyte (Figure 8B), circulating lymphocyte (Figure 8E), neutrophil (Figure 8F), eosinophil (Figure 8G) red blood cell count (Figure

8H), and platelet count (Figure 8I) proportions. Similar to Figure 4A and Figure 4B, plasma DPP4 activity was increased with LPS-induced inflammation (Figure 8C), but protein remained unchanged (Figure 8D). We found no differences in circulating DPP4 activity or protein between *Dpp4*$^{+/+}$ and *Dpp4*$^{Cx3cr1-/-}$ mice before and after LPS injection (Figure 8C-D). This may be because other cells and tissues contribute to the circulating pool of DPP4 in plasma(140, 211) rather than mononuclear phagocytes. LPS-induced inflammation decreased lymphocyte proportions (Figure 8E) while increasing monocyte (Figure 8B), neutrophil (Figure 8F), and eosinophil (Figure 8G) proportions, independent of genotype. This is because LPS stimulates pattern recognition receptors like TLR4 to induce the innate immune response. Monocyte emigration is dependent on its microenvironment, where increased myelopoiesis leads to increased population, but bone marrow mesenchymal stem cells secrete important chemokines like MCP1 to drive extravasation into the blood vessels from the bone marrow(212). Interestingly, we found that the proportions of lymphocytes in the circulation of *Dpp4*$^{Cx3cr1-/-}$ mice were higher before and after LPS injection when compared to *Dpp4*$^{+/+}$ and *Dpp4*$^{-/-}$ mice (Figure 8E). While monocyte proportions were lower before LPS induction but not after (Figure 8B), neutrophil proportions were lower before and after (Figure 8F), and eosinophils were only lower after LPS injection compared to both *Dpp4*$^{+/+}$ and *Dpp4*$^{-/-}$ mice (Figure 4H). This was surprising as *Dpp4*$^{-/-}$ mice had similar trends as *Dpp4*$^{+/+}$ or showed the opposite trends from the *Dpp4*$^{Cx3cr1-/-}$ mice compared to *Dpp4*$^{+/+}$ mice, where lymphocytes were decreased (Figure 8E) and neutrophils were increased (Figure 8F), both only after LPS injection. DPP4 is important in regulating myelopoiesis in the bone marrow as it can regulate the activity of colony-stimulating factors like GM-CSF and G-CSF(168, 169). However,

deletion of *Dpp4* should increase myeloid cell proportions, as seen in the neutrophil proportions in *Dpp4*$^{-/-}$ mice after LPS injections. *Cx3cr1*-expressing cells are important in regulating blood mononuclear phagocyte levels, where deletion will decrease these populations(103, 106). Evidently, DPP4 within these cells has a role in regulating immune cell homeostasis within circulation that cannot be fully elucidated as of yet, however, identifying the role of DPP4 in these cell populations and hematopoiesis and why the phenotype is changed from whole-body deletions should be further studied.

4.1.2 Genetic deletion of *Dpp4* does not alter EDPR1 levels or lipid metabolism in cold-housed mice.

Although EPDR1 has been thoroughly evaluated in terms of its role in cancer development(175–177, 213–215), it also has an emerging role as a batokine(152) and regulating glucose and lipid metabolism. EPDR1 is increased in metabolic diseases like type 2 diabetes(184) and coronary artery disease(183). These studies identified a mechanistic role of EPDR1 in regulating glucose (183, 184) and lipid metabolism(183). It has also been shown to be differentially expressed in brown adipose tissue compared to white adipose tissue(182). Our lab identified that DPP4 can cleave two dipeptides off the N-terminal of EPDR1 (Figure 9), and knowing the roles of DPP4 in the regulation of BAT metabolism, where after high-fat diet feeding, DPP4 deletion decreased adiposity of BAT, resembling more metabolically active tissue, and decreased *Ucp1*, an essential protein in BAT activity(152). For these reasons, we were interested in the roles of EPDR1 in metabolic regulation. Knowing that EPDR1 is differentially expressed in BAT(182), we used cold temperatures to stimulate BAT activity in *Dpp4*$^{+/+}$ and *Dpp4*$^{-/-}$ mice (Figure 11). To validate the model,

we weighed interscapular BAT, subcutaneous WAT, epidydimal WAT (Figure 11A), and transcript expression of thermogenic genes in iBAT (Figure 11B). We found no increase in iBAT in cold-housed mice compared to warm-housed mice, however, both forms of WAT were decreased (Figure 11A), confirming that cold-stimulation affected body composition. Surprisingly, *Epdr1* transcript expression was reduced in cold-housed mice, regardless of genotype. Additionally, we saw an increase in *Ucp1* transcript expression in cold-housed mice and *Pgc1α* in cold-housed *Dpp4*$^{-/-}$ mice versus warm-housed *Dpp4*$^{-/-}$ mice, and no differences in *Pparα* (Figure 11B). However, mice were fed a standard-lab diet, and the warm-housed mice were kept at 23°C, which is still a mild cold stimulus for mice, as thermoneutrality is around 29°C(216, 217). For these reasons, we did not see BAT dysfunction as seen previously(152). Additionally, the control mice's BAT was active, accounting for the lack of upregulation of the thermogenic genes(217).

Not surprisingly, we found significant differences in plasma triglycerides at baseline, where cold-house mice had lower levels of circulating triglycerides, independent of genotype (Figure 11C). Total plasma cholesterol was also lower in cold *Dpp4*$^{-/-}$ mice when compared to warm-housed mice, but not their cold *Dpp4*$^{+/+}$ counterpart (Figure 11D). Although there is a lack of differences in metabolic regulation, possibly due to housing temperatures(217), we can identify increased cold stimulus in the cold mice as baseline triglycerides were lower (Figure 11C). More work is needed to uncover the role of EPDR1 cleavage by DPP4 in lipid metabolism.

4.1.3 Circulating DPP4 and EPDR1 are not strong signatures of dyslipidemia in humans.

DPP4 has been implicated in many metabolic diseases, where the major consensus is that increased levels are associated with worse metabolic parameters, such as obesity, insulin resistance, and dyslipidemia(157, 170, 202, 218–220). This is why it is promising as a signature of different metabolic diseases. On the other hand, EPDR1 has been identified as a biomarker in various cancers(175, 176, 214), it is elevated in brown adipose tissue(182), in patients with CAD(183), and in patients with type 2 diabetes mellitus(184). We used an *apoe*$^{-/-}$ model fed a standard lab diet to simulate dyslipidemia and metabolic dysfunction (Table 2, Figures 13-14). Apolipoprotein E is a major regulator of plasma lipids, regulating the interaction of lipoproteins with different lipoprotein receptors. With the lack of APOE, there is decreased clearance of lipoproteins like very low-density lipoproteins (VLDL) (221, 222), causing hypercholesteremia and spontaneously forming atherosclerotic lesions(221), which is why it is a common model for atherosclerosis studies. Similar to what is seen in the literature, our fasted model developed dyslipidemia, where total cholesterol and LDL cholesterol were elevated, while there was a decrease in HDL cholesterol. Plasma triglycerides were unaffected, and blood glucose was elevated (Table 4), suggesting metabolic dysfunction like insulin resistance.

To further explore the link between DPP4, EPDR1 and metabolic disease, DPP4 protein and activity and EPDR1 protein were measured and analyzed alongside metabolic parameters. Patient samples were taken from the UOHI Biobank, and we separated them into control patients and patients with confirmed CAD. We found that

CAD patients were mostly men, much older on average, and had elevated Hba1c and triglycerides. Most of these patients were dyslipidemic, however, at the time of blood draw, 93% were taking statins, and 28% were taking metformin, so they were normocholesteremic, and had lower levels of total cholesterol, LDLc, and plasma triglycerides, than the control group. Additionally, 92% of control patients were current smokers, with only 5% having never smoked. Smoking is a major risk factor for coronary artery disease(223), and maybe a reason that they have high total cholesterol(224) on average (Table 4). Additionally, with the available dataset statistical adjustment for covariates sex and age was not made possible due to the limited information about age. The small dataset would lead to overcorrected residuals that are not physiologically representative.

Previous meta-analyses and trials have shown that DPP4 inhibition can decrease total cholesterol and triglycerides in humans(151, 225). There is also an increase in DPP4 activity in the circulation of patients with CAD(170) and obese patients(142). Similarly, in mice there is a decrease in plasma total cholesterol, triglycerides, LDLc, and VLDL, which is thought to be mediated through the regulation of SREBP in *Ldlr*$^{-/-}$ mice(226). DPP4 deletion can result in improved glucose control through the increased actions of the incretin hormones and glucose-stimulated insulin secretion(153), with no effects on plasma cholesterol, HDLc, LDLc, and plasma triglycerides in standard lab diet-fed mice, but a decrease in plasma triglycerides in the high-fat high-cholesterol diet-fed mice(227). With the effects of DPP4 inhibition and deletion on glucose and lipid metabolism, we wanted to identify changes in DPP4 protein and activity in an *apoe*$^{-/-}$ mouse model and in patients with confirmed CAD or

risk factors for CAD. Interestingly, patients with confirmed CAD had lower levels of circulating DPP4 protein and activity when compared to the control group (Table 4). Also, contrary to what has been shown(157), we did not see an increase in circulating DPP4 protein in aged mice (Figure 13A), or aged patients (Figure 15B), or a correlation with increased BMI (Figure 15B). We did not see any correlations in mice, however in patients, circulating total cholesterol (Figure 15F) and LDLc (Figure 15G) correlated with circulating DPP4 protein, while HDLc correlated with both DPP4 protein (Figure 15H) and activity (Figure 16G). Although we saw correlations in patients with DPP4 and cholesterol, the *apoe*$^{-/-}$ model affects cholesterol metabolism(221, 222) independently of circulating DPP4 protein and activity. Further work is needed to identify the role of DPP4 in dyslipidemia in mice and humans.

EPDR1 studies have identified increased *Epdr1* expression in adipose tissue of CAD patients(183) and increased *Epdr1* expression in islets of overweight/obese individuals and patients with type 2 diabetes(184). Although these studies identified these increases in metabolic disease, hyperphysiological levels *in vitro* and *in vivo* were beneficial(183, 184). The treatment of insulin-producing pancreatic beta-cells with EPDR1 protein increases insulin secretion(184), which is beneficial for glucose metabolism. Additionally, EPDR1 injection in mice decreases non-HDL cholesterol and plasma glucose(183), while higher expression of *Epdr1* in islets of patients with type 2 diabetes correlates with improved Hba1c(184). Using the *apoe*$^{-/-}$ model and patient samples, we analyzed EPDR1 in circulation and found that it was increased in the aged mice (Figure 14A) and may correlated with LDLc (Figure 14D) and plasma triglycerides (Figure 14E). Interestingly, circulating EPDR1 decreases as age

increases (Figure 16A), the opposite of what we saw in the mice. EPDR1 is elevated in diseased states(183, 184) and the *apoe*$^{-/-}$ mice, however, we did not see any increases in circulating EPDR1 in humans (Table 4), and it did not correlate with BMI (Figure 17A), DPP4 protein (Figure 17C) or activity (Figure 17D), or any other glucose (Figure 17E) or lipid parameter (Figure 17F-I). Although we have identified EPDR1 cleavage in circulation by DPP4, more work is needed to understand the role of this interaction and if it affects glucose and lipid metabolism.

4.2 Future Directions

4.2.1 Understanding the biological relevance of mononuclear phagocyte DPP4 in hematopoiesis.

DPP4 biological activity is complex, as it has protease activity to control the bioactivity of its substrates(139) and non-enzymatic roles in many cells, including but not limited to immune cells like T-cells, dendritic cells, monocytes, and macrophages(202). The most well-characterized function of DPP4 is the enzymatic cleavage of the incretin hormones to regulate glucose metabolism(141, 149). However, it also has substrates involved in regulating hematopoiesis, such as the cleavage of different colony-stimulating factors GM-CSF and G-CSF(168). Additionally, *Cx3cr1*-expressing cells have been implicated in regulating myelopoiesis(103). Our results suggest differential regulation of hematopoiesis in $Dpp4^{Cx3cr1-/-}$ mice when compared to $Dpp4^{+/+}$ mice and $Dpp4^{-/-}$ mice, illustrating differential regulation of the fate determination of progenitor cells into the lymphoid or myeloid lineages and should be further evaluated.

4.2.2 Understanding the role of inflammation on circulating DPP4 activity and protein.

DPP4 can regulate substrates to modulate molecular pathways, including but not limited to the canonical incretin effect, regulating glucose metabolism(141, 149), however, DPP4 regulation during inflammation is not fully understood. There is ubiquitous expression of DPP4(139), and evidence suggests that depending on the tissue or cell expression of DPP4, it can have varying biological functions, which is made apparent when seeing that DPP4 from different tissues can result in different

phenotypic outcomes in mice(141, 192, 227). We show that DPP4 activity increases in circulation after LPS injection, but the protein does not change. This suggests that inflammation can regulate DPP4 activity, which may be a result of hepatic or bone marrow-associated DPP4 shedding(192, 228). However, understanding tissue-specific differences in post-translational modifications should be evaluated.

4.2.3 The glucoregulatory roles of EPDR1.

Elucidating EPDR1's role and its role in glucose metabolism is a promising avenue. Its transcript expression in the islet correlates with reduced Hba1c in people living with type 2 diabetes. It has been identified to regulate TCA cycle intermediates in pancreatic islet beta-cells to increase glucose and pyruvate-stimulated insulin secretion(184). Additionally, exogenous EPDR1 can decrease circulating glucose(183). Although we were unable to generate and validate a model with genetic deletion of *Epdr1*, our preliminary results show worsened glucose tolerance in female *Epdr1*$^{-/-}$ mice (Supplemental Figure 1). This result corroborates the current literature showing that deletion of EPDR1 decreases insulin secretion(184) and that hyperphysiological levels of EPDR1 decrease circulating glucose(183). Identifying the importance of EPDR1 in glucoregulation, however, the regulation of EPDR1 by DPP4 cleavage in glucose metabolism should be further evaluated.

4.3 Limitations

It was identified that LPS injection increases DPP4 activity in circulation, and we show an increase in mRNA expression in BMDMs but no change in DPP4 protein. Important to note is that DPP4 activity could not be measured due to lack of a sensitive enough assay, results from circulating DPP4 could not be corroborated in BMDMs.

During cold-stimulation studies, it is common to singly house the mice to decrease variability and to expose them to the cold. However, individual housing of mice has been shown to increase hypothalamic-pituitary activity and oxidative stress. This chronic emotional stress in the mice can alter glucose and lipid metabolism(229, 230), limiting the applicability of the results. Additionally, our control mice were housed at room temperature, which is a mild cold stimulus, and their thermoneutral temperature is 29°C(216, 217).

Finally, our conditional *Dpp4* deletion model, where *Dpp4* is deleted from cells expressing *Cx3cr1* via tamoxifen induction, has a few drawbacks. The first is that it is induced via tamoxifen gavage, a selective estrogen receptor modulator that has been shown to potentiate the host's innate immune response(231), induce weight loss, poor feeding(232), and could cause Cre toxicity, heart failure and death(233). Also, this model affects a regenerative population of cells, *Cx3cr1* expressing cells are further along in their differentiation(103, 106), meaning that over time, newly differentiated cells will not carry the deletion of *Dpp4* unless there is constant induction via tamoxifen. To mitigate these toxicity and side effects, mice were treated with the efficacious dose of tamoxifen for three days per week, followed by a break in treatment and one more week of treatment. Controls were also treated with tamoxifen, and experiments were performed shortly after induction to decrease the chance of myelorestoration of *Dpp4*-expressing cells(234).

Finally, I began my master’s during the SARS-CoV-2 pandemic. This resulted in quarantines and restrictions, limiting time available in the laboratory, training for new techniques, and potential for experiments.

5. References

1. Martin SS, Aday AW, Almarzooq ZI, Anderson CAM, Arora P, Avery CL, Baker-Smith CM, Barone Gibbs B, Beaton AZ, Boehme AK, Commodore-Mensah Y, Currie ME, Elkind MSV, Evenson KR, Generoso G, Heard DG, Hiremath S, Johansen MC, Kalani R, Kazi DS, Ko D, Liu J, Magnani JW, Michos ED, Mussolino ME, Navaneethan SD, Parikh NI, Perman SM, Poudel R, Rezk-Hanna M, Roth GA, Shah NS, St-Onge M-P, Thacker EL, Tsao CW, Urbut SM, Van Spall HGC, Voeks JH, Wang N-Y, Wong ND, Wong SS, Yaffe K, Palaniappan LP, null null. 2024. 2024 Heart Disease and Stroke Statistics: A Report of US and Global Data From the American Heart Association. Circulation 149:e347–e913.

2. Dunbar SB, Khavjou OA, Bakas T, Hunt G, Kirch RA, Leib AR, Morrison RS, Poehler DC, Roger VL, Whitsel LP. 2018. Projected Costs of Informal Caregiving for Cardiovascular Disease: 2015 to 2035: A Policy Statement From the American Heart Association. Circulation 137:e558–e577.

3. Chaudhry R, Miao JH, Rehman A. 2024. Physiology, CardiovascularStatPearls. StatPearls Publishing, Treasure Island (FL).

4. Olvera Lopez E, Ballard BD, Jan A. 2024. Cardiovascular DiseaseStatPearls. StatPearls Publishing, Treasure Island (FL).

5. Roth GA, Mensah GA, Johnson CO, Addolorato G, Ammirati E, Baddour LM, Barengo NC, Beaton AZ, Benjamin EJ, Benziger CP, Bonny A, Brauer M, Brodmann M, Cahill TJ, Carapetis J, Catapano AL, Chugh SS, Cooper LT, Coresh J, Criqui M, DeCleene N, Eagle KA, Emmons-Bell S, Feigin VL, Fernández-Solà J, Fowkes G, Gakidou E, Grundy SM, He FJ, Howard G, Hu F, Inker L, Karthikeyan G, Kassebaum N, Koroshetz W, Lavie C, Lloyd-Jones D, Lu HS, Mirijello A, Temesgen AM, Mokdad A, Moran AE, Muntner P, Narula J, Neal B, Ntsekhe M, Moraes de Oliveira G, Otto C, Owolabi M, Pratt M, Rajagopalan S, Reitsma M, Ribeiro ALP, Rigotti N, Rodgers A, Sable C, Shakil S, Sliwa-Hahnle K, Stark B, Sundström J, Timpel P, Tleyjeh IM, Valgimigli M, Vos T, Whelton PK, Yacoub M, Zuhlke L, Murray C, Fuster V. 2020. Global Burden of Cardiovascular Diseases and Risk Factors, 1990–2019. J Am Coll Cardiol 76:2982–3021.

6. Wu N, Shen H, Liu H, Wang Y, Bai Y, Han P. 2016. Acute blood glucose fluctuation enhances rat aorta endothelial cell apoptosis, oxidative stress and pro-inflammatory cytokine expression in vivo. Cardiovasc Diabetol 15:109.

7. Hempel A, Maasch C, Heintze U, Lindschau C, Dietz R, Luft FC, Haller H. 1997. High Glucose Concentrations Increase Endothelial Cell Permeability via Activation of Protein Kinase Cα. Circ Res 81:363–371.

8. Esper RJ, Nordaby RA, Vilariño JO, Paragano A, Cacharrón JL, Machado RA. 2006. Endothelial dysfunction: a comprehensive appraisal. Cardiovasc Diabetol 5:4.

9. Hansson GK, Libby P. 2006. The immune response in atherosclerosis: a double-edged sword. Nat Rev Immunol 2006 67 6:508–519.

10. Libby P. 2021. The changing landscape of atherosclerosis. Nat 2021 5927855 592:524–533.

11. Ketelhuth DFJ, Lutgens E, Bäck M, Binder CJ, Van Den Bossche J, Daniel C, Dumitriu IE, Hoefer I, Libby P, O'Neill L, Weber C, Evans PC. 2019. Immunometabolism and atherosclerosis: perspectives and clinical significance: a position paper from the Working Group on Atherosclerosis and Vascular Biology of the European Society of Cardiology. Cardiovasc Res 115:1385–1392.

12. Mercadante AA, Raja A. 2024. Anatomy, ArteriesStatPearls. StatPearls Publishing, Treasure Island (FL).

13. Zhou J, Li Y-S, Chien S. 2014. Shear Stress–Initiated Signaling and Its Regulation of Endothelial Function. Arterioscler Thromb Vasc Biol 34:2191–2198.

14. Chiu J-J, Chien S. 2011. Effects of Disturbed Flow on Vascular Endothelium: Pathophysiological Basis and Clinical Perspectives. Physiol Rev 91:327–387.

15. Davies PF, Civelek M, Fang Y, Fleming I. 2013. The atherosusceptible endothelium: endothelial phenotypes in complex haemodynamic shear stress regions in vivo. Cardiovasc Res 99:315–327.

16. Davies PF. 1995. Flow-mediated endothelial mechanotransduction. Physiol Rev 75:519–560.

17. Akishima Y, Akasaka Y, Ishikawa Y, Lijun Z, Kiguchi H, Ito K, Itabe H, Ishii T. 2005. Role of macrophage and smooth muscle cell apoptosis in association with oxidized low-density lipoprotein in the atherosclerotic development. Mod Pathol 18:365–373.

18. Schwenke DC, Carew TE. 1988. Quantification in vivo of increased LDL content and rate of LDL degradation in normal rabbit aorta occurring at sites susceptible to early atherosclerotic lesions. Circ Res 62:699–710.

19. Schwenke DC, Carew TE. 1989. Initiation of atherosclerotic lesions in cholesterol-fed rabbits. I. Focal increases in arterial LDL concentration precede development of fatty streak lesions. Arterioscler Dallas Tex 9:895–907.

20. Staughton TJ, Lever MJ, Weinberg PD. 2001. Effect of altered flow on the pattern of permeability around rabbit aortic branches. Am J Physiol-Heart Circ Physiol 281:H53–H59.

21. Ramírez CM, Zhang X, Bandyopadhyay C, Rotllan N, Sugiyama MG, Aryal B, Liu X, He S, Kraehling JR, Ulrich V, Lin CS, Velazquez H, Lasunción MA, Li G, Suárez Y, Tellides G, Swirski FK, Lee WL, Schwartz MA, Sessa WC, Fernández-Hernando C. 2019. Caveolin-1 regulates atherogenesis by attenuating LDL transcytosis and vascular inflammation independent of endothelial nitric oxide synthase activation. Circulation 140:225–239.

22. Huang L, Chambliss KL, Gao X, Yuhanna IS, Behling-Kelly E, Bergaya S, Ahmed M, Michaely P, Luby-Phelps K, Darehshouri A, Xu L, Fisher EA, Ge W-P, Mineo C, Shaul PW. 2019. SR-B1 Drives Endothelial Cell LDL Transcytosis via DOCK4 to Promote Atherosclerosis. Nature 569:565–569.

23. Kraehling JR, Chidlow JH, Rajagopal C, Sugiyama MG, Fowler JW, Lee MY, Zhang X, Ramírez CM, Park EJ, Tao B, Chen K, Kuruvilla L, Larriveé B, Folta-Stogniew E, Ola R, Rotllan N, Zhou W, Nagle MW, Herz J, Williams KJ, Eichmann A, Lee WL, Fernández-Hernando C, Sessa WC. 2016. Genome-wide RNAi screen reveals ALK1 mediates LDL uptake and transcytosis in endothelial cells. Nat Commun 7:13516.

24. Zhang X, Fernández-Hernando C. 2020. Transport of low-density lipoproteins (LDL) into the arterial wall: impact in atherosclerosis. Curr Opin Lipidol 31:279–285.

25. García-Cardeña G, Comander J, Anderson KR, Blackman BR, Gimbrone MA. 2001. Biomechanical activation of vascular endothelium as a determinant of its functional phenotype. Proc Natl Acad Sci U S A 98:4478–4485.

26. Jebari-Benslaiman S, Galicia-García U, Larrea-Sebal A, Olaetxea JR, Alloza I, Vandenbroeck K, Benito-Vicente A, Martín C. 2022. Pathophysiology of Atherosclerosis. Int J Mol Sci 23:3346.

27. Moore K, Sheedy F, Fisher E. 2013. Macrophages in atherosclerosis: a dynamic balance. Nat Rev Immunol 13:709–721.

28. Stöger JL, Gijbels MJJ, Velden S van der, Manca M, Loos CM van der, Biessen EAL, Daemen MJAP, Lutgens E, de Winther MPJ de. 2012. Distribution of macrophage polarization markers in human atherosclerosis. Atherosclerosis 225:461–468.

29. Truong R, Thankam FG, Agrawal DK. 2021. Immunological Mechanisms Underlying Sterile Inflammation in the Pathogenesis of Atherosclerosis: Potential Sites for Intervention. Expert Rev Clin Immunol 17:37–50.

30. Chien S. 2003. Molecular and mechanical bases of focal lipid accumulation in arterial wall. Prog Biophys Mol Biol 83:131–151.

31. Georgakis MK, Bernhagen J, Heitman LH, Weber C, Dichgans M. 2022. Targeting the CCL2–CCR2 axis for atheroprotection. Eur Heart J 43:1799–1808.

32. Jongstra-Bilen J, Tai K, Althagafi MG, Siu A, Scipione CA, Karim S, Polenz CK, Ikeda J, Hyduk SJ, Cybulsky MI. 2021. Role of myeloid-derived chemokine CCL5/RANTES at an early stage of atherosclerosis. J Mol Cell Cardiol 156:69–78.

33. Cole JE, Park I, Ahern DJ, Kassiteridi C, Danso Abeam D, Goddard ME, Green P, Maffia P, Monaco C. 2018. Immune cell census in murine atherosclerosis: cytometry by time of flight illuminates vascular myeloid cell diversity. Cardiovasc Res 114:1360–1371.

34. Ley K, Laudanna C, Cybulsky MI, Nourshargh S. 2007. Getting to the site of inflammation: the leukocyte adhesion cascade updated. Nat Rev Immunol 7:678–689.

35. Muller WA. 2011. Mechanisms of Leukocyte Transendothelial Migration. Annu Rev Pathol 6:323–344.

36. Filippi M-D. 2016. Mechanism of Diapedesis: Importance of the Transcellular Route. Adv Immunol 129:25–53.

37. Herter J, Zarbock A. 2013. Integrin Regulation during Leukocyte Recruitment. J Immunol 190:4451–4457.

38. Ginhoux F, Guilliams M. 2016. Tissue-Resident Macrophage Ontogeny and Homeostasis. Immunity 44:439–449.

39. Locati M, Curtale G, Mantovani A. 2020. Diversity, Mechanisms and Significance of Macrophage Plasticity. Annu Rev Pathol 15:123.

40. Sterpetti AV. 2020. Inflammatory Cytokines and Atherosclerotic Plaque Progression. Therapeutic Implications. Curr Atheroscler Rep 22:75.

41. Chinetti-Gbaguidi G, Colin S, Staels B. 2014. Macrophage subsets in atherosclerosis. Nat Rev Cardiol 2014 121 12:10–17.

42. Grootaert MOJ, Bennett MR. 2021. Vascular smooth muscle cells in atherosclerosis: time for a re-assessment. Cardiovasc Res 117:2326–2339.

43. Robichaud S, Rasheed A, Pietrangelo A, Doyoung Kim A, Boucher DM, Emerton C, Vijithakumar V, Gharibeh L, Fairman G, Mak E, Nguyen M-A, Geoffrion M, Wirka R, Rayner KJ, Ouimet M. 2022. Autophagy Is Differentially

Regulated in Leukocyte and Nonleukocyte Foam Cells During Atherosclerosis. Circ Res 130:831–847.

44. Marsch E, Theelen TL, Demandt JAF, Jeurissen M, Van Gink M, Verjans R, Janssen A, Cleutjens JP, Meex SJR, Donners MM, Haenen GR, Schalkwijk CG, Dubois LJ, Lambin P, Mallat Z, Gijbels MJ, Heemskerk JWM, Fisher EA, Biessen EAL, Janssen BJ, Daemen MJAP, Sluimer JC. 2014. Reversal of hypoxia in murine atherosclerosis prevents necrotic core expansion by enhancing efferocytosis. Arterioscler Thromb Vasc Biol 34:2545–2553.

45. Pollard JW. 2009. Trophic macrophages in development and disease. Nat Rev Immunol 9:259–270.

46. Boada-Romero E, Martinez J, Heckmann BL, Green DR. 2020. The clearance of dead cells by efferocytosis. Nat Rev Mol Cell Biol 2020 217 21:398–414.

47. Kavurma MM, Rayner R, Karunakaran D. 2017. The walking dead: macrophage inflammation and death in atherosclerosis. Curr Opin Lipidol 28:91–98.

48. Stiko-Rahm A, Hultgårdh-Nilsson A, Regnström J, Hamsten A, Nilsson J. 1992. Native and oxidized LDL enhances production of PDGF AA and the surface expression of PDGF receptors in cultured human smooth muscle cells. Arterioscler Thromb J Vasc Biol 12:1099–1109.

49. Malech HL, Deleo FR, Quinn MT. 2014. The role of neutrophils in the immune system: An overview. Methods Mol Biol 1124:3–10.

50. Virmani R, Kolodgie FD, Burke AP, Farb A, Schwartz SM. 2000. Lessons From Sudden Coronary Death. Arterioscler Thromb Vasc Biol 20:1262–1275.

51. Spagnoli LG, Mauriello A, Sangiorgi G, Fratoni S, Bonanno E, Schwartz RS, Piepgras DG, Pistolese R, Ippoliti A, Holmes DR. 2004. Extracranial Thrombotically Active Carotid Plaque as a Risk Factor for Ischemic Stroke. JAMA 292:1845–1852.

52. Fahed AC, Jang I-K. 2021. Plaque erosion and acute coronary syndromes: phenotype, molecular characteristics and future directions. Nat Rev Cardiol 18:724–734.

53. Baaten CCFMJ, Nagy M, Bergmeier W, Spronk HMH, van der Meijden PEJ. 2024. Platelet biology and function: plaque erosion vs. rupture. Eur Heart J 45:18–31.

54. Luo X, Lv Y, Bai X, Qi J, Weng X, Liu S, Bao X, Jia H, Yu B. 2021. Plaque Erosion: A Distinctive Pathological Mechanism of Acute Coronary Syndrome. Front Cardiovasc Med 8:711453.

55. Nakajima A, Sugiyama T, Araki M, Seegers LM, Dey D, McNulty I, Lee H, Yonetsu T, Yasui Y, Teng Y, Nagamine T, Nakamura S, Achenbach S, Kakuta T, Jang I-K. 2022. Plaque Rupture, Compared With Plaque Erosion, Is Associated With a Higher Level of Pancoronary Inflammation. JACC Cardiovasc Imaging 15:828–839.

56. Curtis L. Triplitt P. 2012. Examining the Mechanisms of Glucose Regulation 18.

57. Röder PV, Wu B, Liu Y, Han W. 2016. Pancreatic regulation of glucose homeostasis. Exp Mol Med 48:e219.

58. Nakrani MN, Wineland RH, Anjum F. 2024. Physiology, Glucose MetabolismStatPearls. StatPearls Publishing, Treasure Island (FL).

59. Dal Canto E, Ceriello A, Rydén L, Ferrini M, Hansen TB, Schnell O, Standl E, Beulens JW. 2019. Diabetes as a cardiovascular risk factor: An overview of global trends of macro and micro vascular complications. Eur J Prev Cardiol 26:25–32.

60. Einarson TR, Acs A, Ludwig C, Panton UH. 2018. Prevalence of cardiovascular disease in type 2 diabetes: a systematic literature review of scientific evidence from across the world in 2007–2017. Cardiovasc Diabetol 17:83.

61. González P, Lozano P, Ros G, Solano F. 2023. Hyperglycemia and Oxidative Stress: An Integral, Updated and Critical Overview of Their Metabolic Interconnections. Int J Mol Sci 24:9352.

62. Goldin A, Beckman JA, Schmidt AM, Creager MA. 2006. Advanced Glycation End Products. Circulation 114:597–605.

63. Singh VP, Bali A, Singh N, Jaggi AS. 2014. Advanced Glycation End Products and Diabetic Complications. Korean J Physiol Pharmacol Off J Korean Physiol Soc Korean Soc Pharmacol 18:1–14.

64. Wautier JL, Wautier MP, Schmidt AM, Anderson GM, Hori O, Zoukourian C, Capron L, Chappey O, Yan SD, Brett J. 1994. Advanced glycation end products (AGEs) on the surface of diabetic erythrocytes bind to the vessel wall via a specific receptor inducing oxidant stress in the vasculature: a link between surface-associated AGEs and diabetic complications. Proc Natl Acad Sci U S A 91:7742–7746.

65. Bahadoran Z, Mirmiran P, Kashfi K, Ghasemi A. 2023. Vascular nitric oxide resistance in type 2 diabetes. Cell Death Dis 14:1–14.

66. Sweet IR, Gilbert M, Maloney E, Hockenbery DM, Schwartz MW, Kim F. 2009. Endothelial inflammation induced by excess glucose is associated with

cytosolic glucose-6-phosphate but not increased mitochondrial respiration. Diabetologia 52:921–931.

67. Williams SB, Goldfine AB, Timimi FK, Ting HH, Roddy M-A, Simonson DC, Creager MA. 1998. Acute Hyperglycemia Attenuates Endothelium-Dependent Vasodilation in Humans In Vivo. Circulation 97:1695–1701.

68. Hussain MM. 2014. Intestinal Lipid Absorption and Lipoprotein Formation. Curr Opin Lipidol 25:200–206.

69. Hussain MM, Ravi K. K, Zhangyin Z, Jayraz L, Hongya Z, Ahmed B. 1996. Chylomicron assembly and catabolism: role of apolipoproteins and receptors. Biochim Biophys Acta BBA - Lipids Lipid Metab 1300:151–170.

70. Feingold KR. 2000. Introduction to Lipids and Lipoproteins, p. . *In* Feingold, KR, Anawalt, B, Blackman, MR, Boyce, A, Chrousos, G, Corpas, E, de Herder, WW, Dhatariya, K, Dungan, K, Hofland, J, Kalra, S, Kaltsas, G, Kapoor, N, Koch, C, Kopp, P, Korbonits, M, Kovacs, CS, Kuohung, W, Laferrère, B, Levy, M, McGee, EA, McLachlan, R, New, M, Purnell, J, Sahay, R, Shah, AS, Singer, F, Sperling, MA, Stratakis, CA, Trence, DL, Wilson, DP (eds.), Endotext. MDText.com, Inc., South Dartmouth (MA).

71. Chait A, Ginsberg HN, Vaisar T, Heinecke JW, Goldberg IJ, Bornfeldt KE. 2020. Remnants of the Triglyceride-Rich Lipoproteins, Diabetes, and Cardiovascular Disease. Diabetes 69:508–516.

72. Mach F, Baigent C, Catapano AL, Koskinas KC, Casula M, Badimon L, Chapman MJ, De Backer GG, Delgado V, Ference BA, Graham IM, Halliday A, Landmesser U, Mihaylova B, Pedersen TR, Riccardi G, Richter DJ, Sabatine MS, Taskinen M-R, Tokgozoglu L, Wiklund O, ESC Scientific Document Group. 2020. 2019 ESC/EAS Guidelines for the management of dyslipidaemias: lipid modification to reduce cardiovascular risk: The Task Force for the management of dyslipidaemias of the European Society of Cardiology (ESC) and European Atherosclerosis Society (EAS). Eur Heart J 41:111–188.

73. Mortensen MB, Dzaye O, Bøtker HE, Jensen JM, Maeng M, Bentzon JF, Kanstrup H, Sørensen HT, Leipsic J, Blankstein R, Nasir K, Blaha MJ, Nørgaard BL. 2023. Low-Density Lipoprotein Cholesterol Is Predominantly Associated With Atherosclerotic Cardiovascular Disease Events in Patients With Evidence of Coronary Atherosclerosis: The Western Denmark Heart Registry. Circulation 147:1053–1063.

74. Iqbal J, Anwar K, Hussain MM. 2003. Multiple, Independently Regulated Pathways of Cholesterol Transport across the Intestinal Epithelial Cells *. J Biol Chem 278:31610–31620.

75. Iqbal J, Parks JS, Hussain MM. 2013. Lipid Absorption Defects in Intestine-specific Microsomal Triglyceride Transfer Protein and ATP-binding Cassette Transporter A1-deficient Mice. J Biol Chem 288:30432–30444.

76. Repa JJ, Turley SD, Lobaccaro J-MA, Medina J, Li L, Lustig K, Shan B, Heyman RA, Dietschy JM, Mangelsdorf DJ. 2000. Regulation of Absorption and ABC1-Mediated Efflux of Cholesterol by RXR Heterodimers. Science 289:1524–1529.

77. Yang J, Wang L, Jia R. 2020. Role of de novo cholesterol synthesis enzymes in cancer. J Cancer 11:1761–1767.

78. Russell DW. 1992. Cholesterol biosynthesis and metabolism. Cardiovasc Drugs Ther 6:103–110.

79. Shi Q, Chen J, Zou X, Tang X. 2022. Intracellular Cholesterol Synthesis and Transport. Front Cell Dev Biol 10.

80. Ballantyne CM, Banach M, Mancini GBJ, Lepor NE, Hanselman JC, Zhao X, Leiter LA. 2018. Efficacy and safety of bempedoic acid added to ezetimibe in statin-intolerant patients with hypercholesterolemia: A randomized, placebo-controlled study. Atherosclerosis 277:195–203.

81. Thompson PD, MacDougall DE, Newton RS, Margulies JR, Hanselman JC, Orloff DG, McKenney JM, Ballantyne CM. 2016. Treatment with ETC-1002 alone and in combination with ezetimibe lowers LDL cholesterol in hypercholesterolemic patients with or without statin intolerance. J Clin Lipidol 10:556–567.

82. Hedayatnia M, Asadi Z, Zare-Feyzabadi R, Yaghooti-Khorasani M, Ghazizadeh H, Ghaffarian-Zirak R, Nosrati-Tirkani A, Mohammadi-Bajgiran M, Rohban M, Sadabadi F, Rahimi H-R, Ghalandari M, Ghaffari M-S, Yousefi A, Pouresmaeili E, Besharatlou M-R, Moohebati M, Ferns GA, Esmaily H, Ghayour-Mobarhan M. 2020. Dyslipidemia and cardiovascular disease risk among the MASHAD study population. Lipids Health Dis 19:42.

83. Sheedy FJ, Grebe A, Rayner KJ, Kalantari P, Ramkhelawon B, Carpenter SB, Becker CE, Ediriweera HN, Mullick AE, Golenbock DT, Stuart LM, Latz E, Fitzgerald KA, Moore KJ. 2013. CD36 coordinates NLRP3 inflammasome activation by facilitating the intracellular nucleation from soluble to particulate ligands in sterile inflammation. Nat Immunol 14:812–820.

84. Medina KL. 2016. Chapter 4 - Overview of the immune system, p. 61–76. *In* Pittock, SJ, Vincent, A (eds.), Handbook of Clinical Neurology. Elsevier.

85. McComb S, Thiriot A, Akache B, Krishnan L, Stark F. 2019. Introduction to the Immune System, p. 1–24. *In* Fulton, KM, Twine, SM (eds.), Immunoproteomics: Methods and Protocols. Springer, New York, NY.

86. Aristizábal B, González Á. 2013. Innate immune systemAutoimmunity: From Bench to Bedside [Internet]. El Rosario University Press.

87. Wu Q, Zhang J, Lucas D. 2021. Anatomy of Hematopoiesis and Local Microenvironments in the Bone Marrow. Where to? Front Immunol 12:768439.

88. Mitroulis I, Kalafati L, Hajishengallis G, Chavakis T. 2018. Myelopoiesis in the Context of Innate Immunity. J Innate Immun 10:365–372.

89. Marshall JS, Warrington R, Watson W, Kim HL. 2018. An introduction to immunology and immunopathology. Allergy Asthma Clin Immunol 14:49.

90. Kraus RF, Gruber MA. 2021. Neutrophils—From Bone Marrow to First-Line Defense of the Innate Immune System. Front Immunol 12.

91. Sokol CL, Luster AD. 2015. The Chemokine System in Innate Immunity. Cold Spring Harb Perspect Biol 7:a016303.

92. Krueger A, Łyszkiewicz M, Heissmeyer V. 2022. Post-transcriptional control of T-cell development in the thymus. Immunol Lett 247:1–12.

93. Ma D, Wei Y, Liu F. 2013. Regulatory mechanisms of thymus and T cell development. Dev Comp Immunol 39:91–102.

94. Kondo M, Weissman IL, Akashi K. 1997. Identification of Clonogenic Common Lymphoid Progenitors in Mouse Bone Marrow. Cell 91:661–672.

95. Akashi K, Traver D, Miyamoto T, Weissman IL. 2000. A clonogenic common myeloid progenitor that gives rise to all myeloid lineages. Nature 404:193–197.

96. Ruddle NH, Akirav EM. 2009. Secondary Lymphoid Organs: Responding to Genetic and Environmental Cues in Ontogeny and the Immune Response. J Immunol Baltim Md 1950 183:2205–2212.

97. Lewis SM, Williams A, Eisenbarth SC. 2019. Structure-function of the immune system in the spleen. Sci Immunol 4:eaau6085.

98. van Krieken JH, te Velde J. 1988. Normal histology of the human spleen. Am J Surg Pathol 12:777–785.

99. Anderson AO, Anderson ND. 1975. Studies on the structure and permeability of the microvasculature in normal rat lymph nodes. Am J Pathol 80:387–418.

100. Gretz JE, Norbury CC, Anderson AO, Proudfoot AEI, Shaw S. 2000. Lymph-Borne Chemokines and Other Low Molecular Weight Molecules Reach High Endothelial Venules via Specialized Conduits While a Functional Barrier Limits Access to the Lymphocyte Microenvironments in Lymph Node Cortex. J Exp Med 192:1425–1440.

101. Toda G, Yamauchi T, Kadowaki T, Ueki K. 2020. Preparation and culture of bone marrow-derived macrophages from mice for functional analysis. STAR Protoc 2:100246.

102. Weischenfeldt J, Porse B. 2008. Bone Marrow-Derived Macrophages (BMM): Isolation and Applications. Cold Spring Harb Protoc 2008:pdb.prot5080.

103. Gutknecht MF, Bouton AH. 2014. Functional significance of mononuclear phagocyte populations generated through adult hematopoiesis. J Leukoc Biol 96:969–980.

104. Novakowski KE, Loukov D, Chawla V, Bowdish DME. 2017. Bacterial Binding, Phagocytosis, and Killing: Measurements Using Colony Forming Units. Methods Mol Biol 1519:297–309.

105. Zhou J, Nefedova Y, Lei A, Gabrilovich D. 2018. Neutrophils and PMN-MDSC: Their biological role and interaction with stromal cells. Semin Immunol 35:19–28.

106. Landsman L, Bar-On L, Zernecke A, Kim K-W, Krauthgamer R, Shagdarsuren E, Lira SA, Weissman IL, Weber C, Jung S. 2009. CX3CR1 is required for monocyte homeostasis and atherogenesis by promoting cell survival. Blood 113:963–972.

107. Hume DA. 2006. The mononuclear phagocyte system. Curr Opin Immunol 18:49–53.

108. van Furth R, Cohn ZA, Hirsch JG, Humphrey JH, Spector WG, Langevoort HL. 1972. The mononuclear phagocyte system: a new classification of macrophages, monocytes, and their precursor cells. Bull World Health Organ 46:845–852.

109. Bruce Sundstrom J, A. Ansari A. 1995. Comparative study of the role of professional versus semiprofessional or nonprofessional antigen presenting cells in the rejection of vascularized organ allografts. Transpl Immunol 3:273–289.

110. Chesnut RW, Grey HM. 1985. Antigen presenting cells and mechanisms of antigen presentation. Crit Rev Immunol 5:263–316.

111. Rastogi I, Jeon D, Moseman JE, Muralidhar A, Potluri HK, McNeel DG. 2022. Role of B cells as antigen presenting cells. Front Immunol 13:954936.

112. Roche PA, Furuta K. 2015. The ins and outs of MHC class II-mediated antigen processing and presentation. Nat Rev Immunol 15:203–216.

113. Naito M. 2008. Macrophage differentiation and function in health and disease. Pathol Int 58:143–155.

114. Kareva I, Hahnfeldt P. 2013. The emerging “Hallmarks” of metabolic reprogramming and immune evasion: Distinct or linked? Cancer Res 73:2737–2742.

115. Park BS, Lee J-O. 2013. Recognition of lipopolysaccharide pattern by TLR4 complexes. Exp Mol Med 45:e66–e66.

116. Areschoug T, Gordon S. 2009. Scavenger receptors: role in innate immunity and microbial pathogenesis. Cell Microbiol 11:1160–1169.

117. Taban Q, Mumtaz PT, Masoodi KZ, Haq E, Ahmad SM. 2022. Scavenger receptors in host defense: from functional aspects to mode of action. Cell Commun Signal 20:2.

118. Onyishi CU, Desanti GE, Wilkinson AL, Lara-Reyna S, Frickel E-M, Fejer G, Christophe OD, Bryant CE, Mukhopadhyay S, Gordon S, May RC. 2023. Toll-like receptor 4 and macrophage scavenger receptor 1 crosstalk regulates phagocytosis of a fungal pathogen. Nat Commun 14:4895.

119. Freire-de-Lima CG, Xiao YQ, Gardai SJ, Bratton DL, Schiemann WP, Henson PM. 2006. Apoptotic Cells, through Transforming Growth Factor-β, Coordinately Induce Anti-inflammatory and Suppress Pro-inflammatory Eicosanoid and NO Synthesis in Murine Macrophages. J Biol Chem 281:38376–38384.

120. Dalli J, Serhan CN. 2012. Specific lipid mediator signatures of human phagocytes: microparticles stimulate macrophage efferocytosis and pro-resolving mediators. Blood 120:e60–e72.

121. Basil MC, Levy BD. 2016. Specialized pro-resolving mediators: endogenous regulators of infection and inflammation. Nat Rev Immunol 16:51–67.

122. Chan FKM, Luz NF, Moriwaki K. 2015. Programmed necrosis in the cross talk of cell death and inflammation. Annu Rev Immunol 33:79–106.

123. Kim K, Shim D, Lee JS, Zaitsev K, Williams JW, Kim K-W, Jang M-Y, Seok Jang H, Yun TJ, Lee SH, Yoon WK, Prat A, Seidah NG, Choi J, Lee S-P, Yoon S-H, Nam JW, Seong JK, Oh GT, Randolph GJ, Artyomov MN, Cheong C, Choi J-H. 2018. Transcriptome Analysis Reveals Nonfoamy Rather Than Foamy Plaque Macrophages Are Proinflammatory in Atherosclerotic Murine Models. Circ Res 123:1127–1142.

124. Folco EJ, Sukhova GK, Quillard T, Libby P. 2014. Moderate Hypoxia Potentiates Interleukin-1β Production in Activated Human Macrophages. Circ Res 115:875–883.

125. Gordon S, Martinez FO. 2010. Alternative Activation of Macrophages: Mechanism and Functions. Immunity 32:593–604.

126. Wang L, Zhang S, Wu H, Rong X, Guo J. 2019. M2b macrophage polarization and its roles in diseases. J Leukoc Biol 106:345–358.

127. Zizzo G, Hilliard BA, Monestier M, Cohen PL. 2012. Efficient clearance of early apoptotic cells by human macrophages requires “M2c” polarization and MerTK induction. J Immunol Baltim Md 1950 189:3508–3520.

128. Ferrante CJ, Pinhal-Enfield G, Elson G, Cronstein BN, Hasko G, Outram S, Leibovich SJ. 2013. The adenosine-dependent angiogenic switch of macrophages to an M2-like phenotype is independent of Interleukin-4 receptor alpha (IL4Rα) signaling. Inflammation 36:921–931.

129. Grinberg S, Hasko G, Wu D, Leibovich SJ. 2009. Suppression of PLCβ2 by Endotoxin Plays a Role in the Adenosine A2A Receptor-Mediated Switch of Macrophages from an Inflammatory to an Angiogenic Phenotype. Am J Pathol 175:2439–2453.

130. Fernandez DM, Rahman AH, Fernandez NF, Chudnovskiy A, Amir ED, Amadori L, Khan NS, Wong CK, Shamailova R, Hill CA, Wang Z, Remark R, Li JR, Pina C, Faries C, Awad AJ, Moss N, Bjorkegren JLM, Kim-Schulze S, Gnjatic S, Ma’ayan A, Mocco J, Faries P, Merad M, Giannarelli C. 2019. Single-cell immune landscape of human atherosclerotic plaques. Nat Med 25:1576–1588.

131. Hou P, Fang J, Liu Z, Shi Y, Agostini M, Bernassola F, Bove P, Candi E, Rovella V, Sica G, Sun Q, Wang Y, Scimeca M, Federici M, Mauriello A, Melino G. 2023. Macrophage polarization and metabolism in atherosclerosis. Cell Death Dis 14:1–14.

132. Tsukano H, Gotoh T, Endo M, Miyata K, Tazume H, Kadomatsu T, Yano M, Iwawaki T, Kohno K, Araki K, Mizuta H, Oike Y. 2010. The Endoplasmic Reticulum Stress-C/EBP Homologous Protein Pathway-Mediated Apoptosis in Macrophages Contributes to the Instability of Atherosclerotic Plaques. Arterioscler Thromb Vasc Biol 30:1925–1932.

133. Domschke G, Gleissner CA. 2019. CXCL4-induced macrophages in human atherosclerosis. Cytokine 122:154141.

134. Kadl A, Meher AK, Sharma PR, Lee MY, Doran AC, Johnstone SR, Elliott MR, Gruber F, Han J, Chen W, Kensler T, Ravichandran KS, Isakson BE, Wamhoff BR, Leitinger N. 2010. Identification of a novel macrophage phenotype that develops in response to atherogenic phospholipids via Nrf2. Circ Res 107:737–746.

135. Nielsen MJ, Møller HJ, Moestrup SK. 2010. Hemoglobin and Heme Scavenger Receptors. Antioxid Redox Signal 12:261–273.

136. Boyle JJ. 2012. Heme and haemoglobin direct macrophage Mhem phenotype and counter foam cell formation in areas of intraplaque haemorrhage. Curr Opin Lipidol 23:453.

137. Boyle JJ, Johns M, Kampfer T, Nguyen AT, Game L, Schaer DJ, Mason JC, Haskard DO. 2012. Activating Transcription Factor 1 Directs Mhem Atheroprotective Macrophages Through Coordinated Iron Handling and Foam Cell Protection. Circ Res 110:20–33.

138. Philippidis P, Mason J c., Evans B j., Nadra I, Taylor K m., Haskard D o., Landis R c. 2004. Hemoglobin Scavenger Receptor CD163 Mediates Interleukin-10 Release and Heme Oxygenase-1 Synthesis | Circulation Research. Circ Res 94:119–126.

139. Mulvihill EE, Drucker DJ. 2014. Pharmacology, Physiology, and Mechanisms of Action of Dipeptidyl Peptidase-4 Inhibitors. Endocr Rev 35:992–1019.

140. Baggio LL, Varin EM, Koehler JA, Cao X, Lokhnygina Y, Stevens SR, Holman RR, Drucker DJ. 2020. Plasma levels of DPP4 activity and sDPP4 are dissociated from inflammation in mice and humans. Nat Commun 2020 111 11:1–12.

141. Mulvihill EE, Varin EM, Gladanac B, Campbell JE, Ussher JR, Baggio LL, Yusta B, Ayala J, Burmeister MA, Matthews D, Bang KWA, Ayala JE, Drucker DJ. 2017. Cellular Sites and Mechanisms Linking Reduction of Dipeptidyl Peptidase-4 Activity to Control of Incretin Hormone Action and Glucose Homeostasis. Cell Metab 25:152–165.

142. Rao X, Zhao S, Braunstein Z, Mao H, Razavi M, Duan L, Wei Y, Toomey AC, Rajagopalan S, Zhong J. 2019. Oxidized LDL upregulates macrophage DPP4 expression via TLR4/TRIF/CD36 pathways. EBioMedicine 41:50–61.

143. Terasaki M, Nagashima M, Nohtomi K, Kohashi K, Tomoyasu M, Sinmura K, Nogi Y, Katayama Y, Sato K, Itoh F, Watanabe T, Hirano T. 2013. Preventive Effect of Dipeptidyl Peptidase-4 Inhibitor on Atherosclerosis Is Mainly Attributable to Incretin's Actions in Nondiabetic and Diabetic Apolipoprotein E-Null Mice. PLoS ONE 8:e70933.

144. Reimann F, Habib AM, Tolhurst G, Parker HE, Rogers GJ, Gribble FM. 2008. Glucose Sensing in L Cells: A Primary Cell Study. Cell Metab 8:532–539.

145. Wang SY, Chi MM-Y, Li L, Moley KH, Wice BM. 2003. Studies with GIP/Ins cells indicate secretion by gut K cells is KATP channel independent. Am J Physiol-Endocrinol Metab 284:E988–E1000.

146. Kuhre RE, Gribble FM, Hartmann B, Reimann F, Windeløv JA, Rehfeld JF, Holst JJ. 2014. Fructose stimulates GLP-1 but not GIP secretion in mice, rats, and humans. Am J Physiol - Gastrointest Liver Physiol 306:G622–G630.

147. Reimann F, Williams L, da Silva Xavier G, Rutter GA, Gribble FM. 2004. Glutamine potently stimulates glucagon-like peptide-1 secretion from GLUTag cells. Diabetologia 47:1592–1601.

148. Tolhurst G, Heffron H, Lam YS, Parker HE, Habib AM, Diakogiannaki E, Cameron J, Grosse J, Reimann F, Gribble FM. 2012. Short-Chain Fatty Acids Stimulate Glucagon-Like Peptide-1 Secretion via the G-Protein–Coupled Receptor FFAR2. Diabetes 61:364–371.

149. Lamont BJ, Drucker DJ. 2008. Differential Antidiabetic Efficacy of Incretin Agonists Versus DPP-4 Inhibition in High Fat–Fed Mice. Diabetes 57:190–198.

150. Mathur V, Alam O, Siddiqui N, Jha M, Manaithiya A, Bawa S, Sharma N, Alshehri S, Alam P, Shakeel F. 2023. Insight into Structure Activity Relationship of DPP-4 Inhibitors for Development of Antidiabetic Agents. Molecules 28:5860.

151. Monami M, Lamanna C, Desideri CM, Mannucci E. 2012. DPP-4 Inhibitors and Lipids: Systematic Review and Meta-Analysis. Adv Ther 29:14–25.

152. Conarello SL, Li Z, Ronan J, Roy RS, Zhu L, Jiang G, Liu F, Woods J, Zycband E, Moller DE, Thornberry NA, Zhang BB. 2003. Mice lacking dipeptidyl peptidase IV are protected against obesity and insulin resistance. Proc Natl Acad Sci U S A 100:6825–6830.

153. Marguet D, Baggio L, Kobayashi T, Bernard A-M, Pierres M, Nielsen PF, Ribel U, Watanabe T, Drucker DJ, Wagtmann N. 2000. Enhanced insulin secretion and improved glucose tolerance in mice lacking CD26. Proc Natl Acad Sci U S A 97:6874–6879.

154. Matheeussen V, Waumans Y, Martinet W, Van Goethem S, Van der Veken P, Scharpé S, Augustyns K, De Meyer GRY, De Meester I. 2013. Dipeptidyl peptidases in atherosclerosis: expression and role in macrophage differentiation, activation and apoptosis. Basic Res Cardiol 108:350.

155. Ervinna N, Mita T, Yasunari E, Azuma K, Tanaka R, Fujimura S, Sukmawati D, Nomiyama T, Kanazawa A, Kawamori R, Fujitani Y, Watada H. 2013. Anagliptin, a DPP-4 Inhibitor, Suppresses Proliferation of Vascular Smooth Muscles and Monocyte Inflammatory Reaction and Attenuates Atherosclerosis in Male apo E-Deficient Mice. Endocrinology 154:1260–1270.

156. Wang H, Li Y, Zhang X, Xu Z, Zhou J, Shang W. 2020. DPP-4 Inhibitor Linagliptin Ameliorates Oxidized LDL-Induced THP-1 Macrophage Foam Cell Formation and Inflammation. Drug Des Devel Ther 14:3929.

157. Lamers D, Famulla S, Wronkowitz N, Hartwig S, Lehr S, Ouwens DM, Eckardt K, Kaufman JM, Ryden M, Müller S, Hanisch F-G, Ruige J, Arner P, Sell H,

Eckel J. 2011. Dipeptidyl Peptidase 4 Is a Novel Adipokine Potentially Linking Obesity to the Metabolic Syndrome. Diabetes 60:1917–1925.

158. Fahed G, Aoun L, Bou Zerdan M, Allam S, Bou Zerdan M, Bouferraa Y, Assi HI. 2022. Metabolic Syndrome: Updates on Pathophysiology and Management in 2021. Int J Mol Sci 23:786.

159. Shah Z, Kampfrath T, Deiuliis JA, Zhong J, Pineda C, Ying Z, Xu X, Lu B, Moffatt-Bruce S, Durairaj R, Sun Q, Mihai G, Maiseyeu A, Rajagopalan S. 2011. Chronic DPP-4 Inhibition Reduces Atherosclerosis and Inflammation via Effects on Monocyte Recruitment and Chemotaxis. Circulation 124:2338–2349.

160. Vittone F, Liberman A, Vasic D, Ostertag R, Esser M, Walcher D, Ludwig A, Marx N, Burgmaier M. 2012. Sitagliptin reduces plaque macrophage content and stabilises arteriosclerotic lesions in Apoe−/− mice. Diabetologia 55:2267–2275.

161. Patoulias DI, Boulmpou A, Teperikidis E, Katsimardou A, Siskos F, Doumas M, Papadopoulos CE, Vassilikos V. 2021. Cardiovascular efficacy and safety of dipeptidyl peptidase-4 inhibitors: A meta-analysis of cardiovascular outcome trials. World J Cardiol 13:585–592.

162. Gantz I, Chen M, Suryawanshi S, Ntabadde C, Shah S, O'Neill EA, Engel SS, Kaufman KD, Lai E. 2017. A randomized, placebo-controlled study of the cardiovascular safety of the once-weekly DPP-4 inhibitor omarigliptin in patients with type 2 diabetes mellitus. Cardiovasc Diabetol 16:112.

163. Scirica BM, Bhatt DL, Braunwald E, Steg PG, Davidson J, Hirshberg B, Ohman P, Frederich R, Wiviott SD, Hoffman EB, Cavender MA, Udell JA, Desai NR, Mosenzon O, McGuire DK, Ray KK, Leiter LA, Raz I, SAVOR-TIMI 53 Steering Committee and Investigators. 2013. Saxagliptin and cardiovascular outcomes in patients with type 2 diabetes mellitus. N Engl J Med 369:1317–1326.

164. White WB, Cannon CP, Heller SR, Nissen SE, Bergenstal RM, Bakris GL, Perez AT, Fleck PR, Mehta CR, Kupfer S, Wilson C, Cushman WC, Zannad F. 2013. Alogliptin after Acute Coronary Syndrome in Patients with Type 2 Diabetes. N Engl J Med 369:1327–1335.

165. Green JB, Bethel MA, Armstrong PW, Buse JB, Engel SS, Garg J, Josse R, Kaufman KD, Koglin J, Korn S, Lachin JM, McGuire DK, Pencina MJ, Standl E, Stein PP, Suryawanshi S, Van de Werf F, Peterson ED, Holman RR. 2015. Effect of Sitagliptin on Cardiovascular Outcomes in Type 2 Diabetes. N Engl J Med 373:232–242.

166. Rosenstock J, Perkovic V, Johansen OE, Cooper ME, Kahn SE, Marx N, Alexander JH, Pencina M, Toto RD, Wanner C, Zinman B, Woerle HJ,

Baanstra D, Pfarr E, Schnaidt S, Meinicke T, George JT, von Eynatten M, McGuire DK, for the CARMELINA Investigators. 2019. Effect of Linagliptin vs Placebo on Major Cardiovascular Events in Adults With Type 2 Diabetes and High Cardiovascular and Renal Risk: The CARMELINA Randomized Clinical Trial. JAMA 321:69–79.

167. Rosenstock J, Kahn SE, Johansen OE, Zinman B, Espeland MA, Woerle HJ, Pfarr E, Keller A, Mattheus M, Baanstra D, Meinicke T, George JT, Eynatten M von, McGuire DK, Marx N, Investigators for the C. 2019. Effect of Linagliptin vs Glimepiride on Major Adverse Cardiovascular Outcomes in Patients With Type 2 Diabetes: The CAROLINA Randomized Clinical Trial. JAMA 322:1155–1166.

168. Broxmeyer HE, Hoggatt J, O'Leary HA, Mantel C, Chitteti BR, Cooper S, Messina-Graham S, Hangoc G, Farag S, Rohrabaugh SL, Ou X, Speth J, Pelus LM, Srour EF, Campbell TB. 2012. Dipeptidylpeptidase 4 negatively regulates colony-stimulating factor activity and stress hematopoiesis. Nat Med 18:1786–1796.

169. Ou X, O'Leary HA, Broxmeyer HE. 2013. Implications of DPP4 modification of proteins that regulate stem/progenitor and more mature cell types. Blood 122:161–169.

170. Rao X, Deiuliis JA, Mihai G, Varghese J, Xia C, Frieman MB, Sztalryd C, Sun XJ, Quon MJ, Taylor SI, Rajagopalan S, Zhong J. 2018. Monocyte DPP4 Expression in Human Atherosclerosis Is Associated With Obesity and Dyslipidemia. Diabetes Care 41:e1–e3.

171. Shinjo T, Nakatsu Y, Iwashita M, Sano T, Sakoda H, Ishihara H, Kushiyama A, Fujishiro M, Fukushima T, Tsuchiya Y, Kamata H, Nishimura F, Asano T. 2015. DPP-IV inhibitor anagliptin exerts anti-inflammatory effects on macrophages, adipocytes, and mouse livers by suppressing NF-κB activation. Am J Physiol-Endocrinol Metab 309:E214–E223.

172. Diaz-Jimenez D, Petrillo MG, Busada JT, Hermoso MA, Cidlowski JA. 2020. Glucocorticoids mobilize macrophages by transcriptionally up-regulating the exopeptidase DPP4. J Biol Chem 295:3213–3227.

173. Wei Y, Xiong ZJ, Li J, Zou C, Cairo CW, Klassen JS, Privé GG. 2019. Crystal structures of human lysosomal EPDR1 reveal homology with the superfamily of bacterial lipoprotein transporters. 1. Commun Biol 2:1–13.

174. Nimmrich I, Erdmann S, Melchers U, Chtarbova S, Finke U, Hentsch S, Hoffmann I, Oertel M, Hoffmann W, Müller O. 2001. The novel ependymin related gene *UCC1* is highly expressed in colorectal tumor cells. Cancer Lett 165:71–79.

175. Chen R, Zhang Y. 2020. EPDR1 correlates with immune cell infiltration in hepatocellular carcinoma and can be used as a prognostic biomarker. J Cell Mol Med 24:12107–12118.

176. Riffo-Campos ÁL, Castillo J, Vallet-Sánchez A, Ayala G, Cervantes A, López-Rodas G, Franco L. 2016. In silico RNA-seq and experimental analyses reveal the differential expression and splicing of EPDR1 and ZNF518B genes in relation to KRAS mutations in colorectal cancer cells. Oncol Rep 36:3627–3634.

177. El-Masry OS, Alamri AM, Alzahrani F, Alsamman K. 2022. ADAMTS14, ARHGAP22, and EPDR1 as potential novel targets in acute myeloid leukaemia. Heliyon 8:e09065.

178. Park S, Daily JW, Song MY, Kwon H-K. 2020. Gene-gene and gene-lifestyle interactions of AKAP11, KCNMA1, PUM1, SPTBN1, and EPDR1 on osteoporosis risk in middle-aged adults. Nutr Burbank Los Angel Cty Calif 79–80:110859.

179. Staats KA, Wu T, Gan BS, O'Gorman DB, Ophoff RA. 2016. Dupuytren's disease susceptibility gene, EPDR1, is involved in myofibroblast contractility. J Dermatol Sci 83:131–137.

180. Khor CC, Do T, Jia H, Nakano M, George R, Abu-Amero K, Duvesh R, Chen LJ, Li Z, Nongpiur ME, Perera SA, Qiao C, Wong H-T, Sakai H, Barbosa de Melo M, Lee M-C, Chan AS, Azhany Y, Dao TLH, Ikeda Y, Perez-Grossmann RA, Zarnowski T, Day AC, Jonas JB, Tam POS, Tran TA, Ayub H, Akhtar F, Micheal S, Chew PTK, Aljasim LA, Dada T, Luu TT, Awadalla MS, Kitnarong N, Wanichwecharungruang B, Aung YY, Mohamed-Noor J, Vijayan S, Sarangapani S, Husain R, Jap A, Baskaran M, Goh D, Su DH, Wang H, Yong VK, Yip LW, Trinh TB, Makornwattana M, Nguyen TT, Leuenberger EU, Park K-H, Wiyogo WA, Kumar RS, Tello C, Kurimoto Y, Thapa SS, Pathanapitoon K, Salmon JF, Sohn YH, Fea A, Ozaki M, Lai JSM, Tantisevi V, Khaing CC, Mizoguchi T, Nakano S, Kim C-Y, Tang G, Fan S, Wu R, Meng H, Nguyen TTG, Tran TD, Ueno M, Martinez JM, Ramli N, Aung YM, Reyes RD, Vernon SA, Fang SK, Xie Z, Chen XY, Foo JN, Sim KS, Wong TT, Quek DT, Venkatesh R, Kavitha S, Krishnadas SR, Soumittra N, Shantha B, Lim B-A, Ogle J, de Vasconcellos JPC, Costa VP, Abe RY, de Souza BB, Sng CC, Aquino MC, Kosior-Jarecka E, Fong GB, Tamanaja VC, Fujita R, Jiang Y, Waseem N, Low S, Pham HN, Al-Shahwan S, Craven ER, Khan MI, Dada R, Mohanty K, Faiq MA, Hewitt AW, Burdon KP, Gan EH, Prutthipongsit A, Patthanathamrongkasem T, Catacutan MAT, Felarca IR, Liao CS, Rusmayani E, Istiantoro VW, Consolandi G, Pignata G, Lavia C, Rojanapongpun P, Mangkornkanokpong L, Chansangpetch S, Chan JCH, Choy BNK, Shum JWH, Than HM, Oo KT, Han AT, Yong VH, Ng X-Y, Goh SR, Chong YF, Hibberd ML, Seielstad M, Png E, Dunstan SJ, Chau NVV, Bei J, Zeng YX, Karkey A, Basnyat B, Pasutto F, Paoli D, Frezzotti P, Wang JJ, Mitchell P,

Fingert JH, Allingham RR, Hauser MA, Lim ST, Chew SH, Ebstein RP, Sakuntabhai A, Park KH, Ahn J, Boland G, Snippe H, Stead R, Quino R, Zaw SN, Lukasik U, Shetty R, Zahari M, Bae HW, Oo NL, Kubota T, Manassakorn A, Ho WL, Dallorto L, Hwang YH, Kiire CA, Kuroda M, Djamal ZE, Peregrino JIM, Ghosh A, Jeoung JW, Hoan TS, Srisamran N, Sandragasu T, Set SH, Doan VH, Bhattacharya SS, Ho C-L, Tan DT, Sihota R, Loon S-C, Mori K, Kinoshita S, Hollander AI den, Qamar R, Wang Y-X, Teo YY, Tai E-S, Hartleben-Matkin C, Lozano-Giral D, Saw SM, Cheng C-Y, Zenteno JC, Pang CP, Bui HTT, Hee O, Craig JE, Edward DP, Yonahara M, Neto JM, Guevara-Fujita ML, Xu L, Ritch R, Liza-Sharmini AT, Wong TY, Al-Obeidan S, Do NH, Sundaresan P, Tham CC, Foster PJ, Vijaya L, Tashiro K, Vithana EN, Wang N, Aung T. 2016. Genome-wide association study identifies five new susceptibility loci for primary angle closure glaucoma. Nat Genet 48:556–562.

181. Valle MCD, Sleat DE, Sohar I, Wen T, Pintar JE, Jadot M, Lobel P. 2006. Demonstration of Lysosomal Localization for the Mammalian Ependymin-related Protein Using Classical Approaches Combined with a Novel Density Shift Method *. J Biol Chem 281:35436–35445.

182. Deshmukh AS, Peijs L, Beaudry JL, Jespersen NZ, Nielsen CH, Ma T, Brunner AD, Larsen TJ, Bayarri-Olmos R, Prabhakar BS, Helgstrand C, Severinsen MCK, Holst B, Kjaer A, Tang-Christensen M, Sanfridson A, Garred P, Privé GG, Pedersen BK, Gerhart-Hines Z, Nielsen S, Drucker DJ, Mann M, Scheele C. 2019. Proteomics-Based Comparative Mapping of the Secretomes of Human Brown and White Adipocytes Reveals EPDR1 as a Novel Batokine. Cell Metab 30:963-975.e7.

183. Koplev S, Seldin M, Sukhavasi K, Ermel R, Pang S, Zeng L, Bankier S, Di Narzo A, Cheng H, Meda V, Ma A, Talukdar H, Cohain A, Amadori L, Argmann C, Houten SM, Franzén O, Mocci G, Meelu OA, Ishikawa K, Whatling C, Jain A, Jain RK, Gan L-M, Giannarelli C, Roussos P, Hao K, Schunkert H, Michoel T, Ruusalepp A, Schadt EE, Kovacic JC, Lusis AJ, Björkegren JLM. 2022. A mechanistic framework for cardiometabolic and coronary artery diseases. Nat Cardiovasc Res 2022 11 1:85–100.

184. Cataldo LR, Gao Q, Argemi-Muntadas L, Hodek O, Cowan E, Hladkou S, Gheibi S, Spégel P, Prasad RB, Eliasson L, Scheele C, Fex M, Mulder H, Moritz T. 2022. The human batokine EPDR1 regulates β-cell metabolism and function. Mol Metab 66:101629.

185. Salgado FJ, Vela E, Martín M, Franco R, Nogueira M, Cordero OJ. 2000. Mechanisms of CD26/dipeptidyl peptidase IV cytokine-dependent regulation on human activated lymphocytes. Cytokine 12:1136–1141.

186. Andrikou E, Tsioufis C, Andrikou I, Leontsinis I, Tousoulis D, Papanas N. 2019. GLP-1 receptor agonists and cardiovascular outcome trials: An update. Hellenic J Cardiol 60:347–351.

187. Marx N, Husain M, Lehrke M, Verma S, Sattar N. 2022. GLP-1 Receptor Agonists for the Reduction of Atherosclerotic Cardiovascular Risk in Patients With Type 2 Diabetes. Circulation 146:1882–1894.

188. Chen L, Shan Y, Weng Y, Sui Z, Zhang X, Liang Z, Zhang L, Zhang Y. 2016. Hydrophobic Tagging-Assisted N-Termini Enrichment for In-Depth N-Terminome Analysis. Anal Chem 88:8390–8395.

189. Lakso M, Pichel JG, Gorman JR, Sauer B, Okamoto Y, Lee E, Alt FW, Westphal H. 1996. Efficient in vivo manipulation of mouse genomic sequences at the zygote stage. Proc Natl Acad Sci 93:5860–5865.

190. Yona S, Kim K-W, Wolf Y, Mildner A, Varol D, Breker M, Strauss-Ayali D, Viukov S, Guilliams M, Misharin A, Hume DA, Perlman H, Malissen B, Zelzer E, Jung S. 2013. Fate Mapping Reveals Origins and Dynamics of Monocytes and Tissue Macrophages under Homeostasis. Immunity 38:79–91.

191. Mulvihill EE, Varin EM, Ussher JR, Campbell JE, Bang KWA, Abdullah T, Baggio LL, Drucker DJ. 2016. Inhibition of Dipeptidyl Peptidase-4 Impairs Ventricular Function and Promotes Cardiac Fibrosis in High Fat–Fed Diabetic Mice. Diabetes 65:742–754.

192. Baggio LL, Varin EM, Koehler JA, Cao X, Lokhnygina Y, Stevens SR, Holman RR, Drucker DJ. 2020. Plasma levels of DPP4 activity and sDPP4 are dissociated from inflammation in mice and humans. 1. Nat Commun 11:3766.

193. Röhrborn D, Eckel J, Sell H. 2014. Shedding of dipeptidyl peptidase 4 is mediated by metalloproteases and up-regulated by hypoxia in human adipocytes and smooth muscle cells. FEBS Lett 588:3870–3877.

194. Nargis T, Kumar K, Ghosh AR, Sharma A, Rudra D, Sen D, Chakrabarti S, Mukhopadhyay S, Ganguly D, Chakrabarti P. 2017. KLK5 induces shedding of DPP4 from circulatory Th17 cells in type 2 diabetes. Mol Metab 6:1529–1539.

195. Waget A, Cabou C, Masseboeuf M, Cattan P, Armanet M, Karaca M, Castel J, Garret C, Payros G, Maida A, Sulpice T, Holst JJ, Drucker DJ, Magnan C, Burcelin R. 2011. Physiological and Pharmacological Mechanisms through which the DPP-4 Inhibitor Sitagliptin Regulates Glycemia in Mice. Endocrinology 152:3018–3029.

196. Varin EM, Mulvihill EE, Beaudry JL, Pujadas G, Fuchs S, Tanti J-F, Fazio S, Kaur K, Cao X, Baggio LL, Matthews D, Campbell JE, Drucker DJ. 2019. Circulating Levels of Soluble Dipeptidyl Peptidase-4 Are Dissociated from Inflammation and Induced by Enzymatic DPP4 Inhibition. Cell Metab 29:320-334.e5.

197. Noels H, Theelen W, Sternkopf M, Jankowski V, Moellmann J, Kraemer S, Lehrke M, Marx N, Martin L, Marx G, Jankowski J, Goetzenich A, Stoppe C.

2018. Reduced post-operative DPP4 activity associated with worse patient outcome after cardiac surgery. Sci Rep 8:11820.

198. Aït Slimane T, Lenoir C, Sapin C, Maurice M, Trugnan G. 2000. Apical Secretion and Sialylation of Soluble Dipeptidyl Peptidase IV Are Two Related Events. Exp Cell Res 258:184–194.

199. Fan H, Meng W, Kilian C, Grams S, Reutter W. 1997. Domain-Specific N-Glycosylation of the Membrane Glycoprotein Dipeptidylpeptidase IV (CD26) Influences its Subcellular Trafficking, Biological Stability, Enzyme Activity and Protein Folding. Eur J Biochem 246:243–251.

200. Ji F, Zhou M, Zhu H, Jiang Z, Li Q, Ouyang X, Lv Y, Zhang S, Wu T, Li L. 2022. Integrative Proteomic Analysis of Multiple Posttranslational Modifications in Inflammatory Response. Genomics Proteomics Bioinformatics 20:163–176.

201. Liu J, Qian C, Cao X. 2016. Post-Translational Modification Control of Innate Immunity. Immunity 45:15–30.

202. Zhong J, Rao X, Deiuliis J, Braunstein Z, Narula V, Hazey J, Mikami D, Needleman B, Satoskar AR, Rajagopalan S. 2013. A Potential Role for Dendritic Cell/Macrophage-Expressing DPP4 in Obesity-Induced Visceral Inflammation. Diabetes 62:149–157.

203. Horiuchi T, Mitoma H, Harashima S, Tsukamoto H, Shimoda T. 2010. Transmembrane TNF-α: structure, function and interaction with anti-TNF agents. Rheumatol Oxf Engl 49:1215–1228.

204. Anderson P, Phillips K, Stoecklin G, Kedersha N. 2004. Post-transcriptional regulation of proinflammatory proteins. J Leukoc Biol 76:42–47.

205. Nishida S, Matsumura T, Senokuchi T, Murakami-Nishida S, Ishii N, Morita Y, Yagi Y, Motoshima H, Kondo T, Araki E. 2020. Inhibition of inflammation-mediated DPP-4 expression by linagliptin increases M2 macrophages in atherosclerotic lesions. Biochem Biophys Res Commun 524:8–15.

206. Zore T, Palafox M, Reue K. 2018. Sex differences in obesity, lipid metabolism, and inflammation—A role for the sex chromosomes? Mol Metab 15:35–44.

207. Bhattacharya S, Sadhukhan D, Saraswathy R. 2024. Role of sex in immune response and epigenetic mechanisms. Epigenetics Chromatin 17:1.

208. Deny M, Arroba Nuñez LA, Romano M, Denis O, Casimir G, Chamekh M. 2022. Sex difference in innate inflammatory response and macrophage polarization in Streptococcus agalactiae-induced pneumonia and potential role of microRNA-223-3p. Sci Rep 12:17126.

209. Becerra-Díaz M, Lerner AD, Yu DH, Thiboutot JP, Liu MC, Yarmus LB, Bose S, Heller NM. 2021. Sex differences in M2 polarization, chemokine and IL-4 receptors in monocytes and macrophages from asthmatics. Cell Immunol 360:104252.

210. Keselman A, Fang X, White PB, Heller NM. 2017. Estrogen Signaling Contributes to Sex Differences in Macrophage Polarization during Asthma. J Immunol 199:1573–1583.

211. McKillop AM, Stevenson CL, Moran BM, Abdel-Wahab YHA, Flatt PR. 2018. Tissue expression of DPP-IV in obesity-diabetes and modulatory effects on peptide regulation of insulin secretion. Peptides 100:165–172.

212. Shi C, Jia T, Mendez-Ferrer S, Hohl TM, Serbina NV, Lipuma L, Leiner I, Li MO, Frenette PS, Pamer EG. 2011. Bone Marrow Mesenchymal Stem and Progenitor Cells Induce Monocyte Emigration in Response to Circulating Toll-like Receptor Ligands. Immunity 34:590–601.

213. Gimeno-Valiente F, Riffo-Campos ÁL, Ayala G, Tarazona N, Gambardella V, Rodríguez FM, Huerta M, Martínez-Ciarpaglini C, Montón-Bueno J, Roselló S, Roda D, Cervantes A, Franco L, López-Rodas G, Castillo J. 2020. EPDR1 up-regulation in human colorectal cancer is related to staging and favours cell proliferation and invasiveness. Sci Rep 10:3723.

214. Yang Y, Zhang H, Liu Z, Zhao F, Liang G. 2021. EPDR1 is related to stages and metastasize in bladder cancer and can be used as a prognostic biomarker. BMC Urol 21:71.

215. Zhao Z, Wang Z, Wang P, Liu S, Li Y, Yang X. 2021. EPDR1, Which Is Negatively Regulated by miR-429, Suppresses Epithelial Ovarian Cancer Progression via PI3K/AKT Signaling Pathway. Front Oncol 11.

216. Tian XY, Ganeshan K, Hong C, Nguyen KD, Qiu Y, Kim J, Tangirala RK, Tonotonoz P, Chawla A. 2016. Thermoneutral housing accelerates metabolic inflammation to potentiate atherosclerosis but not insulin resistance. Cell Metab 23:165–178.

217. Ganeshan K, Chawla A. 2017. Warming the mouse to model human diseases. Nat Rev Endocrinol 13:458–465.

218. Lee JY, Jang BK, Song MK, Kim HS, Kim M-K. 2017. Association between Serum Dipeptidyl Peptidase-4 Concentration and Obesity-related Factors in Health Screen Examinees. J Obes Metab Syndr 26:188–196.

219. Love KM, Liu Z. 2021. DPP4 Activity, Hyperinsulinemia, and Atherosclerosis. J Clin Endocrinol Metab 106:1553–1565.

220. Herz CT, Brix JM, Ludvik B, Schernthaner G, Schernthaner G-H. 2021. Decrease of dipeptidyl peptidase 4 activity is associated with weight loss after bariatric surgery. Obes Surg 31:2545–2550.

221. Joven J, Rull A, Ferré N, Escolà-Gil JC, Marsillach J, Coll B, Alonso-Villaverde C, Aragones G, Claria J, Camps J. 2007. The results in rodent models of atherosclerosis are not interchangeable: The influence of diet and strain. Atherosclerosis 195:e85–e92.

222. Hinder LM, Vincent AM, Hayes JM, McLean LL, Feldman EL. 2013. Apolipoprotein E Knockout as the Basis for Mouse Models of Dyslipidemia-Induced Neuropathy. Exp Neurol 239:102–110.

223. Salehi N, Janjani P, Tadbiri H, Rozbahani M, Jalilian M. 2021. Effect of cigarette smoking on coronary arteries and pattern and severity of coronary artery disease: a review. J Int Med Res 49:03000605211059893.

224. Rao Ch. S, Subash Y. E. 2013. The Effect of Chronic Tobacco Smoking and Chewing on the Lipid Profile. J Clin Diagn Res JCDR 7:31–34.

225. Cha S-A, Park Y-M, Yun J-S, Lim T-S, Song K-H, Yoo K-D, Ahn Y-B, Ko S-H. 2017. A comparison of effects of DPP-4 inhibitor and SGLT2 inhibitor on lipid profile in patients with type 2 diabetes. Lipids Health Dis 16:58.

226. Yano W, Inoue N, Ito S, Itou T, Yasumura M, Yoshinaka Y, Hagita S, Goto M, Nakagawa T, Inoue K, Tanabe S, Kaku K. 2017. Mechanism of lipid-lowering action of the dipeptidyl peptidase-4 inhibitor, anagliptin, in low-density lipoprotein receptor-deficient mice. J Diabetes Investig 8:155–160.

227. Trzaskalski NA, Vulesevic B, Nguyen M-A, Jeraj N, Fadzeyeva E, Morrow NM, Locatelli CAA, Travis N, Hanson AA, Nunes JRC, O'Dwyer C, Veen JN van der, Lorenzen-Schmidt I, Seymour R, Pulente SM, Clément AC, Crawley AM, Jacobs RL, Doyle M-A, Cooper CL, Kim K-H, Fullerton MD, Mulvihill EE. 2023. Hepatocyte-derived DPP4 regulates portal GLP-1 bioactivity, modulates glucose production, and when absent influences NAFLD progression. JCI Insight 8.

228. Baumeier C, Schlüter L, Saussenthaler S, Laeger T, Rödiger M, Alaze SA, Fritsche L, Häring H-U, Stefan N, Fritsche A, Schwenk RW, Schürmann A. 2017. Elevated hepatic DPP4 activity promotes insulin resistance and non-alcoholic fatty liver disease. Mol Metab 6:1254–1263.

229. Kalliokoski O, Jacobsen KR, Darusman HS, Henriksen T, Weimann A, Poulsen HE, Hau J, Abelson KSP. 2013. Mice Do Not Habituate to Metabolism Cage Housing–A Three Week Study of Male BALB/c Mice. PLoS ONE 8:e58460.

230. Schipper L, van Heijningen S, Karapetsas G, van der Beek EM, van Dijk G. 2020. Individual housing of male C57BL/6J mice after weaning impairs growth and predisposes for obesity. PLoS ONE 15:e0225488.

231. Sfogliarini C, Pepe G, Dolce A, Della Torre S, Cesta MC, Allegretti M, Locati M, Vegeto E. 2022. Tamoxifen Twists Again: On and Off-Targets in Macrophages and Infections. Front Pharmacol 13:879020.

232. Donocoff RS, Teteloshvili N, Chung H, Shoulson R, Creusot RJ. 2020. Optimization of tamoxifen-induced Cre activity and its effect on immune cell populations. Sci Rep 10:15244.

233. Bersell K, Choudhury S, Mollova M, Polizzotti BD, Ganapathy B, Walsh S, Wadugu B, Arab S, Kühn B. 2013. Moderate and high amounts of tamoxifen in αMHC-MerCreMer mice induce a DNA damage response, leading to heart failure and death. Dis Model Mech 6:1459–1469.

234. Jacquelin S, Licata F, Dorgham K, Hermand P, Poupel L, Guyon E, Deterre P, Hume DA, Combadière C, Boissonnas A. 2013. CX3CR1 reduces Ly6Chigh-monocyte motility within and release from the bone marrow after chemotherapy in mice. Blood 122:674–683.

6. Appendix

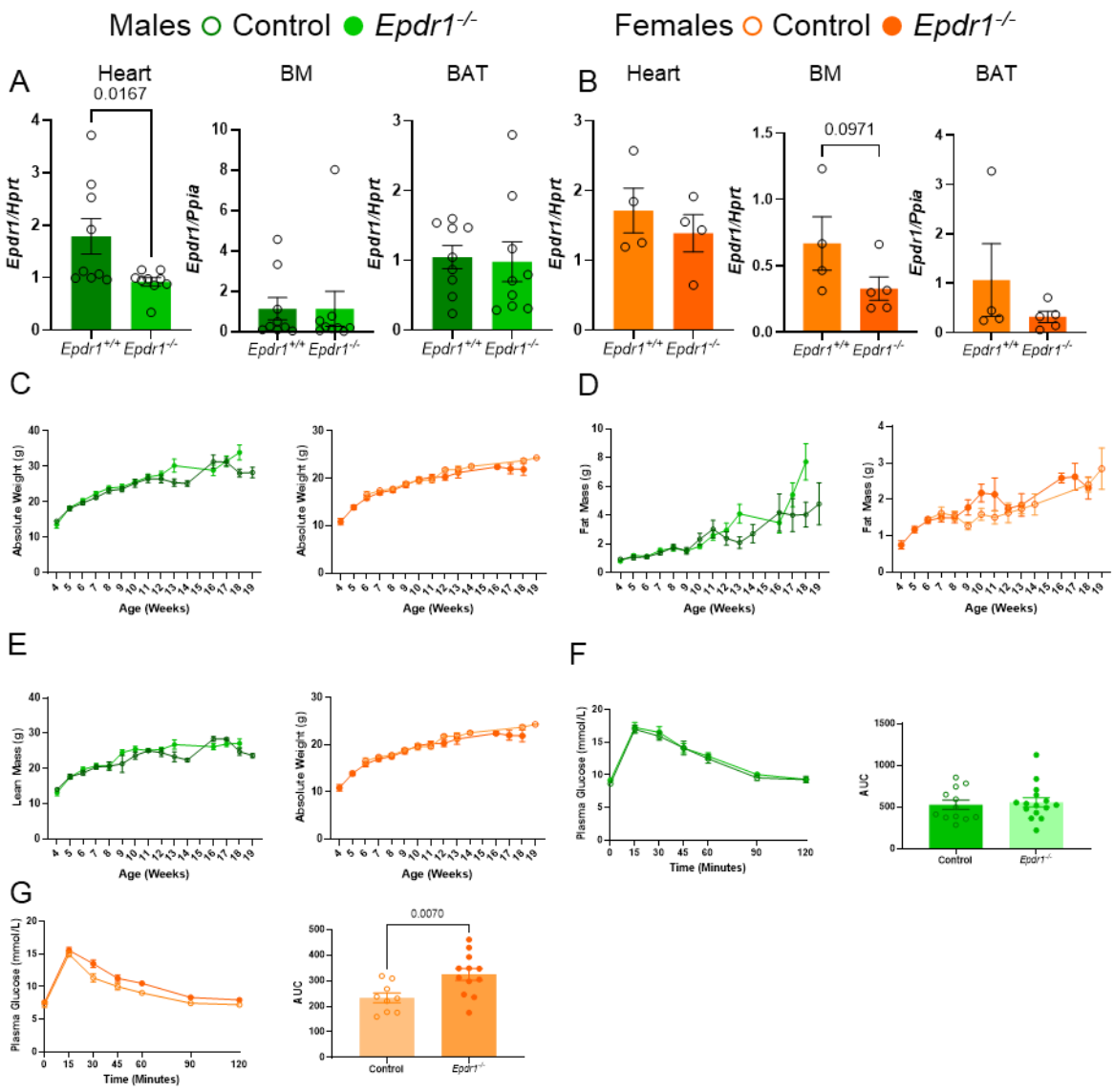
Males ○ Control ● Epdr1-/-
Females ○ Control ● Epdr1-/-
A
Heart
BM
BAT
0.0167
Epdr1/Hprt
Epdr1/Ppia
Epdr1+/+ Epdr1-/-
B
0.0971
C
D
Absolute Weight (g)
Fat Mass (g)
Age (Weeks)
E
F
Lean Mass (g)
Plasma Glucose (mmol/L)
Time (Minutes)
AUC
Control
Epdr1-/-
G
0.0070

Supplemental Figure 1. Female *Epdr1*$^{-/-}$ mice have worsened glucose tolerance. Male (green) and female (orange) control and *Epdr1*$^{-/-}$ mice (A) underwent EchoMRI from 4-19 weeks of age (B-D). Glucose tolerance tests were performed on 8–11-week-old mice (E-F). Statistical analyses performed multiple unpaired student t-test with welch correction (A-C) an unpaired two-tailed student t-test with welch correction (D-E) and an unpaired one-tailed student t-test with welch correction (F). Statistical outliers were excluded based off the ROUT method with a false discovery rate of 1%, n=4-8.

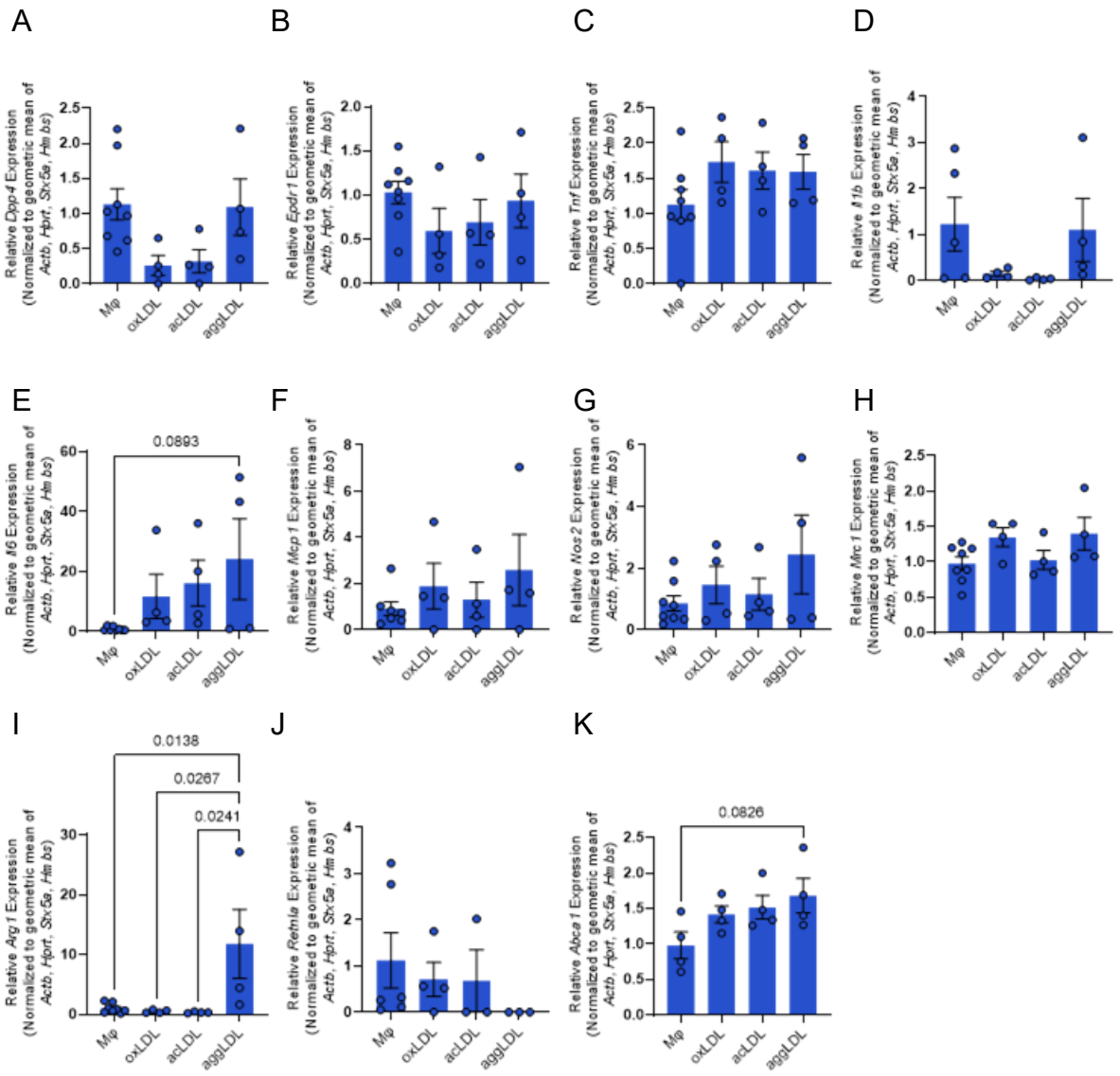
A
B
C
D
E
F
G
H
I
J
K
Relative Dpp4 Expression (Normalized to geometric mean of Actb, Hprt, Stx5a, Hm bs)
Relative Epdr1 Expression (Normalized to geometric mean of Actb, Hprt, Stx5a, Hm bs)
Relative Tnf Expression (Normalized to geometric mean of Actb, Hprt, Stx5a, Hm bs)
Relative Il1b Expression (Normalized to geometric mean of Actb, Hprt, Stx5a, Hm bs)
Relative Il6 Expression (Normalized to geometric mean of Actb, Hprt, Stx5a, Hm bs)
Relative Mcp1 Expression (Normalized to geometric mean of Actb, Hprt, Stx5a, Hm bs)
Relative Nos2 Expression (Normalized to geometric mean of Actb, Hprt, Stx5a, Hm bs)
Relative Mrc1 Expression (Normalized to geometric mean of Actb, Hprt, Stx5a, Hm bs)
Relative Arg1 Expression (Normalized to geometric mean of Actb, Hprt, Stx5a, Hm bs)
Relative Retnla Expression (Normalized to geometric mean of Actb, Hprt, Stx5a, Hm bs)
Relative Abca1 Expression (Normalized to geometric mean of Actb, Hprt, Stx5a, Hm bs)
0.0893
0.0138
0.0267
0.0241
0.0826
Mφ
oxLDL
acLDL
aggLDL

Supplemental Figure 2. *Dpp4* transcript expression is unchanged after 48h of lipid loading treatment.

Bone marrow was isolated from male eight- to twelve-week-old *Dpp4*$^{+/+}$ mice and differentiated into BMDMs. After 48h of treatment, macrophages (Mφ), or foam cells stimulated with oxidized LDL (oxLDL), acylated LDL (acLDL), or aggregated LDL (aggLDL). Transcript expression was measured using RT-qPCR in male BMDMs, Data is shown as mean ± SEM. Significance was determined by an ordinary one-way ANOVA with Tukey's multiple comparisons (A-K). Statistical outliers were excluded based off the ROUT method with a false discovery rate of 1%, n=4-8.

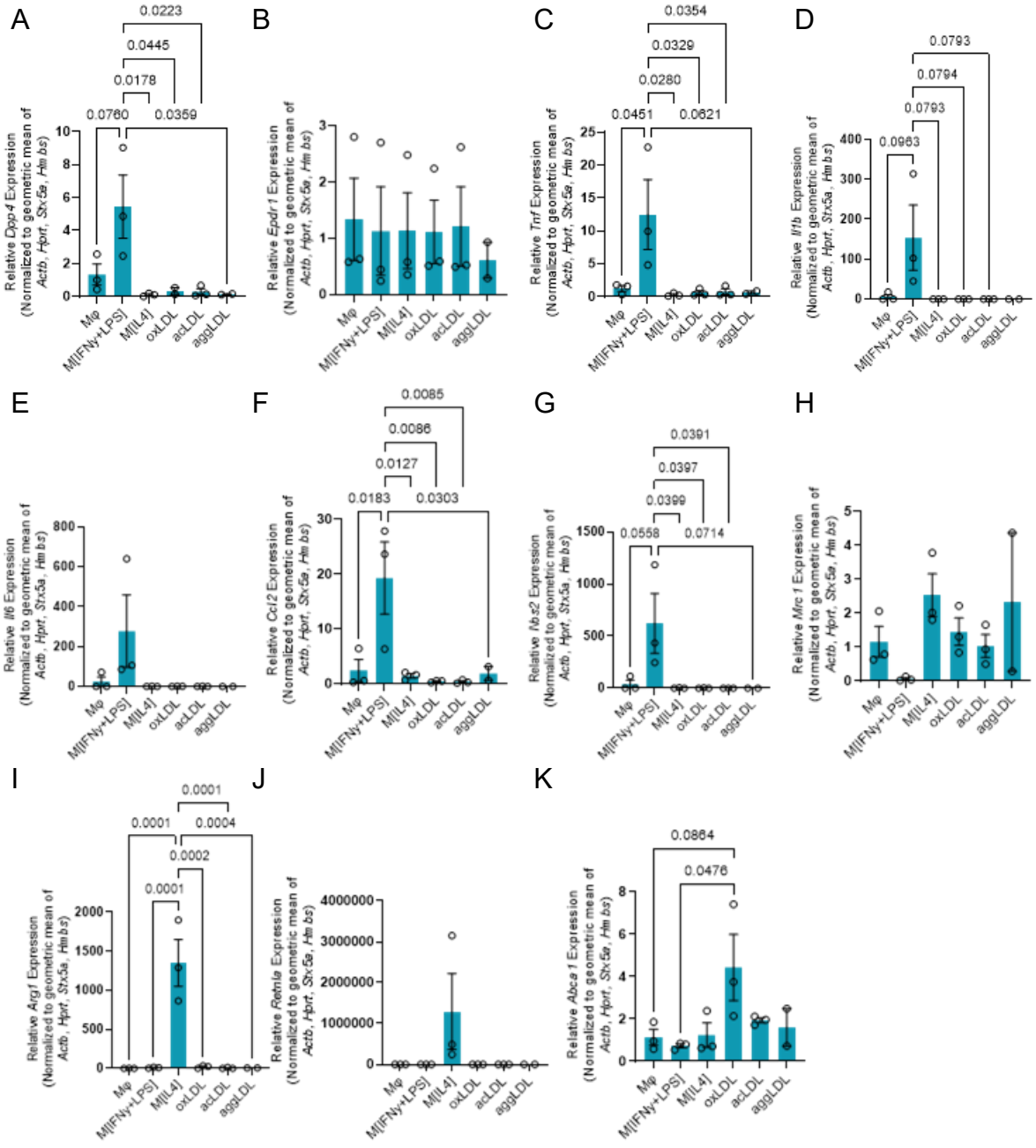
A
B
C
D
E
F
G
H
I
J
K
Mφ
M[IFNγ+LPS]
M[IL4]
oxLDL
acLDL
aggLDL

Supplemental Figure 3. *Dpp4* transcript expression is increase in pro-inflammatory macrophages.

Bone marrow was isolated from male eight- to twelve-week-old *Dpp4*$^{+/+}$ mice and differentiated into BMDMs. After 24h of treatment, macrophages (Mφ), treatment media with IFNγ and LPS (M[IFNγ+LPS]), treatment media with IL4 (M[IL4]), or foam cells stimulated with oxidized LDL (oxLDL), acylated LDL (acLDL), or aggregated LDL (aggLDL). Transcript expression was measured using RT-qPCR in male BMDMs, Data is shown as mean ± SEM. Significance was determined by an ordinary one-way ANOVA with Tukey's multiple comparisons (A-K), n=3.

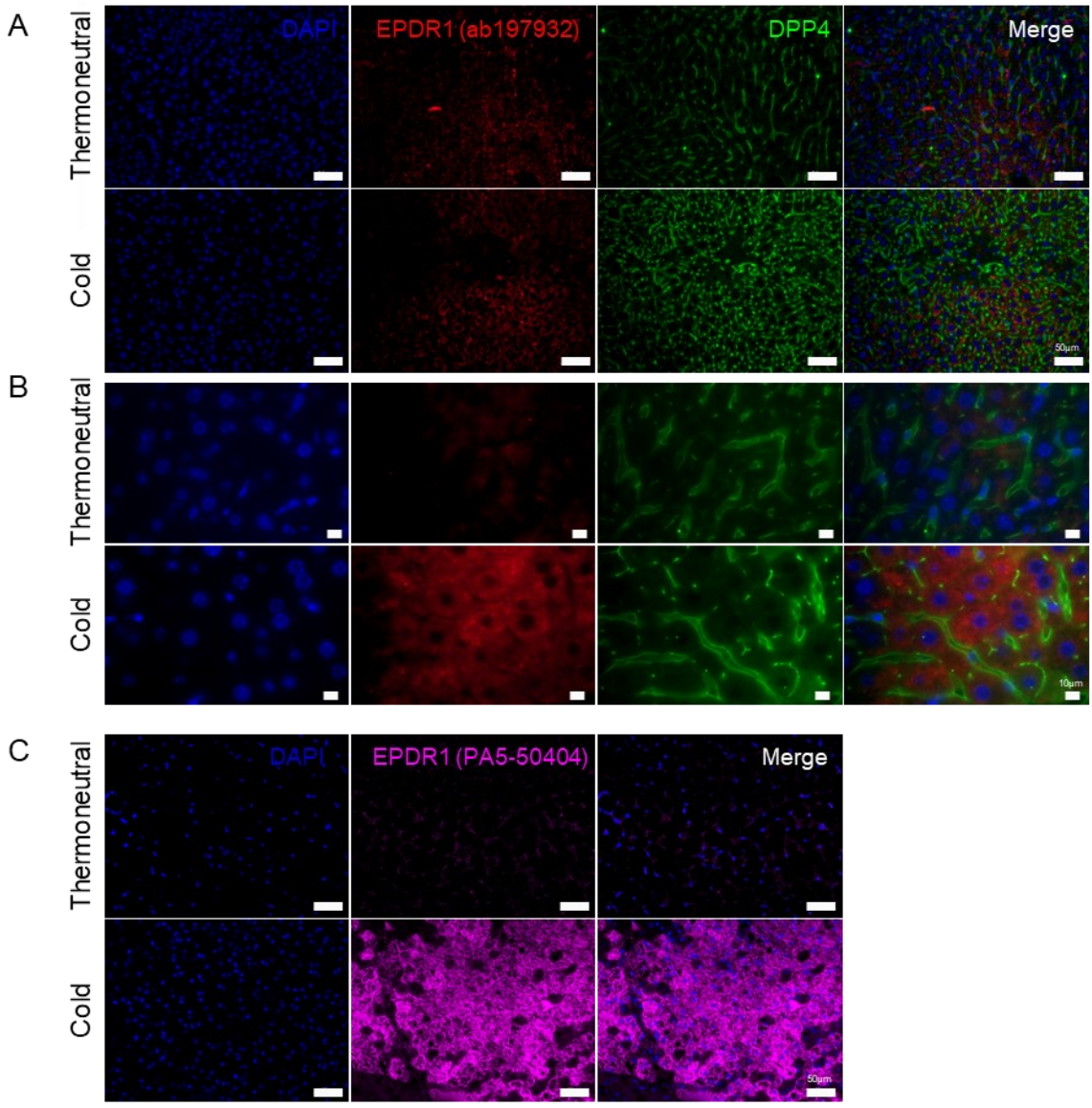

Supplemental Figure 4. Validation of EPDR1 antibodies in cold-stimulated brown adipose tissue.

Male wildtype thermoneutral and cold-stimulated mice was stained for EPDR1 and DPP4 using ab197932 (A-B) at 20X (A) or 63X (B) or EPDR1 using (PA5-50404) at 20X (C). Data shown is representative, n=3.

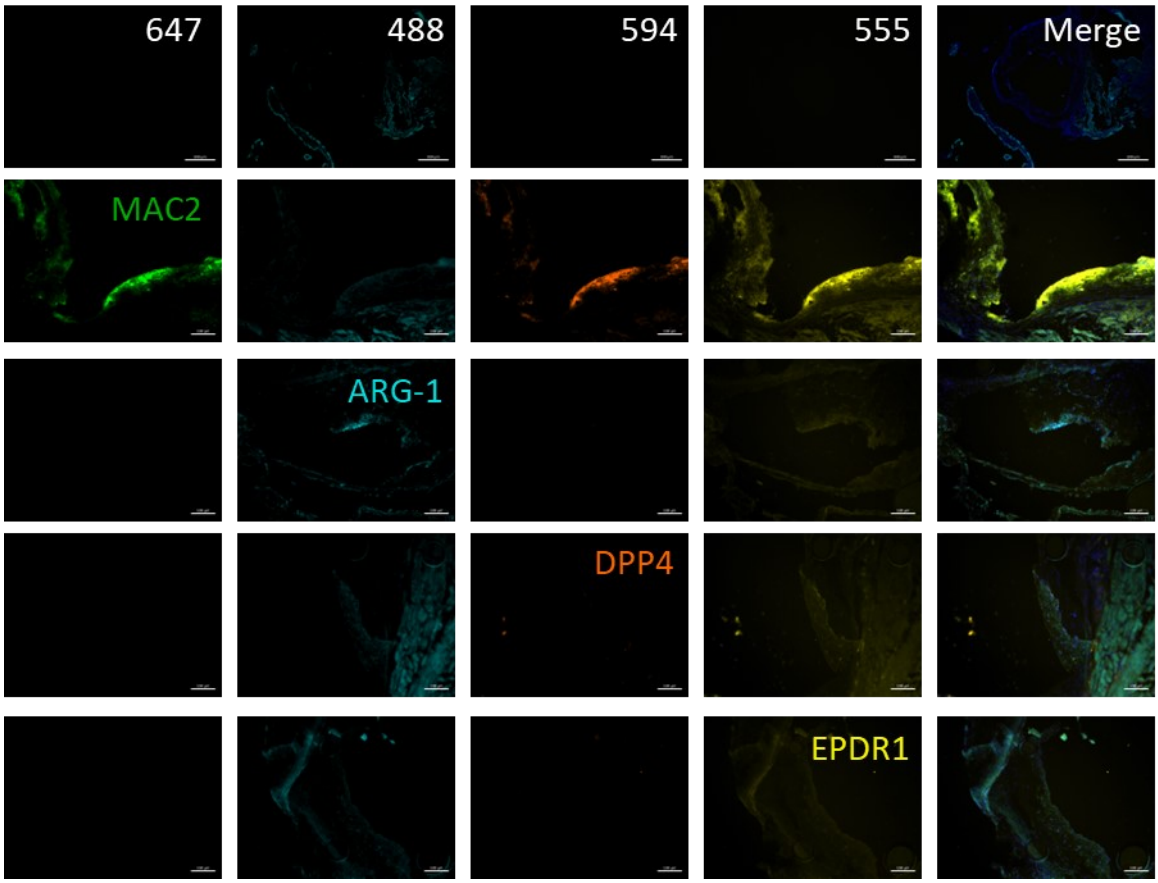

Supplemental Figure 5. Fluorescence spillover of multiple channels into the 647nm.

Staining of MAC2, ARG1, DPP4, and EPDR1, atherosclerotic lesions of *apoe*$^{-/-}$ mice aged fed a high-fat diet for 26 weeks by immunohistochemistry. Slides were fixed, permeabilized with Triton X-100, and stained with primary antibodies anti-MAC2, anti-ARG1, anti-DPP4, and anti-EPDR1, then treated with a secondary antibody as described under “Methods”.

7. Curriculum Vitae

Andrew Clément

Education

2021–present	University of Ottawa Ottawa, Ontario Canada MSc. Candidate Biochemistry Supervisor: Dr. Erin Mulvihill
2019–2021	University of Ottawa Ottawa, Ontario Canada Bachelor of Science (Honours) Translational and Molecular Medicine Honours thesis Supervisor: Dr. Morgan Fullerton

Awards and Other Honours

Sept. 2022–Aug. 2023	Canada Graduate Scholarships — Master's ($35000)
Sept. 2022 – Aug. 2024	University of Ottawa Heart Institute Cardiac Endowment Fund ($40,000)
May 2023	ORAL Basic (Honorable) Award 2023 ($150)
Sept. 2021–Aug. 2022	CI3 Graduate Studentship ($15,000)
Sept. 2021–Aug. 2022	Étoiles Académiques
Sept. 2017, May 2021	Admission Scholarship ($3,000, $15,000)
Sept. 2019–Feb. 2021	Merit Scholarship ($5,000)
Sept. 2019–Feb 2021	Deans Honour List

Publications

Trzaskalski NA, Vulesevic B, Nguyen MA, Jeraj N, Fadzeyeva E, Morrow NM, Locatelli CA, Travis N, Hanson AA, Nunes JR, O'Dwyer C, van der Veen JN, Lorenzen-Schmidt I, Seymour R, Pulente SM, **Clément AC**, Crawley AM, Jacobs RL, Doyle MA, Cooper CL, Kim KH, Fullerton MD, Mulvihill EE. Hepatocyte-derived DPP4 regulates portal GLP-1 bioactivity, modulates glucose production, and when absent influences NAFLD progression. JCI Insight. 2023 Jan 24;8(2):e154314. doi: 10.1172/jci.insight.154314. PMID: 36472923; PMCID: PMC9977314.

Morrow NM, Locatelli CAA, Trzaskalski NA, Klein CT, Hanson AA, Alhadi H, Tripathi I, **Clément AC**, Imran S, Lorenzen-Schmidt I, Mulvihill EE. Adaptation to short-term extreme fat consumption alters intestinal lipid handling in male and female mice. Biochim Biophys Acta Mol Cell Biol Lipids. 2022 Nov;1867(11):159208. doi: 10.1016/j.bbalip.2022.159208. Epub 2022 Aug 1. PMID: 35926775.

Presentations

2024	Oral Presentation: Novel Role for DPP4 in Inflammation and Atherosclerosis Work in Progress (WIP) Trainee Seminars, University of Ottawa Heart Institute, Ottawa, Canada
2024	Oral Presentation: Novel Role for DPP4 in Inflammation and Atherosclerosis Biochemistry, Microbiology, and Immunology (BMI) Seminar Day, University of Ottawa, Ottawa, Canada
2023	Oral Presentation: Novel Role for DPP4 in Inflammation and Atherosclerosis Ottawa Cardiovascular Research Day, University of Ottawa Heart Institute, Ottawa, Canada
2023	Poster Presentation: Novel Role for DPP4 in Macrophage Polarization and Atherosclerosis Biochemistry, Microbiology, and Immunology (BMI) Seminar Day, University of Ottawa, Ottawa, Canada
2022	Poster Presentation: Novel Role for DPP4 in Macrophage Polarization and Atherosclerosis Canadian Lipid and Vascular Summit, Whistler, British Columbia, Canada
2022	Oral Presentation: DPP4 and MERP-1 and Their Roles in Atherosclerosis Biochemistry, Microbiology, and Immunology (BMI) Seminar Day, University of Ottawa, Ottawa, Canada
2022	Poster Presentation: DPP4 and MERP-1 and Their Roles in Atherosclerosis Biochemistry, Microbiology, and Immunology (BMI) Symposium, Montebello, Quebec
2021	Oral Presentation DPP4, MERP-1 And Their Roles in Macrophage Polarization and Atherosclerosis

	Work in Progress (WIP) Trainee Seminars, University of Ottawa Heart Institute, Ottawa, Canada
2021	Oral Presentation: CREBH Normalizes Dyslipidemia and Halts Atherosclerosis in Diabetes by Decreasing Circulating Remnant Lipoproteins Metabolism Journal Club, Ottawa, Canada
2020	Poster Presentation: Making them last: Suppressing In Vitro Dedifferentiation of Mouse Primary Hepatocytes TMM Poster Day, Ottawa, Canada